# IMPACT MODIFIED POLY(ETHYLENE TEREPHTHALATE)-ORGANOCLAY NANOCOMPOSITES

A THESIS SUBMITTED TO
THE GRADUATE SCHOOL OF NATURAL AND APPLIED SCIENCES
OF
MIDDLE EAST TECHNICAL UNIVERSITY

BY

ELİF ALYAMAÇ

IN PARTIAL FULFILLMENT OF THE REQUIREMENTS
FOR
THE DEGREE OF MASTER OF SCIENCE
IN
CHEMICAL ENGINEERING

JULY 2004

Approval of the Graduate School of Natural and Applied Sciences

Prof. Dr. Canan Özgen
Director

I certify that this thesis satisfies all the requirements as a thesis for the degree of Master of Science.

Prof. Dr. Timur Doğu
Head of Department

This is to certify that we have read this thesis and that in our opinion it is fully adequate, in scope and quality, as a thesis and for the degree of Master of Science.

Prof. Dr. Ülkü Yılmazer
Supervisor

Examining Committee Members

Prof. Dr. Nurcan Baç (METU, Che) _____

Prof. Dr. Ülkü Yılmazer (METU, Che) _____

Prof. Dr. Erdal Bayramlı (METU, Chem) _____

Assoc. Prof. Dr. Cevdet Kaynak (METU, Mete) _____

Assoc. Prof. Dr. Göknur Bayram (METU, Che) _____

**I hereby declare that all information in this document has been obtained and presented in accordance with academic rules and ethical conduct. I also declare that, as required by these rules and conduct, I have fully cited and referenced all material and results that are not original to this work.**

Name, Last name : Elif Alyamaç

Signature :

# ABSTRACT

## IMPACT MODIFIED POLY(ETHYLENE TEREPHTHALATE)-ORGANOCLAY NANOCOMPOSITES

Alyamaç, Elif
M.S., Department of Chemical Engineering
Supervisor: Prof. Dr. Ülkü YILMAZER

July 2004, 113 pages

This study was conducted to investigate the effects of component concentrations and addition order of the components, on the final properties of ternary nanocomposites composed of poly(ethylene terephthalate), organoclay, and an ethylene/methyl acrylate/glycidyl methacylate (E-MA-GMA) terpolymer acting as an impact modifier for PET.

In this context, first, the optimum amount of the impact modifier was determined by melt compounding binary PET-terpolymer blends in a corotating twin-screw extruder. The amount of the impact modifier (5 wt. %) resulting in the highest Young's modulus and reasonable elongation at break was selected owing to its balanced mechanical properties. Thereafter, by using 5 wt. % terpolymer content, the effects of organically modified clay concentration and addition order of the components on ternary nanocomposites were systematically investigated.

Mechanical testing revealed that different addition orders of the materials significantly affected mechanical properties. Among the investigated addition orders, the best sequence of component addition (PI-C) was the one in which poly(ethylene terephthalate) was first compounded with E-MA-GMA. Later, this

mixture was compounded with the organoclay in the subsequent run. Young's modulus of not extruded pure PET increased by 67% in samples with 5 wt. % E-MA-GMA plus 5 wt. % clay loading. The highest percent elongation at break was obtained as 300%, for the addition order of PI-C, with 1 wt. % clay content, which is nearly 50 fold higher than that obtained for pure PET.

In X-ray diffraction analysis, extensive layer separation associated with delamination of the original clay structure occurred in PI-C and CI-P sequences with both 1 and 3 wt. % clay contents. X-ray diffraction patterns showed that, at these conditions exfoliated structures resulted as indicated by the disappearence of any peaks due to the diffraction within the consecutive clay layers.

**Keywords:** poly(ethylene terephthalate), impact modification, organoclay, nanocomposites, extrusion

# ÖZ

## DARBE DAYANIMI İYİLEŞTİRİLMİŞ POLİETİLEN TEREFTALAT- ORGANİK KİL NANOKOMPOZİTLERİ

Alyamaç, Elif
Yüksek Lisans, Kimya Mühendisliği
Tez Yöneticisi: Prof. Dr. Ülkü Yılmazer

Temmuz 2004, 113 sayfa

Bu çalışma, amorf polietilen tereftalat (PET), organik kil ve PET için darbe iyileştirici olarak davranan etilen/metil akrilat/glisidil metakrilat (E-MA-GMA) terpolimerinden oluşan üçlü nanokompozit sistemlerinin özelliklerine, bileşen konsantrasyonlarının ve bileşen ekleme sırasının etkisini incelemek amacıyla yürütülmüştür.

Bu çerçevede, ilk olarak, aynı yönde dönen çift vidalı ekstrüderde PET ve darbe iyileştiricili sistemler eriyik halde karıştırılarak, en uygun darbe iyileştirici miktarı belirlenmiştir. Young modülü yüksek, kopmadaki uzama değeri makul olan darbe iyileştirici miktarı (ağırlıkça %5) dengeli mekanik özelliklerinden dolayı seçilmiştir. Daha sonra, organik kil miktarı ve bileşenlerin ekleme sırasının, ağırlıkça %5 darbe iyileştirici içeren, üçlü nanokompozit sistemleri üzerindeki etkisi sistematik olarak incelenmiştir.

Mekanik testler, malzemelerin ekleme sırasının mekanik özellikleri büyük ölçüde etkilediğini göstermiştir. PET' in önce E-MA-GMA ile, daha sonra da organik kille karıştırılması, en iyi ekleme sırası olmuştur. Ağırlıkça %5 kil ve %5 E-MA-GMA içeren numunelerde Young modülü, ekstrüzyon işlemine maruz kalmamış PET' e kıyasla %67 artış göstermiştir. En yüksek kopmada uzama %300 olup bu değer saf PET' inkinin yaklaşık 50 katıdır, ve ağırlıkça %1 kil içeren PI-C sıralamasında elde edilmiştir.

X-ışını kırınımı analizinde, kilin orijinal yapısının dağılmasına bağlı olarak gözlemlenen tabaka açılması, PI-C ve CI-P sıralamalarında, ağırlıkça hem %1 hem de %3 kil içeriğinde oluşmuştur. X-ışını kırınımı grafiklerinde, çok iyi dağılmış yapının oluştuğu, ardışık tabakalar arasında kırılmaya bağlı olarak görülen tepe eğrilerinin kaybolmasından anlaşılmıştır.

**Anahtar Kelimeler:** poli(etilen tereftalat), darbe dayanımı iyileştirilmesi, organik kil, nanokompozitler, ekstrüzyon

To my family

## ACKNOWLEDGEMENTS

I would like to express my deepest gratitude to my supervisor Prof. Dr. Ülkü Yılmazer, for his continuous support, encouragement and guidance throughout this study.

I am very grateful to Assoc. Prof. Dr. Göknur Bayram from Department of Chemical Engineering for giving me every opportunity to use the instruments in her laboratory. I also would like to thank Prof. Dr. Erdal Bayramlı from Department of Chemistry for letting me use the injection molding machine in his laboratory and Prof. Dr Teoman Tinçer from Department of Chemistry for providing me the impact test instrument in his laboratory.

Special thanks go to Cengiz Tan from Department of Metallurgical and Materials Engineering for SEM Analysis and Mihrican Açıkgöz from Department of Chemical Engineering for DSC Analysis.

İnciser Girgin and Bilgin Çiftçi from General Directorate of Mineral Research and Exploration, for X-Ray Diffraction Analysis, are gratefully acknowledged. I am also thankful to all my friends in Polymer Research Group for their cooperation and friendship.

Last but not the least; I wish to express my sincere thanks to my family for supporting, encouraging, and loving me all through my life.

# TABLE OF CONTENTS

# LIST OF TABLES

TABLE

# LIST OF FIGURES

# NOMENCLATURE

| | |
|---|---|
| $A_0$ | Original, undeformed cross-sectional area, $mm^2$ |
| b | Width of beam tested, mm |
| c | velocity of light, m/s |
| d | Depth of beam tested, mm |
| d | Plane spacing, Å |
| D | Distance, mm |
| E | Modulus of Elasticity, MPa |
| $E_B$ | Modulus of elasticity in bending, MPa |
| F | Tensile Load, N |
| h | Plank's constant, J.sec |
| L | Support span, mm |
| $L_0$ | Initial gauge length, mm |
| ΔL | Change in sample length, mm |
| m | Slope of the tangent to the initial straight-line portion of the load-deflection curve, N/mm |
| M | Monovalent cation |
| n | Order of diffraction |
| P | Load at a given point on the load-deflection curve, N |
| R | Maximum strain in the outer fibers, mm/mm |
| S | Stress in the outer fibers at midspan, MPa |
| T | Thickness, mm |
| $T_c$ | Crystallization temperature, °C |
| $T_g$ | Glass transition temperature, °C |
| $T_m$ | Melting temperature, °C |
| W | Width, mm |
| x | Degree of isomorphous substitution |

*Greek Letters*

| | |
|---|---|
| $\epsilon$ | Tensile strain, mm/mm |
| $\lambda$ | Wavelength, nm |
| $\nu$ | Frequency |
| $\sigma$ | Tensile stress(nominal), MPa |
| $\sigma_m$ | Tensile strength, MPa |
| $\theta$ | Scattering angle, ° |

*Abbreviations*

| | |
|---|---|
| APET | Amorphous Poly(Ethylene Terephthalate) |
| ASTM | American Society for Testing and Materials |
| BHET | Bis (β-Hydroxyethyl) Terephthalate |
| CEC | Cation Exchange Capacity |
| DMT | Dimethyl Terephthalate |
| DSC | Differential Scanning Calorimetry |
| EG | Ethylene Glycol |
| E-GMA | Ethylene-Glycidyl Methacrylate |
| E-MA-GMA | Ethylene-Methyl Acrylate-Glycidyl Methacrylate |
| EPR | Ethylene-co-Propylene Rubber |
| GMA | Glycidyl Methacrylate |
| HT | Hydrogenated Tallow |
| IV | Intrinsic Viscosity |
| MFI | Melt Flow Index |
| MMT | Montmorillonite |
| PET | Poly(Ethylene Terephthalate) |
| PLS | Polymer Layered Silicate |
| PTA | Purified Terephthalic Acid |
| SAXS | Small Angle X-ray Scattering |
| SEM | Scanning Electron Microscopy |
| TEM | Transmission Electron Microscopy |
| TPA | Terephthalic Acid |
| WAXS | Wide Angle X-ray Scattering |
| XRD | X-Ray Diffraction |

# CHAPTER 1

# INTRODUCTION

Composite materials are a new class of materials that combine two or more distinctly dissimilar components into a suitable form. While each component retains its identity, the new composite material displays macroscopic properties superior to its parent constituents, particularly in terms of mechanical properties and economic value (Broutman and Krock, 1967).

In recent years, it is found that when fillers are dispersed in polymers on the nanometer scale, composites obtained show improved properties compared to conventional polymer composites. Among these properties improved by the presence of nanofillers are mechanical, thermal, physical and barrier properties. This new class of composites is called polymer matrix nanocomposites (Giannelis, 1996).

Today, studies are being conducted globally, using almost all types of polymer matrices. Consequently, current reports on poly(ethylene terephthalate) based nanocomposites (Pinnavaia and Beall, 2000) and impact modification of poly(ethylene terephthalate) (Chapleau and Huneault, 2003) exist in the literature. However, there are no studies on nanocomposites formed from organically modified clay as the reinforcing agent and impact modified poly(ethylene terephthalate) as the matrix.

Poly(ethylene terephthalate) is a thermoplastic polyester having poor impact resistance and high notch sensitivity. Additionally, in PET/clay nanocomposites, addition of clay sometimes imparts drawbacks to the resulting material such as brittleness. For this reason, impact modification of PET can be achieved by dispersing elastomeric polymers in the polymer matrix.

In this study, the effects of component concentrations and addition order of the components, on the final properties of ternary nanocomposites composed of amorphous poly(ethylene terephthalate) matrix, organically modified clay, and an ethylene/methyl acrylate/glycidyl methacylate (E-MA-GMA) terpolymer were systematically investigated.

In this context, first, the amount of the terpolymer acting as an impact modifier for PET was optimized by melt compounding binary PET-terpolymer blends. The amount of the impact modifier resulting in the highest elastic modulus and reasonable elongation at break was selected owing to its balanced mechanical properties. Thereafter, by using the optimum impact modifier concentration, the effects of organically modified clay concentration and addition order of the components were systematically investigated by preparing ternary nanocomposites formed from organically modified clay as the nanofiller and impact modified poly(ethylene terephthalate) as the matrix.

All formulations were prepared by melt compounding of the components with a two-step mixing procedure in a corotating twin-screw extruder. Prior to characterization, standard test specimens were injection molded. Mechanical tests conducted on each composition included the investigation of tensile strength, Young's modulus, tensile stress at yield, percent elongation at break, flexural modulus, flexural strength and impact strength. The morphology was analyzed by X-Ray Diffraction and Scanning Electron Microscopy. Flow characteristics, melting and crystallization behavior of the compositions were also studied by Melt Flow Index Measurements and Differential Scanning Calorimetry Analysis, respectively.

At the end of the study, the processing parameters of the nanocomposites were optimized using the properties synergistically derived from the three components.

# CHAPTER 2

# BACKGROUND

## 2.1 Composites

A composite is a multiphase material that exhibits a significant proportion of the properties of both constituent phases such that a better combination of properties is realized. Many composite materials are composed of just two phases; one is termed the matrix, which is continuous and surrounds the other phase, often called the dispersed phase. The properties of composites are a function of the properties of the constituent phases, their relative amounts, and the geometry of the dispersed phase. "Dispersed phase geometry" in this context means the shape of the particles and the particle size, distribution, and orientation (Callister, 1997).

### 2.1.1 Polymer Matrix Composites

Polymers, metals, and ceramics are all used as matrix materials in composites, depending on the particular requirements. Polymers are unquestionably the most widely used matrix materials in modern composites (Gibson, 1994). Polymers have advantages over other types of materials, such as metals and ceramics, because their low processing costs, low weight and properties such as transparency and toughness form unique combinations. Many polymers have useful characteristics, such as tensile strength, modulus, elongation and impact strength and make them more cost effective than metals and ceramics (Sawyer and Grubb, 1987).

A polymer is defined as a long-chain molecule built up by the repetition of small, simple chemical units. In some cases the repetition is linear, much as a chain is built up from its links. In other cases the chains are branched or

interconnected to form three-dimensional networks. The repeat unit of the polymer is usually equivalent or nearly equivalent to the monomer, or starting material from which the polymer is formed (Billmeyer, 1984).

Polymers are divided into two broad categories: thermoplastics and thermosets. In a thermoplastic polymer, individual molecules are linear in structure with no chemical linking between them. They are held in place by weak secondary bonds such as van der Waals forces and hydrogen forces. With the application of heat and pressure, these intermolecular bonds in a solid thermoplastic polymer can be temporarily broken and the molecules can be moved relative to each other to flow into new positions. Upon cooling, the molecules freeze in their new positions, restoring the secondary bonds between them and resulting in a new solid shape. Thus, a thermoplastic polymer can be heat-softened, melted and reshaped as many times as desired.

In a thermoset polymer, on the other hand, the molecules are chemically joined together by cross-links, forming a rigid, three-dimensional network structure. Once these cross-links are formed during the polymerization reaction, the thermoset polymer can not be melted and reshaped by the application of heat and pressure.

The primary consideration in the selection of a matrix is its basic mechanical properties including tensile modulus, tensile strength, and fracture toughness. The most important advantage of thermoplastic polymers over thermoset polymers is their high impact strength and fracture resistance, which in turn impart excellent damage tolerance characteristics to the composite material (Schwartz, 1997). In general, thermoplastic polymers have higher strains to failure than thermoset polymers, which may provide a better resistance to matrix microcracking in the composite laminate.

## 2.2 Nanocomposites

For some time, particles have been added to polymers in order to improve the stiffness and the toughness of the materials, to enhance their barrier properties, to enhance their resistance to fire and ignition or just simply to reduce cost. In recent years, it was found that when the fillers are dispersed in polymers on the nanometer scale, the materials possessed unique properties typically not shared by their more conventional microcomposite counterparts. This new class of materials is called nanocomposites (Giannelis, 1996).

Nanocomposites already look attractive for molded car parts such as body panels and under-hood components, as well as electrical/electronic parts, power-tool housings, lawnmowers, aircraft interiors, and applier components. On the packaging side, nanocomposites can slow down transmission of gases and moisture vapor through plastics by creating a "tortuous path" for gas molecules to thread their way among the obstructing platelets (Sherman L.M., 1999).

Polymer nanocomposites are particle-filled polymers in which at least one dimension of the dispersed particles is in the nanometer range. One can distinguish three types of polymer nanocomposites, depending on how many dimensions of the dispersed particles are in the nanometer range. When all three dimensions are on the nanometer scale, they are called isodimensional nanoparticles or zero-dimension reinforcing particles (Mark, 1996; Herron and Thorn, 1998); when two dimensions are in the nanometer scale and the third is larger, they are called nanotubes/nanofibers or one-dimension reinforcing particles (Favier et al., 1997; Chazeau et al., 1999). This type of nanocomposite is extensively studied because reinforcing nanofillers yield materials with exceptional properties.

The third type of nanocomposites has fillers with only one dimension in the nanometer range that reinforce the material in two dimensions. For this type of nanocomposite, the fillers are present in a form of sheets with a thickness of a few nanometers and hundred to thousands nanometers of length and width (Alexandre and Dubois, 2000). In our study, we have focused on the third type of nanocomposites which is to be explained in the following section.

## 2.3 Polymer-Layered Silicate Nanocomposites

After layered silicates are dispersed on a nanometer scale into the polymer matrix, nanocomposites exhibit significantly improved mechanical, thermal, optical and physico-chemical properties when compared with pure polymer or conventional composites. Improvements may include, for instance, increased modulus, strength, heat resistance, decreased gas permeability and flammability.

The unprecedented mechanical properties of polymer layered silicate nanocomposites (PLS) were first demonstrated by researchers at Toyota using nylon nanocomposites (Kojima et al., 1993). They showed that a doubling of the tensile modulus and strength is achieved for nylon-layered silicate nanocomposites containing as little as 2 vol. % inorganic material.

PLS nanocomposites have several advantages (Giannelis, 1999) e.g. (a) they are lighter in weight compared to conventionally filled polymers because high degrees of stiffness and strength are realized with far less high density inorganic material; (b) they exhibit outstanding diffusional barrier properties without requiring a multipolymer layered design, allowing for recycling; and (c) their mechanical properties are potentially superior to unidirectional fiber reinforced polymers, because reinforcement from the inorganic layers will occur in two rather than in one dimension. Uses for this new class of composites can be found in aerospace, automotive, electronics and biotechnology applications, to list only a few (Schmidt et al., 2002).

### 2.3.1 Layered Silicates

The layered silicates used in polymer-layered silicate nanocomposites, like the better known members of the group, talc and mica, belong to the structural family of 2:1 phyllosilicates. Their crystal structure consists of multi-layers. Each layer is made up of two silica tetrahedral sheets and an edge-shared octahedral sheet of either aluminum or magnesium hydroxide. Their structure is shown in Figure 2.1 and their chemical formulas are given in Table 2.1.

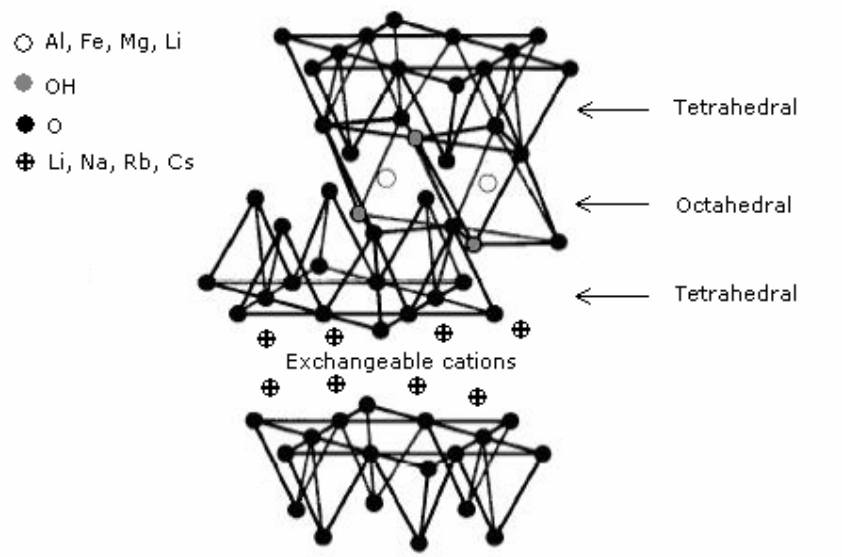


**Figure 2.1.** Structure of 2:1 layered silicates (Giannelis et al., 1999).

The layer thickness is around 1 nm and the lateral dimensions of these layers may vary from 30 nm to several microns or even larger. Stacking of the layers leads to a regular Van der Waals gap between the silicate layers which is called the interlayer or gallery. Negative charges are generated by isomorphic substitution within the layers (for example, $Al^{3+}$ replaced by $Mg^{2+}$ or by $Fe^{2+}$, or $Mg^{2+}$ replaced by $Li^{+}$). These negative charges are counterbalanced by alkali or alkaline earth cations situated in the interlayers.

Montmorillonite, hectorite, and saponite are the most commonly used layered silicates. In the older literature, the term "montmorillonite" was frequently used as a group name for any swelling 2:1 clay mineral as well as the name of a specific mineral. Presently, smectite is the group name and montmorillonite is restricted to a mineral name belonging to that group (Giese and Van Oss, 2002). In France, Damour and Salvetat gave the name montmorillonite to a mineral found in a region of central France. The famous French chemist, Henry LeChatelier, studied montmorillonite and in 1887 correctly identified it as being a hydrated aluminum silicate (Seymour and Deanin, 1987).

All of these silicates are characterized by a large active surface area (700-800 $m^2/g$ in the case of montmorillonite), a moderate negative surface charge (cation exchange capacity) (CEC) and layer morphology.

**Table 2.1** Chemical structures of commonly used layered silicates.

| Layered silicates | General Formula* |
|---|---|
| Montmorillonite | $M_x(Al_{4-x}Mg_x)Si_8O_{20}(OH)_4$ |
| Hectorite | $M_x(Mg_{6-x}Li_x)Si_8O_{20}(OH)_4$ |
| Saponite | $M_xMg_6(Si_{8-x}Al_x)O_{20}(OH)_4$ |

*M = monovalent cation; x = degree of isomorphous substitution.

The performance improvements of polymer nanocomposites depend to a large extent on the distribution and arrangement of the layered silicates as a result of intercalation or exfoliation, and on the interfacial bonding between the layered silicates and the polymer (Le Baron et al., 1999).

Layered silicates are hydrophilic and most polymers are hydrophobic. In order to enhance the mineral-polymer interaction, hydrophilic phyllosilicates are rendered more organophilic by exchanging the hydrated cations of the interlayer with cationic surfactants such as alkylammonium or alkylphosphonium (Pinnavaia and Beall, 2000). The interlayer spacing is usually larger for modified layered silicates because organic cations are bulkier than hydrated inorganic cations. The modified layered silicates have lower surface energy and are more compatible with organic polymer matrices. In addition, the organic cations may provide various functional groups that can react with the polymer chain to increase adhesion between the inorganic filler and the organic polymer matrix (Giannelis, 1998).

### 2.3.2 Structures of Polymer-Layered Silicate Nanocomposites

Nanocomposites can be classified into three categories according to the degree of dispersion of silicates. This depends on the nature of the components used including polymer matrix, layered silicate, and organic cation. If the polymer can not intercalate between the silicate sheets, a microcomposite is obtained. This phase separated composite has the same properties as conventional microcomposites.

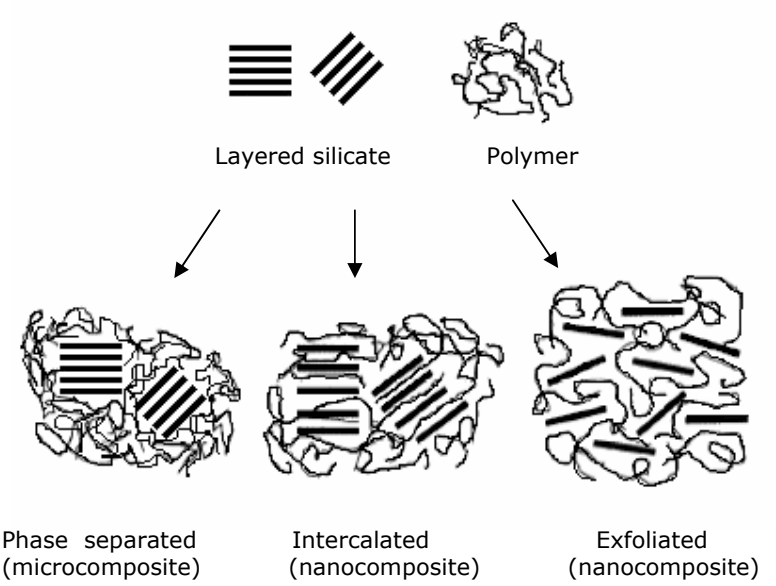


**Figure 2.2** Schematic illustrations of a phase separated; an intercalated; and an exfoliated polymer-layered silicate nanocomposites.

Beyond this traditional class of polymer-filler composites, two types of nanocomposites can be obtained: Intercalated structures are formed when a single (or sometimes more) extended polymer chain is intercalated between the silicate layers. The result is a well ordered multilayer structure of alternating polymeric and inorganic layers (Beyer, 2002).

In an exfoliated or delaminated nanocomposite, the silicates are completely and uniformly dispersed in the continuous polymer matrix. Usually, the clay content of an exfoliated nanocomposite is much lower than that of an intercalated nanocomposite (Yoon et al., 2001).

The delamination configuration is of particular interest because it maximizes the polymer-clay interactions, making the entire surface of the layers available for the polymer. This should lead to the most significant changes in mechanical and physical properties. Possible polymer-layered silicate structures are given in Figure 2.2.

## 2.4 Preparative Methods of Polymer-Layered Silicate Nanocomposites

The preparative methods are divided into three main groups according to the starting materials and processing techniques.

### 2.4.1 In-situ Intercalative Polymerization Method

In this method, the layered silicate is swollen within the liquid monomer or a monomer solution so the polymer formation can occur between the intercalated sheets. Polymerization can be initiated either by heat or radiation, by the diffusion of a suitable initiator, or by an organic initiator or catalyst fixed through cation exchange inside the interlayer before the swelling step. It is the first method used to synthesize polymer-layered silicate nanocomposites based on polyamide 6 (Fukushima et al., 1988).

### 2.4.2 Solution Intercalation Method

This is based on a solvent system in which the polymer is soluble and the silicate layers are swellable. The layered silicate is first swollen in a solvent, such as water, chloroform, or toluene. When the polymer and layered silicate solutions are mixed, the polymer chains intercalate and displace the solvent within the interlayer of the silicate (Sinha Ray et al., 2003). Upon solvent removal, the intercalated structure remains resulting in PLS nanocomposite.

### 2.4.3 Melt Intercalation Method

This method was first reported by Vaia et al. in 1993. The process involves annealing a mixture of polymer and layered silicates above melting point of the polymer. During the anneal, the polymer chains diffuse from the bulk polymer melt into the van der Waals galleries between the silicate layers (Vaia et al., 1995). This method is quite general and is broadly applicable to a range of commodity polymers from essentially non-polar polystyrene, to weakly polar poly(ethylene terephthalate), to strongly polar nylon.

It has great advantages over either in-situ intercalative polymerization or solution intercalation. First, this method is environmentally benign due to the absence of organic solvents. Second, it is compatible with current industrial process, such as extrusion and injection molding. The melt intercalation method

allows the use of polymers which were previously not suitable for in situ polymerization or solution intercalation. Besides, it is a quite effective technology for the case of polyolefin-based nanocomposites (Hasegawa et al., 2000).

## 2.5 Polymer Processing

### 2.5.1 Extrusion

In principle, the extrusion process comprises the forcing of a plastic or molten material through a shaped die by means of pressure (Morton-Jones D.H., 1989). In addition to the shaping of parts by the extrusion process, extrusion is the most efficient and widely used process for melting plastic resin as part of the process of adding or mixing fillers, colorants, and other additives into the molten plastic. Extrusion can be used to shape the part directly after this mixing or an extruder can be used as the melting device that is coupled with other shaping processes (Strong, 1996). Examples of the use of extruders as integral parts of other plastic forming operations would include injection molding, blow molding, and foam making. The advantages and disadvantages of extrusion are summarized in Table 2.2.

**Table 2.2** Comparison of extrusion to other plastics molding processes.

| Advantages | Disadvantages |
|---|---|
| Continuous | Limited complexity of parts |
| High production volumes | Uniform cross-sectional shape only |
| Low cost per pound | |
| Efficient melting | |
| Many types of raw materials | |
| Good mixing (compounding) | |

Twin-screw extruders are a widely used type of extruders. They exist in corotating and counterrotating versions; the screws could be non-intermeshing, partially intermeshing or closely intermeshing. With corotating twin-screw extruders, the melt contained in one screw channel is transferred to the other channel with each rotation. The transport mechanism (drag forces) is comparable to that of a single-screw extruder. The melt however is exposed to a greater shear stress due to the increased path length through the extruder.

Such extruders are almost exclusively employed for compounding (Ullmann's Encyclopedia of Industrial Chemistry, 1992).

### 2.5.2 Injection Molding

Many well known thermoplastic processes rely on an extrusion system to provide the heat-softened material for manipulation into a final finished article. Injection molding is an obvious and possibly the oldest example of this where a thermoplastic material is forced by a ram through a heating chamber and then to a nozzle or die and finally into a closed mold where the material takes up the required form (Fisher, 1976).

There are several configurations of injection units in use today. The simplest, first generation plunger and torpedo machines are still being made, but the most widely used type is the reciprocating single-screw injection unit (Schwartz, 1997). The most important process parameters controlled by the injection unit are the following.

#### 2.5.2.1 Melt Temperature

The temperature of the melt when it penetrates into the mold is controlled by the temperature control system of the injection unit but may also be affected by the injection speed and by the level of back pressure.

#### 2.5.2.2 Injection Speed

This is the speed at which the screw advances during the mold filling step. Modern machines are equipped with variable injection speed control- a profile of speeds rather than a single constant value is used to fill the mold. Typical mold filling starts at a low speed to prevent jetting; speed is increased during the middle part of filling and reduced again toward the end to allow smooth and accurate transition to pressure control, which takes over when the mold is full.

#### 2.5.2.3 Injection Pressure

The pressure exerted by the screw on the melt is not constant during the mold filling stage. Injection pressure builds up as the mold is filled and as the

resistance to flow increases. It is only when the mold is full that a transfer from speed control to pressure control takes place. Injection pressure is the principle variable during the holding stage.

## 2.6 Polymer Characterization

Once a new material is developed, its properties should be evaluated and usually compared with the properties of already known materials to verify the proposed reaction. Analysis of properties of newly developed material is also important in determining the applications for which the material can be used. There are various analytical and evaluative methods currently available. Many of them are equipped with high technology device with computer programs. Although there is no single test that can provide all the answers needed, one can obtain a good picture of the type of material by combining the results of various tests. The methods and their standard procedures used in this study will be discussed in the following sections.

### 2.6.1 Mechanical Properties

There are a variety of methods which are useful in predicting mechanical properties of polymers. However, it is essential that there should be some consistency in the manner in which tests are conducted, and in the interpretation of their results. This consistency is accomplished by using standardized testing techniques. Establishment and publication of these standards are often coordinated by professional societies. In the United States the most active organization is the American Society for Testing and Materials (ASTM). Its annual book of ASTM standards comprises numerous volumes, which are issued and updated yearly; a large number of these standards relate to mechanical testing techniques. Three of the more commonly employed testing techniques based on ASTM standards are tensile, flexural and impact tests.

#### 2.6.1.1 Tensile Test

Standard test method for tensile properties (ASTM D638M-91a) employs specimens of a specified shape, typically a dogbone, as depicted in Figure 3.10. During the test, a specimen is deformed, usually to fracture, with a gradually increasing tensile load that is applied uniaxially along the long axis of a

specimen. The length of the center section is called the initial gauge length $L_0$. The force F is measured at the fixed end as a function of elongation.

$$\sigma = F / A_0 \tag{2.1}$$

$$\epsilon = \Delta L / L_0 \tag{2.2}$$

where $A_0$ is the original, undeformed cross-sectional area of the gauge region and $\Delta L$ is the change in sample length as a result of the applied force.

Tensile stress (nominal), $\sigma$ is the tensile load per unit area of minimum original cross-section, with the gauge boundaries, carried by the test specimen at any given moment. It is expressed in force per unit area, usually in megapascals, (Equation 2.1).

Tensile strength, $\sigma_m$ is the maximum tensile stress sustained by the specimen during a tension test. When the maximum stress occurs at the yield point, it is designated tensile strength at yield. When the maximum stress occurs at break, it is designated tensile strength at break.

Tensile strain, $\epsilon$ is the ratio of the elongation to the gauge length of the test specimen, that is, the change in length per unit of original length. It is expressed as a dimensionless ratio, as shown in Equation 2.2.

It is seen in Equation 2.3 that modulus of elasticity, E is the ratio of stress (nominal) to corresponding strain below the proportional limit of a material. It is expressed in force per unit area, usually in megapascals. It is also known as elastic modulus or Young's modulus.

$$E = \sigma / \epsilon \tag{2.3}$$

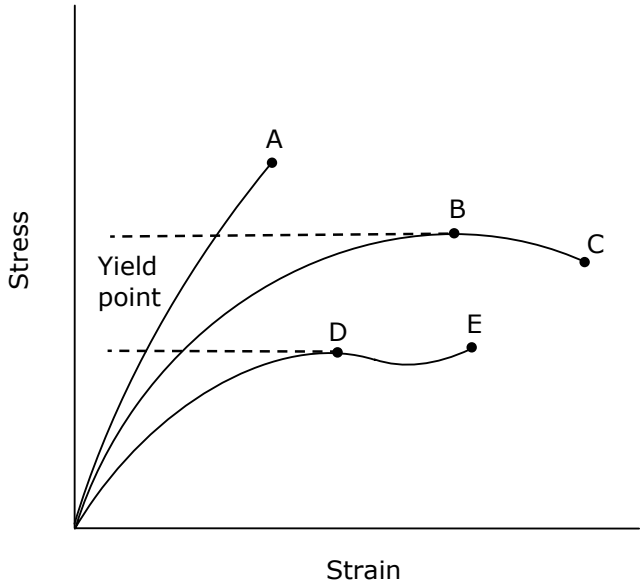


**Figure 2.3** Tensile designations.

In Figure 2.3, A and E designate tensile strength at break and elongation at break. B is the point showing both tensile strength at yield and elongation at yield. On the other hand, point C presents tensile stress at break and elongation at break. Lastly, D displays tensile stress at yield and elongation at yield.

2.6.1.2 Flexural Test

ASTM D790M-92 test method covers the determination of flexural properties of polymers using a three-point or four-point loading system.

Three-point loading system utilizes center loading on a simply supported beam. A bar of rectangular cross-section is tested in flexure as a beam. The bar rests on two supports and is loaded by means of a loading nose midway between the supports (Figure 3.11).

When the specimen is tested in flexure as a simple beam supported at two points and loaded at the midpoint, the maximum stress in the outer fibers occurs at midspan. This stress may be calculated for any point on the load-deflection curve by the following equation:

$$S = 3PL/2bd^2 \qquad (2.4)$$

where S is stress in the outer fibers at midspan (MPa), P is load at a given point on the load-deflection curve (N), L is support span (mm), b is width of beam tested (mm), and d is depth of beam tested (mm).

The maximum strain in the outer fibers occurs at midspan as well, and may be calculated as follows:

$$r = 6Dd/L^2 \quad (2.5)$$

where r is maximum strain in the outer fibers (mm/mm), D is maximum deflection of the center of the beam (mm), d is depth of beam tested (mm), and L is support span (mm).

The tangent modulus of elasticity, often called flexural modulus, is the ratio within the elastic limit of stress to corresponding strain and shall be expressed in megapascals. It is calculated by drawing a tangent to the steepest initial straight-line portion of the load-deflection curve and using Equation 2.6.

$$E_B = L^3m/4bd^3 \quad (2.6)$$

where $E_B$ is modulus of elasticity in bending (MPa), L is support span (mm), b is width of beam tested (mm), d is depth of beam tested (mm), and m is slope of the tangent to the initial straight-line portion of the load-deflection curve (N/mm).

2.6.1.3 Impact Test

Another popular method of testing (ASTM D256-92) the mechanical performance of polymers involves impact loading. Here, a specimen, often with a sharp notch cut in it, is struck a sudden blow, causing failure. Impact tests measure the energy required for failure when a standard specimen receives a rapid stress loading.

The impact strength of a polymer can be measured employing a number of techniques including Izod and Charpy tests. For both Izod and Charpy tests, a

weight is released, causing the specimens to be struck. The energy to break values are determined from the loss in the kinetic energy of the weight.

Impact tests are not limited to the basic Charpy and Izod methods. Special purpose tests, sometimes very highly instrumented, are used to characterize polymer blends and composites (Sperling, 1997).

### 2.6.2 Thermal Analysis

Thermal analysis represents a wide range of analytical techniques designed to assess the response of materials to thermal stimuli, typically temperature change. Various techniques evaluate changes in enthalpy, specific heat, thermal conductivity and diffusivity, linear and volumetric expansion, mechanical and viscoelastic properties with temperature.

#### 2.6.2.1 Differential Scanning Calorimetry

The differential scanning calorimeter (DSC) is the instrument that has dominated the field of thermal analysis in the past decade. The term DSC was coined in 1963 at Perkin-Elmer to describe a new thermal analyzer they had developed (Watson et al., 1964). It measures heat flows and temperatures associated with exothermic and endothermic transitions. The ease with which important properties such as transitions, heat capacity, reaction, and crystallization kinetics are characterized has made the DSC widely used in the plastics laboratory (Lobo and Bonilla, 2003).

In DSC analysis, two identical small sample pans are instrumented to operate at the same temperature and can be programmed up or down in temperature at the same rate. A sample is placed in one, and the other is left empty. Instrumentation is provided to measure the electrical power necessary to keep the two sample pans at the same temperature. If a temperature is encountered at which the sample undergoes a change of phase or state, more or less power will be needed to keep the sample pan at the same temperature as the reference pan (depending on whether the reaction is exothermic or endothermic).

Since power is the value being recorded, the area under the peak is the electrical equivalent of the heat of the reaction. To measure heat capacity in this

calorimeter, the sample pan and reference pan are first brought to some temperature and then heated at some constant rate. Since the reference pan is empty, it will require a smaller amount of electrical power to achieve this rate (Encyclopedia of Polymer Science and Technology, 1970).

Some advantages of the differential scanning calorimeter are that relatively short times are required to make a determination and that small sample size is sufficient. The disadvantage is that it is a comparative rather than an absolute method.

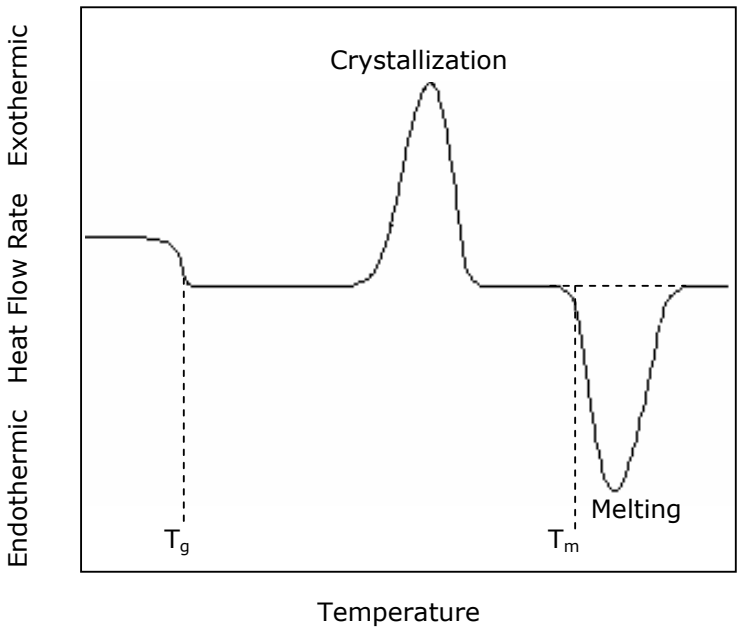


**Figure 2.4** Schematic DSC curve.

DSC is routinely used for investigation, selection, comparison, and end-use performance of materials. It is used in academic, industrial, and government research facilities, as well as quality control and production operations. Material properties measured include glass transitions, melting point, freezing point, boiling point, decomposition point, crystallization, phase changes, melting, crystallization, product stability, cure and cure kinetics, and oxidative stability.

At $T_g$, the heat capacity of the sample suddenly increases, requiring more power (relative to the reference) to maintain the temperatures the same. This differential heat flow to the sample (endothermic) causes a drop in the DSC curve (Figure 2.4). At $T_m$, the sample crystals want to melt at constant temperature, so a sudden input of large amounts of heat is required to keep the sample temperature even with the reference temperature. This results in the characteristic endothermic melting peak. Crystallization, in which large amounts of heat are given off at constant temperature, gives rise to a similar but exothermic peak. By measuring the net energy flow to or form the sample, heat capacities and heat of fusion can be determined (Rosen, 1993).

### 2.6.3 Melt Viscosity/Rheology Measurements

Some type of melt viscosity is included in the specification for almost every polymeric or plastic product. This is because viscosity is related to the molecular weight and to the performance of a polymer. Equipment used for rheological measurements range from the simple and ubiquitous melt flow indexer to the precise and quantitative capillary and cone-and-plate rheometers (Lobo and Bonilla, 2003).

#### 2.6.3.1 Melt Flow Index

The melt flow index test method is used to monitor the quality of plastic materials. The quality of the material is indicated in this test by melt flow rate through a specified die under prescribed conditions of temperature, load, and piston position in the barrel, as timed measurement is being made. The melt flow rate through a specified capillary die is inversely proportional to the melt viscosity of the material, if the melt flow rate is measured under constant load and temperature. The melt viscosity of the material or melt flow rate is related to the molecular weight of the material if the molecular structures are the same.

The extrusion plastometer as specified in ASTM D1238-79 is equipped with a piston rod assembly and weights, removable orifice of L/D=4/1, temperature controller and temperature readout, orifice drill, charging tool, and cylinder cleaning tool.

### 2.6.4 Morphological Analysis

In order for one to fundamentally understand and further improve the surface, interfacial, or thin-film properties of polymers, a complete morphological characterization of surface and interfacial regions is required. The importance of surface characterization is immediately apparent if one considers the influence of processing conditions on polymeric materials. For example, following the extrusion or molding of polymers, surface characterization commonly reveals the presence of a skin/core effect. Morphological and chemical composition differences occur in the surface region and can drastically influence the properties of the polymeric material for the chosen application (Chou et al., 1994).

#### 2.6.4.1 Scanning Electron Microscopy

Due to the great depth of focus, relatively simple image interpretation, and ease of sample preparation, SEM is the preferred technique for viewing specimen detail at a resolution well exceeding that of the light microscope. The SEM images vividly display the three-dimensional characteristics of the object surface under examination (Concise Encyclopedia of Polymer Science and Engineering, 1990).

Scanning electron microscope, although diffraction-limited, achieves its resolution by scanning a very finely focused beam of very short-wavelength electrons across a surface and by the detection of either the back-scattered or secondary electrons in a raster pattern in order to build up an image on a television monitor (Kirk and Othmer, 1995).

SEM sample preparation is relatively easy and usually involves only mounting on a specimen-stub; however, for nonconducting specimens a conductive coating is applied to the surface to prevent charging. This coating process is acceptable provided the coating does not cover the morphological features of interest. Unfortunately, the electron beam can damage the polymer specimen. Types of beam damage include cross-linking and dimensional shrinkage, loss of crystallinity, or, in certain radiation-sensitive polymers such as electron beam resists, chain scission and mass loss (Grubb, 1974).

### 2.6.5 X-Ray Diffraction

The method of X-ray diffraction and scattering is one of the oldest and most widely used techniques available for the study of polymer structures. A beam of X-rays incident to a material is partly absorbed and partly scattered, and the rest is transmitted unmodified. The scattering of X-rays occurs as a result of interaction with electrons in the material. The X-rays scattered from different electrons interfere with each other and produce a diffraction pattern that varies with scattering angle. The variation of the scattered and diffracted intensity with angle provides information on the electron density distribution, and hence the atomic positions, within the material.

The word diffraction is generally preferred when the specimen under study has regularity in its structure so that the detected X-rays exhibit well-defined intensity maxima. Other scattering techniques are also employed in the study of polymers, i.e., the scattering of light, neutrons, and electrons. The basic principles governing the scattering and diffraction of these different types of electromagnetic waves and particles are very similar. The differences in the wavelength and the mode of interaction with matter, however, make one radiation more suitable than another for studying some particular aspects of polymer structure.

X-ray scattering (or diffraction) techniques are usually categorized into wide-angle X-ray scattering (WAXS) and small-angle X-ray scattering (SAXS). In the former, the desired information on the polymer structure is contained in the intensities at large scattering angles and, in the latter, at small scattering angles. In general terms, WAXS is used to obtain structural information on a scale of 1 nm or smaller, and SAXS on a scale of 1-1000 nm (Concise Encyclopedia of Polymer Science and Engineering, 1990).

#### 2.6.5.1 Principles of X-Ray Scattering and Diffraction

In the spectrum of electromagnetic radiation, X-rays lie between the ultraviolet rays and gamma rays. Those X-rays used for structure analysis have wavelengths $\lambda$ in the range of 0.05-0.25 nm. Most work on polymers is done with the Cu K$\alpha$ emission line, a doublet with an average wavelength equal to 0.154 nm. In view of the wave-particle duality, it is in some cases useful to

consider X-rays to consist of photons of energy $h\nu$ , where h is Plank's constant and the frequency $\nu$ is given by $c/\lambda$ (c= velocity of light). Thus, the Cu K$\alpha$ line consists of photons of energy 8.04 keV. A high intensity x-ray beam is one with a high flux of photons (Concise Encyclopedia of Polymer Science and Engineering, 1990).

Normally the sample is irradiated with a collimated beam of X-rays, and the intensity of the scattered X-rays is measured as a function of scattering direction. The scattering angle, that is, the direction of the scattered beam in relation to the incident beam, is customarily denoted by 2θ.

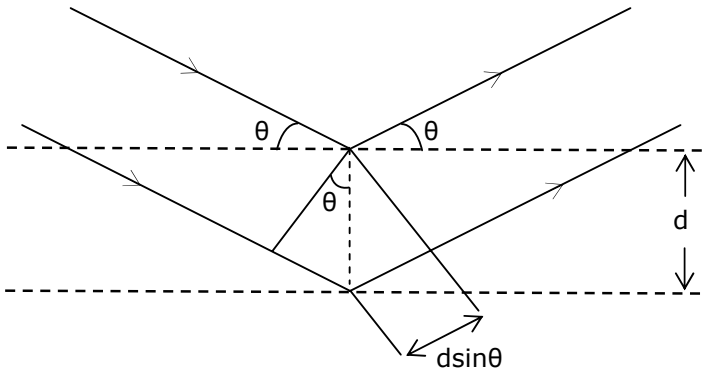


**Figure 2.5** Diffraction of x rays by planes of atoms (Callister, 1997).

The incident X-ray wave is reflected specularly (mirror-like) as it leaves the crystal planes, but most of the wave energy continues through to subsequent planes where additional reflected waves are produced. Then, as shown in Figure 2.5 where the plane spacing is denoted d, the path length difference for waves reflected from successive planes is 2d sinθ. Note that the scattering angle (the angle between the original and outgoing rays) is 2θ.

Constructive interference of the reflected waves occurs when this distance is an integral of the wavelength. The Bragg condition for the angles of the diffraction peaks is thus:

$$n\lambda = 2d\sin\theta \quad (2.7)$$

where n is an integer called the order of diffraction.

## 2.7 Poly(ethylene terephthalate)

Poly(ethylene terephthalate), or PET, is a typical member of the polyester family composed of repeated units of (-$CH_2CH_2$-OOC-$C_6H_4$-COO-) containing a phenyl group ($C_6H_4$). First synthesized in the early 1940s (Billmeyer, 1984), PET was initially recognized as a semicrystalline melt-spun fiber. Soon afterwards biaxial films of PET were developed. The structure of PET is illustrated in Figure 2.6. PET is widely used as an engineering thermoplastic for packaging, electronics, and other applications. Worldwide production of PET has expanded enormously: production now reaches several million metric tons annually.

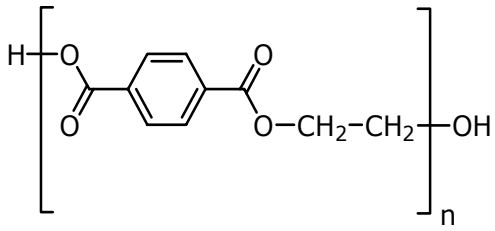


**Figure 2.6** Chemical structure of PET.

### 2.7.1 Chemistry

PET is a polycondensation polymer that is most commonly produced from a reaction of ethylene glycol (EG) with either purified terephthalic acid (PTA) or dimethyl terephthalate (DMT), using a continuous melt-phase polymerization process. In many cases, melt-phase polymerization is followed by solid-state polymerization. Melt-phase polycondensation is used to prepare fiber-grade PET or a precursor resin which is then solid-state polymerized to achieve higher molecular weight or intrinsic viscosity. Melt polymerization is usually carried out at around 285°C. Due to increased rate of thermal degradation of PET by further increase in temperature or time of polymerization, final intrinsic viscosity (IV) is usually kept below 0.6 (Polymeric Materials Encyclopedia, 1996).

2.7.1.1 Melt-Phase Polycondensation

PET can be prepared by direct esterification of terephthalic acid and ethylene glycol or transesterification of dimethyl terephthalate with ethylene glycol. In both cases, starting materials are petroleum derivatives. One basic feedstock for PET is ethane, which is converted to ethylene oxide and finally to ethylene glycol (EG). Another important feedstock is para-xylene, which is oxidized to yield terephthalic acid (TPA). Terephthalic acid is purified by reaction with methanol to form dimethyl terephthalate (DMT). Synthesis from DMT follows the scheme given in Figure 2.7.

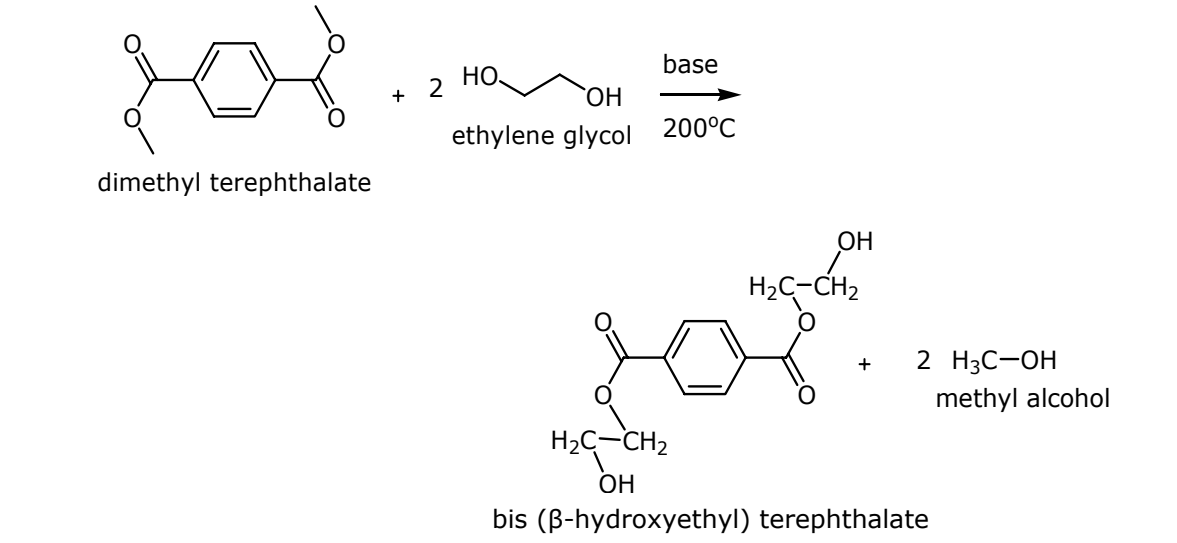


**Figure 2.7** Synthesis of PET with the transesterification reaction of DMT and EG.

During synthesis of PET, DMT and excess EG are first heated to 200°C in the presence of a basic catalyst. Distillation of the mixture results in the loss of methanol (bp, 64.7°C) and the formation of a new ester called bis (β-hydroxyethyl) terephthalate (BHET). When BHET is heated to a higher temperature (~280°C), ethylene glycol (bp, 198°C) distills and polymerization (second transesterification) takes place (Solomons, 1996).

BHET acts as the monomer for polymerization to yield PET. The transesterification reaction of BHET to produce PET and EG is carried out at a temperature well above the boiling point of ethylene glycol and above the melting point of the polymer. In both types of melt-polymerization processes, the highest molecular weight attainable is limited by two factors: high viscosity of the melt, which makes removal of ethylene glycol difficult, and traces of EG, BHET, and oligomers present at equilibrium due to the rapid reversible nature of the transesterification reaction (Polymeric Materials Encyclopedia, 1996).

Commercial synthesis of PET does not lead entirely to a pure linear poly (ethylene terephthalate) structure. The bulk polymer made by the melt-phase process contains small amounts of cyclic ethylene terephthalate such as trimers, tetramers, and pentamers (Kirk and Othmer, 1995). More detailed information about the chemistry of PET preparation, kinetics of melt-phase polycondensation, and manufacturing processes can be found in many sources.

### 2.7.2 Morphology

Poly(ethylene terephthalate) is a crystallizable polymer whose morphology can vary widely depending on the fabrication process. The polymer can be obtained as a glassy or amorphous transparent solid by rapidly quenching the melt below the glass transition temperature $T_g$. Amorphous PET is of little commercial significance because it has low mechanical properties, high gas permeation rates, and low dimensional stability. The properties of a polymer depend on its structural arrangement and are closely related to the internal morphological structure of the polymer. When PET is heated above its $T_g$, it crystallizes rapidly, forming an opaque material exhibiting spherulitic superstructures. This morphology can also be obtained by slow cooling of the polymer melt.

### 2.7.3 Degradation

Poly(ethylene terephthalate) like other polyesters can experience various degradation processes such as thermal degradation under the influence of heat alone, oxidative degradation upon heating in the presence of atmospheric oxygen, hydrolytic degradation in the presence of moisture, photo-oxidative degradation under the influence of light and oxygen, radiochemical degradation under the influence of ionizing radiation, and chemical degradation in the presence of various reagents (Polymeric Materials Encyclopedia, 1996).

In hydrolytic degradation, the chemical reaction of PET with water at elevated temperatures leads to a reduction in molecular weight and the formation of carboxyl and hydroxyl end groups. The amount of hydrolytic degradation in the melt is larger when the material has previously been dried in an air atmosphere rather than in a vacuum or inert environment.

Thermal-oxidative degradation of PET causes a more severe reduction of molecular weight and increase in the formation of gaseous products than purely thermal degradation. When we melt PET in the presence of air, degradation increases rapidly with increasing temperature.

The rate of degradation increases in the following order as a result of melting and drying conditions: vacuum drying-nitrogen melting, air drying-nitrogen melting, vacuum drying-air melting, and air drying-air melting (highest degradation). In this study, vacuum drying was applied on PET prior to melt compounding; however PET was melted in an air rather than in a nitrogen environment.

The degradation processes of PET can be controlled by physical factors such as processing temperatures, residence time in the melt, drying temperature and time, melt and drying environments, and moisture content, and chemical factors such as molecular weight or intrinsic viscosity and polymerization conditions.

## 2.8 Literature Survey on Poly(ethylene terephthalate)

The literature is replete with studies on both impact modifications of PET and PET-clay nanocomposites. In this study, we have focused on impact modified PET-organoclay nanocomposites. However, to the best of our knowledge, no study on the impact modified PET/clay nanocomposites has been reported. Previous studies on impact modification of PET and PET-clay nanocomposites are summarized in the following sections.

### 2.8.1 Impact Modification of PET

Loyens et al. (2002b) evaluated various modifiers with and without functional groups for ultimate mechanical properties of rubber modified semicrystalline PET. The most toughening route for PET was provided by dispersing a preblend of ethylene-co-propylene rubber (EPR) and a low amount of ethylene-glycidyl methacrylate copolymers (E-GMAx) (x; percent of GMA by weight). They stated that the ternary PET/ (EPR/E-GMA8) blends displayed highly increased impact strengths and reasonable elongation at break.

From the earlier results of Loyens and his coworkers (2002a), it is known that very effective compatibilization of PET/elastomer blends is obtained in the presence of glycidyl methacrylate functional groups. In addition, Hert et al. (1992) used several GMA holding co- and terpolymers to improve the impact toughness of PET.

Xanthos et al. prepared a review in 1991 about the use of suitably functionalized blend constituents. They presented that the compatibilization reaction of PET and ethylene-acrylic ester-GMA terpolymer occurred between epoxy group of the terpolymer with carboxyl group of PET.

Chapleau et al. (2003) investigated the mechanical performance of PET containing different polyolefin-based copolymers used as impact modifiers. The addition of the modifiers containing GMA resulted in a decrease of the tensile modulus and tensile strength, whereas the elongation at break and toughness were generally increased compared to pure PET.

The addition of GMA grafted polyolefins has also been showed to be useful for the reactive compatibilization of blends of polyolefins with PET (Kalfoglou et

al., 1995). Kalfoglou and his coworkers reported that in such blends, a polyolefin-polyester graft copolymer was generated in situ by a reaction involving the grafted epoxy moieties and the carboxyl/hydroxyl polyester end groups.

### 2.8.2 PET/Clay Nanocomposites

Davis et al. (2002) studied poly(ethylene terephthalate)/montmorillonite nanocomposites compounded via melt-blending in a corotating mini twin-screw extruder. They found that nanocomposites compounded with 1, 2-dimethyl-3-N-hexadecyl imidazolium treated MMT showed high levels of dispersion and delamination. They also examined that alternative mixing conditions, longer residence times, and higher screw speeds resulted in lower quality nanocomposites.

Ke at al. (1999) dispersed organically modified montmorillonite in PET by in-situ polymerization. Complete delamination was not achieved, but the tensile modulus of the nanocomposites increased as much as 3 times over that of pure PET.

Tsai et al. (2000) reported nanocomposites of PET and clay by utilizing an amphoteric surfactant and an antimony acetate catalyst. Their nanocomposites showed higher flexural strength and modulus than pure PET with 3 wt. % loading of the silicate.

Imai et al. (2002) developed a new compatibilizer suitable for the PET-expandable fluorine mica nanocomposites prepared by in-situ polymerization. This new compatibilizer connected PET through covalent bonds and mica through ionic bonds. They demonstrated that the employment of the compatibilizer provided nanocomposites with a high modulus.

# CHAPTER 3

# EXPERIMENTAL

## 3.1 Materials

### 3.1.1 Polymer Matrix

Poly(ethylene terephthalate) was purchased from Sasa Company, Adana, Turkey. PET pellets were in the amorphous form and, thus, the pellets were transparent. Typical properties of APET obtained from the producer are listed in Table 3.1.

**Table 3.1** Typical properties of APET.

| | |
|---|---|
| Intrinsic viscosity (23°C) | 0.57 dl/g |
| $T_g$ | 78°C |
| $T_m$ | 255°C |

### 3.1.2 Layered Silicate

Cloisite 25A, a natural montmorillonite modified with a quaternary ammonium salt, was purchased from Southern Clay Products. Figure 3.1 shows the chemical structure of the quaternary ammonium and its anion, methyl sulfate.

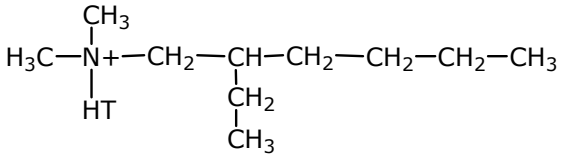

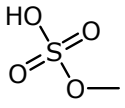

**Figure 3.1** Chemical structures of the quaternary ammonium and the anion; methyl sulfate.

The organophilic clay is prepared via ion exchange reaction between $Na^+$ montmorillonite and a quaternary ammonium salt by the manufacturer. Physical Data of Cloisite 25A are given in Table 3.2.

**Table 3.2** Physical data of Cloisite 25A.

| Clay | d Spacing (Å) | Surface Modification* | Surface Charge (meq/100 g) |
|---|---|---|---|
| C25A | 18.6 | 2MHTL8 | 95 |

* HT = hydrogenated tallow (~65% C18; ~30% C16; ~5% C14),
2M = dimethyl, L8 = 2-ethylhexyl.

3.1.3 Impact Modifier

Lotader GMA AX8900, ethylene-methyl acrylate-glycidyl methacrylate (E-MA-GMA) terpolymer used in this study, was purchased from Atofina Chemicals. Specifications of the terpolymer provided by the manufacturer are given in Table 3.3.

**Table 3.3** Specifications of E-MA-GMA.

| | |
|---|---|
| MFI (190°C / 2.16 kg) | 6 g/10 min |
| Density (23°C) | 0.95 g/cm$^3$ |
| GMA content | 8 wt. % |
| $T_m$ | 65°C |
| Young's modulus | 8 MPa |
| Tensile strength at break | 4 MPa |
| Elongation at break | 1100% |

Lotader GMA AX8900 resin is an impact modifier for extrusion or blow molding grades of polyesters. Figure 3.2 shows its chemical structure.

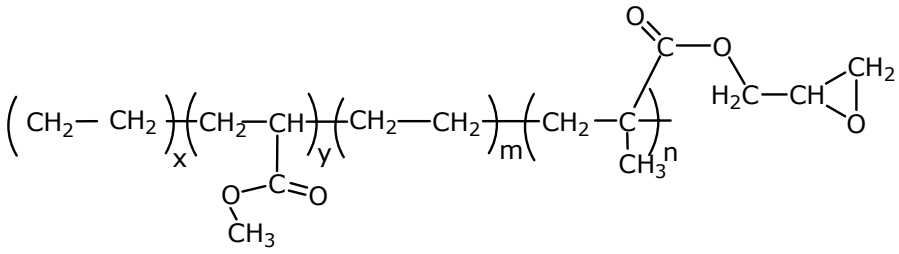

**Figure 3.2** Chemical structure of Lotader GMA AX8900.

The epoxy functionality of GMA reacts with the carboxyl end groups of PET in the melt phase to form a graft copolymer. For this reason, Lotader GMA AX8900 may also be called as a functionalized polymer used as a compatibilizer.

## 3.2 Equipment and Processing

### 3.2.1 Melt Compounding

In this study, Thermoprism TSE 16 TC twin screw extruder was used for the preparation of all the formulations. The type of this extruder is: 16 mm co-rotating, fully intermeshing screws with barrel length of 384 mm. The temperatures of barrel and die were set and the extruder was allowed to stabilize prior to performing any compounding trials. Processing temperatures of mixing zones and die on the twin screw extruder are given in Figure 3.3.

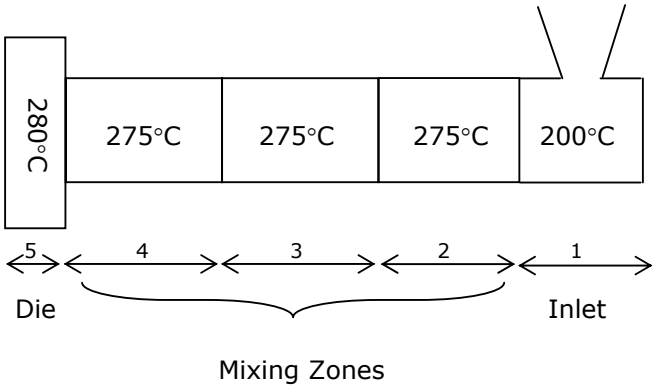


**Figure 3.3** Processing temperatures of inlet, die, and mixing zones.

Temperatures were adjusted using the temperature controllers on the control panel. The screw speed was constant at 350 rpm throughout the experiments. Figure 3.4 shows the experimental set-up for melt compounding of all formulations represented in Table 3.5.

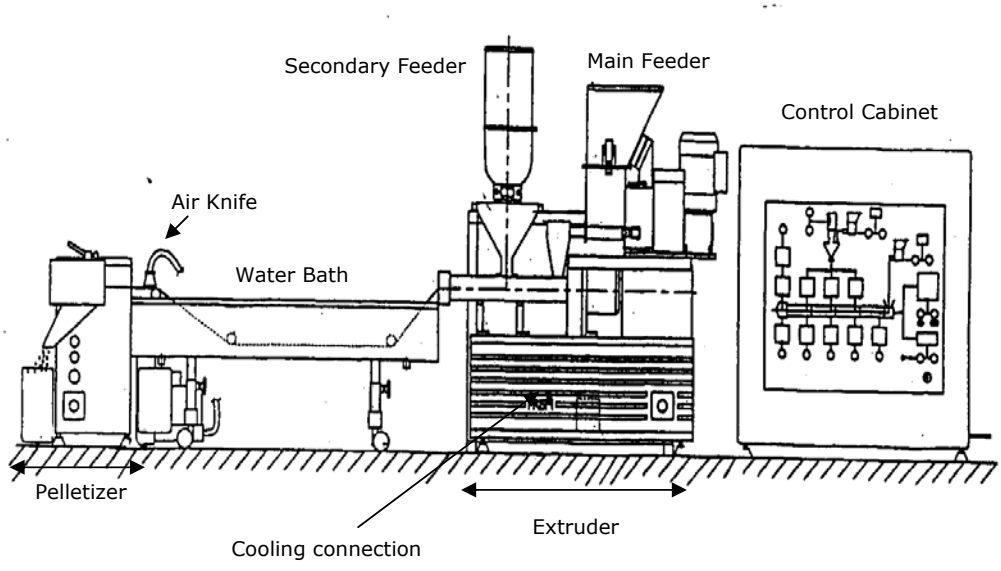


**Figure 3.4** Experimental setup for melt compounding.

Main and secondary feeders illustrated in Figure 3.4 are calibrated before starting to extrusion. Third feeder called vertical force feeder was removed from the illustration for clarity. During melt compounding, the molten product coming out through the die is passed through a water bath fed with cold water. An air knife is attached on the other end of the water bath to remove any excess water from the solidified product. The cooled product is then fed into the pelletizer. The pellets obtained from the pelletizer are packed in plastic bags either to use in a subsequent run or to have them injection molded.

The presence of even small traces of moisture can cause significant hydrolytic degradation of materials. Thus APET, organically modified clay, and the impact modifier used in this study were dried under vacuum, prior to compounding. Table 3.4 shows the drying temperature and time for all the materials.

**Table 3.4** Drying temperature and time for the materials used in the study.

| Material | Drying Temperature, °C | Drying Time, hr. |
|---|---|---|
| APET | 120 | 15 |
| Organoclay | 120 | 15 |
| Impact Modifier | 40 | 12 |

3.2.1.1 Addition Order of the Components

In this study, one of the process parameters was the addition order of the components. The following addition orders were investigated: P, I and C stand for PET, Impact Modifier (Lotader), and Clay respectively.

Sequence 1 (CI-P)

Run 1 Lotader pellets were fed to the extruder from the main feeder. Organoclay particles were added to the molten stream at the second feed port.
Run 2 PET pellets were fed to the system from the main feeder. Pellets of precompounded (Lotader and organoclay) (run 1) inside the second feeder were added to the molten stream at the second feed port (Figure 3.5).

In the first run of the Sequence 1 (CI-P), temperatures were adjusted based on the processing temperature of Lotader. Thus, the barrel temperature profile was 170-190-190-190-200°C. In addition, CI-P with 5 wt. % clay content could not be processed due to problems associated with the high clay loading in the first run.

Sequence 2 (PC-I)

Run 1 PET pellets were fed to the extruder from the main feeder. Organoclay particles inside the second feeder were added to the molten PET at the second feed port.
Run 2 Pellets of precompounded PET and organoclay (run 1) were added to the system from the main feeder. Pellets of Lotader inside the second feeder were fed to the system at the main feed port (Figure 3.6).

Sequence 3 (PI-C)

Run 1 Pellets of Lotader GMA AX8900 and pellets of PET were dry blended and added to the extruder from the main feeder.
Run 2 Pellets of precompounded (run 1) PET and Lotader were fed to the system from the main feeder. Particles of organoclay inside the second feeder were fed to the melt stream at the second feed port (Figure 3.7).

Sequence 4 (All-S) simultaneous feeding

Run 1 Pellets of dry blended (PET and Lotader) inside the main feeder and organoclay particles inside the second feeder were fed to the extruder simultaneously from the main feed port.
Run 2 Pellets of precompounded three components (run 1) were fed to the extruder from the main feeder (Figure 3.8).

Beyond the ternary nanocomposites prepared by different addition orders explained above; binary PET/clay nanocomposites designated as PC in Table 3.5 were also melt blended to be able to compare the effects of impact modifier which was added as the third component in the nanocomposites. All one-step mixing formulations were converted into two-step mixing ones via extruding the product once more. This was done to make the results comparable with each other.

**Table 3.5** Formulation table.

| | Concentration (wt. %) | | |
|---|---|---|---|
| Group name | APET | Organoclay | Impact Modifier |
| P | 100 | - | - |
| PI | 95 | - | 5 |
| PI | 90 | - | 10 |
| PI | 85 | - | 15 |
| PI | 80 | - | 20 |
| PC | 99 | 1 | - |
| PC | 97 | 3 | - |
| PC | 95 | 5 | - |
| PC-I | 94 | 1 | 5 |
| PC-I | 92 | 3 | 5 |
| PC-I | 90 | 5 | 5 |
| PI-C | 94 | 1 | 5 |
| PI-C | 92 | 3 | 5 |
| PI-C | 90 | 5 | 5 |
| CI-P | 94 | 1 | 5 |
| CI-P | 92 | 3 | 5 |
| All-S | 94 | 1 | 5 |
| All-S | 92 | 3 | 5 |
| All-S | 90 | 5 | 5 |

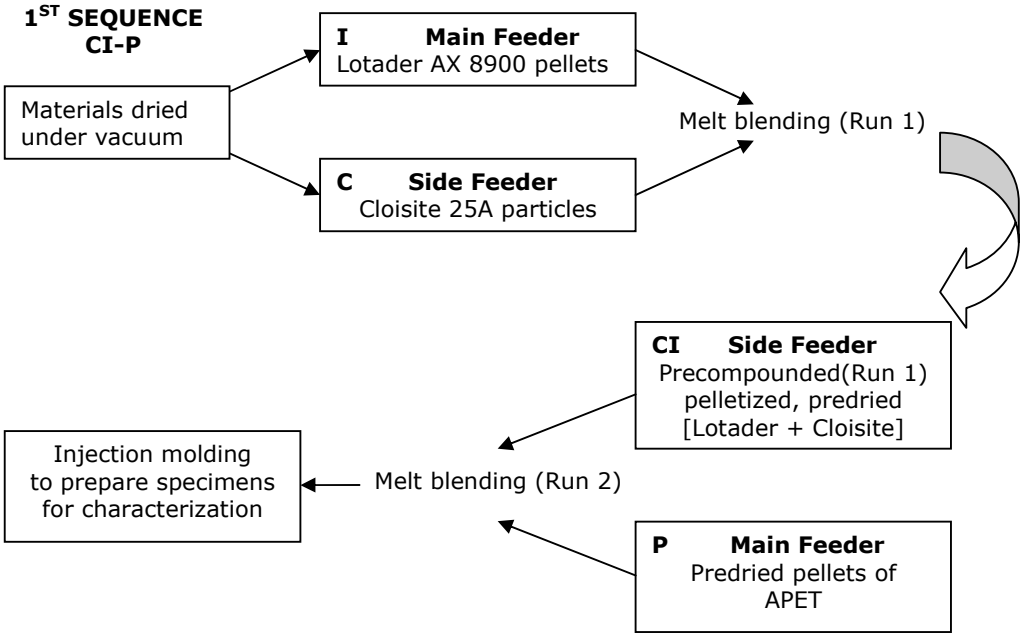


**Figure 3.5** Flowchart of (CI-P) two-step melt compounding procedure.

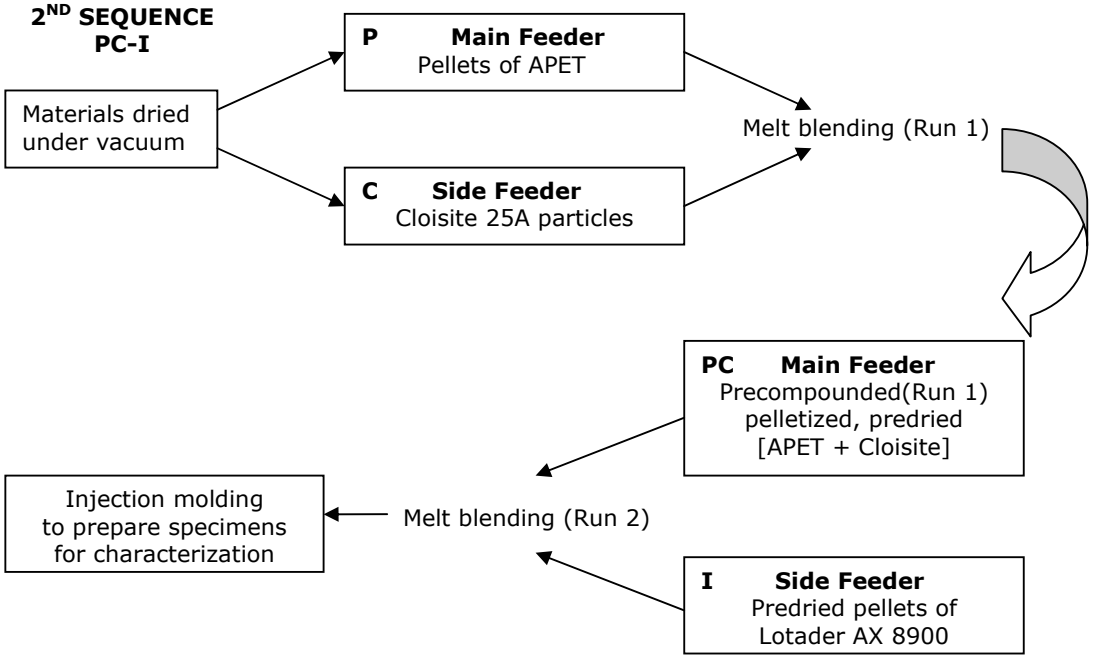


**Figure 3.6** Flowchart of (PC-I) two-step melt compounding procedure.

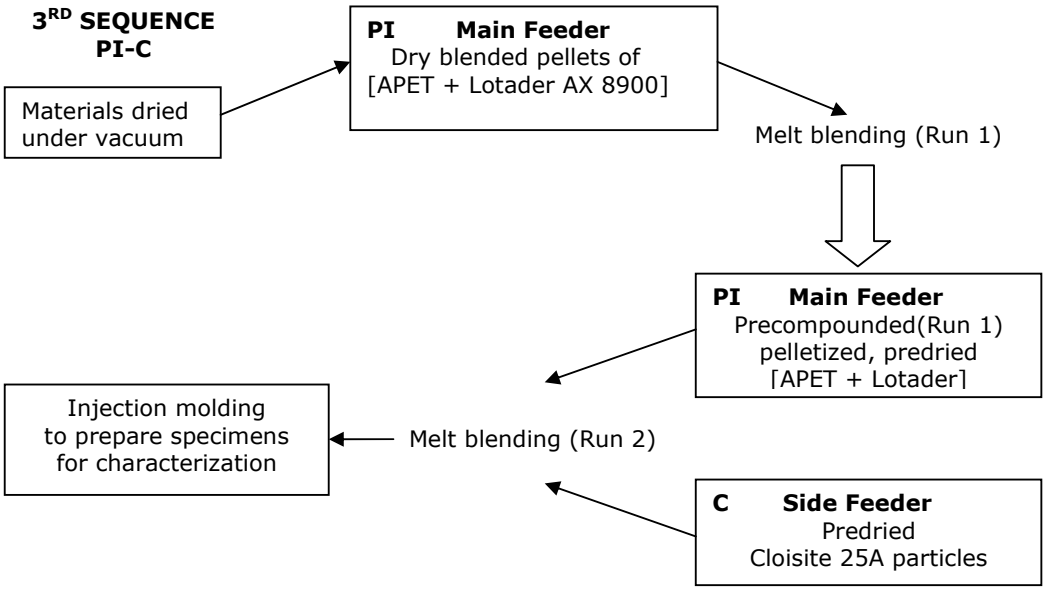


**Figure 3.7** Flowchart of (PI-C) two-step melt compounding procedure.

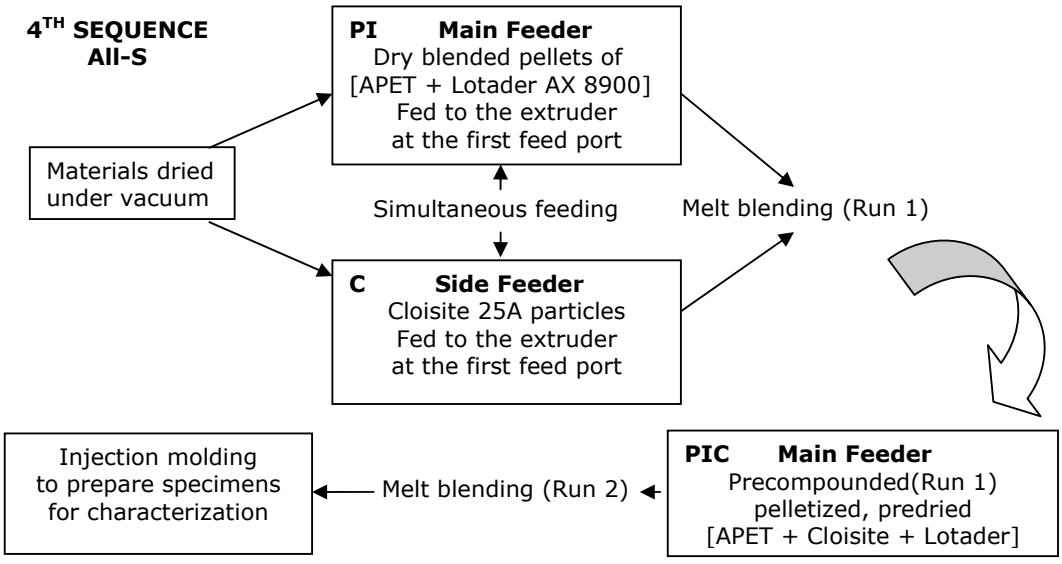


**Figure 3.8** Flowchart of (All-S) two-step melt compounding procedure.

### 3.2.2 Injection Molding

A laboratory scale injection molding machine shown in Figure 3.9 (Microinjector, Daca Instruments) was used to mold the specimens of all melt compounded formulations. All the compounded formulations, in pellet form, were dried before injection molding, for 12-15 hours at 120 °C. Molding parameters given in Table 3.6 were kept constant throughout the molding process.

Water was used as a coolant for the mold temperature controller, which was connected to the mold in order to maintain a constant and specific mold temperature.

**Table 3.6** Molding parameters for all formulations.

| Molding parameters | Unit | Value |
|---|---|---|
| Nozzle temperature | °C | 275 |
| Mold temperature | °C | 18 |
| Fill time | sec | 30 |
| Hold time | min | 1 |
| Injection speed | - | Fast |
| Injection pressure | bar | 8 |

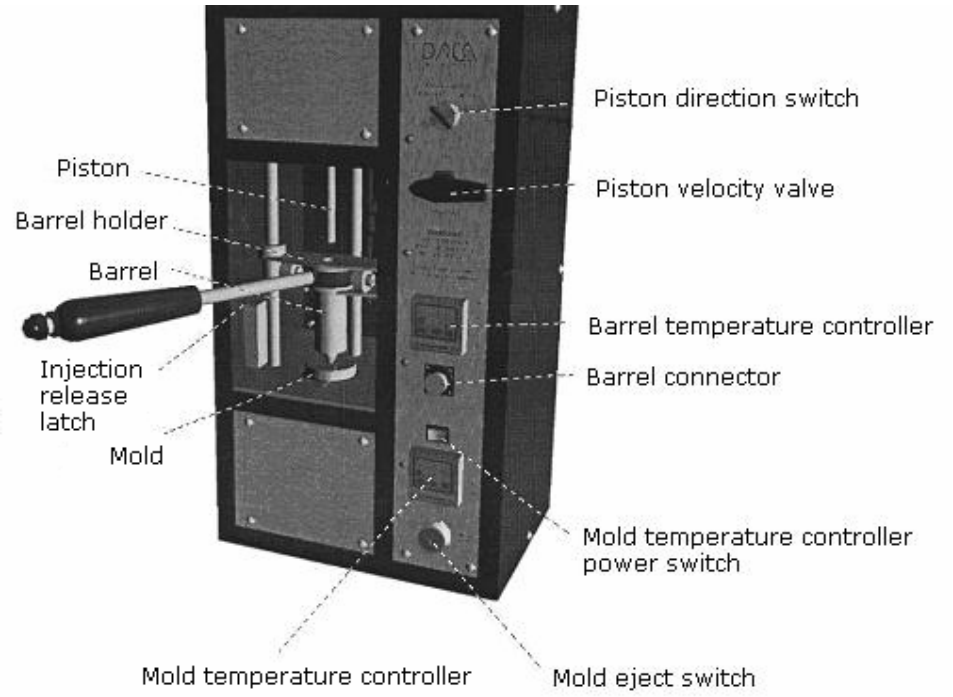


**Figure 3.9** Injection molding machine.

### 3.3 Characterization

3.3.1 Mechanical Testing Procedure and Equipment

Mechanical tests were performed in the standard laboratory atmosphere. At least seven specimens were tested for each formulation. For each series of tests, the arithmetic mean of all values obtained was calculated and reported as the average value for the particular property in question. Standard deviation was also calculated according to American Society for Testing and Materials (ASTM) standards.

Mechanical tests included the investigation of tensile strength, tensile stress at yield, Young's modulus, percent strain at break, flexural modulus, flexural strength and impact strength.

3.3.1.1 Tensile Test

A Lloyd 30K universal testing machine was used to conduct tensile testing of molded samples for all the formulations. The test was performed conforming to ASTM D638M-91a. During the test, the specimen was placed in the grips of the testing machine, taking care that it was properly alligned and the grips were tightened evenly and firmly enough to prevent the slippage of the specimen while testing but not to the point where the specimen would be crushed.

The crosshead speed of the machine was set at the rate of 8mm/min, which was calculated considering the specimen gauge length of 80 mm and strain rate of 0.1 $min^{-1}$. The specimen was pulled at this constant rate of extension until the center of the specimen fails. Tensile extension was recorded as a function of the stress required to stretch the sample to failure.

Typical ASTM tensile test specimen and its dimensions are given in Figure 3.10 and Table 3.7 respectively.

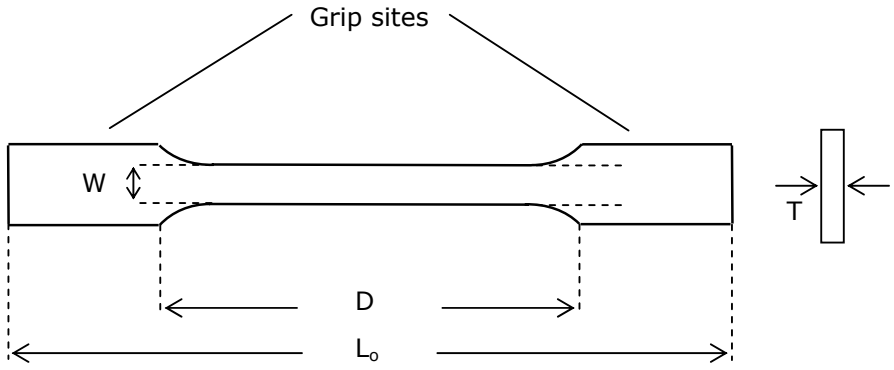


**Figure 3.10** Typical ASTM tensile test specimen.

**Table 3.7** Specifications of injection molded specimen.

| Symbol, Term | Dimensions (mm) |
|---|---|
| D- Distance between Grips | 80 |
| $L_0$ - Length Overall | 112 |
| T- Thickness | 2.10 |
| W- Width of Narrow Section | 7.50 |

3.3.1.2 Flexural Test

In flexural test, three-point loading system was used based on test method-I procedure of ASTM D790M-92. Three-point loading diagram is illustrated in Figure 3.11.

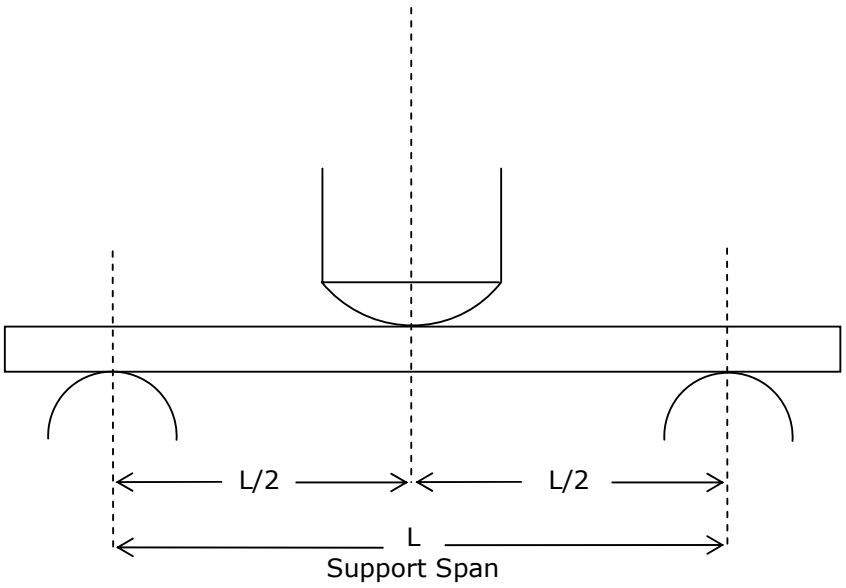


**Figure 3.11** Three-point loading diagram.

The support span was taken as 50 mm throughout the testing of all specimens and the rate of crosshead motion was calculated as 2.08 mm/min according to ASTM standards. For this value of crosshead motion, corresponding strain rate was 0.01 $min^{-1}$.

3.3.1.3 Impact Test

Charpy impact tests were carried out by using a Pendulum Impact Tester of Coesfeld Material Test, based on Test Method-I Procedure A in ASTM D256-91a. Unnotched samples having the same geometry as the tensile specimens given in Table 3.7 were used for impact test. During the test, the specimen was supported at both ends and the striker hit the specimen as shown in Figure 3.12.

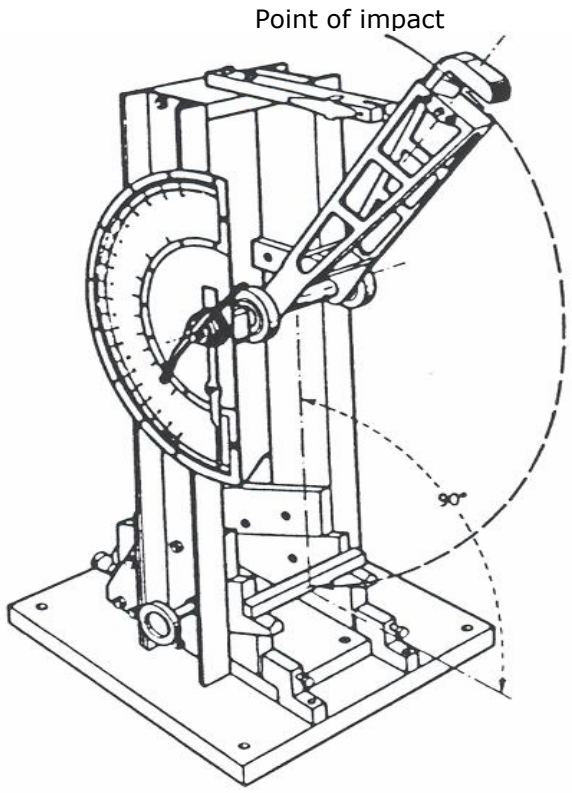


**Figure 3.12** Charpy-type impact instrument.

### 3.3.2 Differential Scanning Calorimetry (DSC) Analysis

Differential scanning calorimetry (DSC) measurements were carried out with a General V4.1.C DuPont 2000 in order to evaluate the possible changes in melting ($T_m$) and glass transition ($T_g$) temperatures due to the presence of impact modifier and organoclay in APET. The effects of different addition orders of the materials during melt compounding were also investigated utilizing thermal properties.

In DSC analysis, 10 mg of sample was cut from the center of an injection molded specimen and was heated from room temperature to 280°C at a rate of 20°C/min. The samples were scanned under nitrogen atmosphere.

### 3.3.3 Scanning Electron Microscopy (SEM) Analysis

Scanning electron microscopy (SEM) analysis was performed by a JEOL JSM-6400 low voltage scanning electron microscope. The analysis was conducted on fracture surfaces of impact specimens. A sample which was not fractured by impact loading was fractured under liquid nitrogen. In all cases, the fractured surfaces were gold-coated and mounted on brass stages prior to viewing with the scanning electron microscope. SEM images were examined in order to investigate the effect of impact modifier and organoclay on the morphology of PET matrix. The SEM photographs were taken at x250 and x3500 magnifications.

### 3.3.4 X-Ray Diffraction Analysis

X-ray diffraction patterns for the composites containing organoclay were collected on an X-ray diffractometer (Philips, PW-3710). Cu Kα ($\lambda = 1.54$ Å) radiation, generated at a voltage of 40 kV and current of 55 mA, was used as an X-ray source. Diffraction angle 2θ was scanned from 1° to 10° at a scanning rate of 3°/min and a step size of 0.02°.

### 3.3.5 Melt Flow Index (MFI)

Melt flow index (MFI) measurements were carried out according to ASTM D1238-79 using Omega Melt Flow Indexer. Conditions of temperature and load were selected as 260°C and 2.16 kg respectively, which were in accordance with material specifications. This method is based on determining the melt index, defined as the mass flow rate of polymer through a specified capillary. Mass flow rate is expressed as grams per 10 min. Since melt flow index values are inversely related to the melt viscosity, changes in viscosity values were evaluated for each formulation.

# CHAPTER 4

# RESULTS AND DISCUSSION

## 4.1 Morphological Analysis

### 4.1.1 X-Ray Diffraction Analysis

X-ray diffraction (XRD) analysis was performed to characterize the layered structures of the nanocomposites. By monitoring the position, shape, and intensity of the basal reflections from the silicate layers, intercalated or exfoliated structure can be identified (Vaia et al., 1996).

In the case of intercalation, polymer chains are inserted between galleries of the clay, and the d-spacing between the galleries is increased. On the other hand, in the case of exfoliation, these individual silicate layers are distributed randomly in a continuous polymer matrix. Consequently, characterizing the formation of a nanocomposite requires measurement of the d-spacing by X-ray diffraction analysis. In Table 4.1, the d-spacing and 2theta values of all compositions are given.

**Table 4.1** X-ray diffraction results of materials containing clay.

| | Peak-1 | Peak-1 | Peak-2 | Peak-2 |
|---|---|---|---|---|
| **Cloisite 25A** | **d-spacing (Å)** | **2theta (deg)** | **d-spacing (Å)** | **2theta (deg)** |
| | 17.94 | 4.92 | **-** | **-** |
| **PC** | | | | |
| **Clay(wt.%)** | **d-spacing (Å)** | **2theta (deg)** | **d-spacing (Å)** | **2theta (deg)** |
| 1 | 30.44 | 2.90 | 15.74 | 5.61 |
| 3 | 31.36 | 2.82 | 15.53 | 5.69 |
| 5 | 33.44 | 2.64 | 16.14 | 5.47 |
| **CI-P** | | | | |
| **Clay(wt.%)** | **d-spacing (Å)** | **2theta (deg)** | **d-spacing (Å)** | **2theta (deg)** |
| 1 | - | - | - | - |
| 3 | - | - | - | - |
| **PC-I** | | | | |
| **Clay(wt.%)** | **d-spacing (Å)** | **2theta (deg)** | **d-spacing (Å)** | **2theta (deg)** |
| 1 | 32.39 | 2.73 | 15.47 | 5.71 |
| 3 | 32.46 | 2.72 | 15.57 | 5.67 |
| 5 | 32.10 | 2.75 | 15.94 | 5.54 |
| **PI-C** | | | | |
| **Clay(wt.%)** | **d-spacing (Å)** | **2theta (deg)** | **d-spacing (Å)** | **2theta (deg)** |
| 1 | - | - | - | - |
| 3 | - | - | - | - |
| 5 | 35.81 | 2.47 | 15.16 | 5.83 |
| **All-S** | | | | |
| **Clay(wt.%)** | **d-spacing (Å)** | **2theta (deg)** | **d-spacing (Å)** | **2theta (deg)** |
| 1 | - | - | - | |
| 3 | 33.69 | 2.62 | 16.88 | 5.23 |
| 5 | 34.35 | 2.57 | 16.47 | 5.36 |

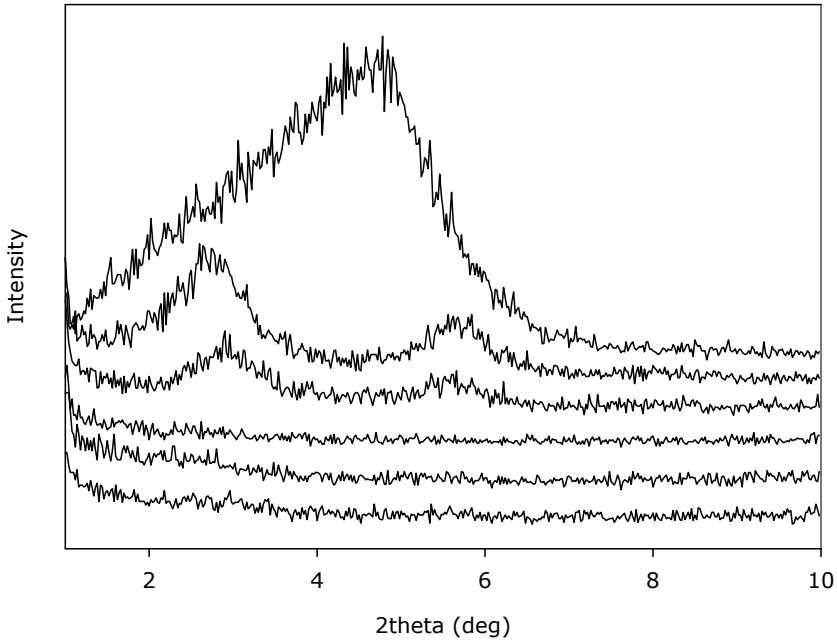


**Figure 4.1** X-ray diffraction patterns of nanocomposites containing 1 wt. % clay. (From top to bottom: C25A, PC-I, PC, All-S, CI-P, and PI-C). The diffraction pattern of C25A is included for comparison.

Figure 4.1 shows XRD patterns of nanocomposites with 1 wt. % clay (Cloisite 25A) loading. The y-axis is shifted for clarity. The d-spacing indicates the interlayer spacing of the silicate layers, which is calculated from the peak position using Bragg's equation. As it is seen in this figure, Cloisite 25A has this peak at 2θ of 4.92°, which corresponds to a d-spacing of 17.94 Å. For PI-C, CI-P, and All-S sequences with 1 wt. % clay content, no peak is detected by XRD, which suggests that they have an exfoliated structure.

In Figure 4.1, the d-spacing is increased from 17.94 Å for pure Cloisite 25A to 32.39 Å for PC-I containing 1 wt. % clay. Whereas, the d-spacing of 30.44 Å for PC containing 1 wt. % clay is relatively smaller than that of the nanocomposite having impact modifier as a third component. This indicates that the presence of impact modifier has an effect on the dispersion of the silicate layers in the polymer matrix.

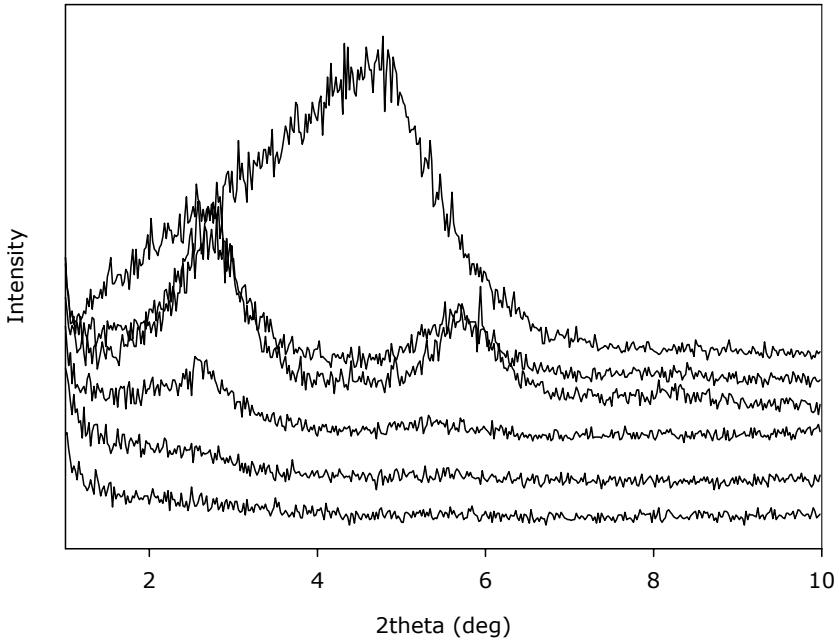


**Figure 4.2** X-ray diffraction patterns of nanocomposites containing 3 wt. % clay. (From top to bottom: C25A, PC-I, PC, All-S, CI-P, and PI-C).

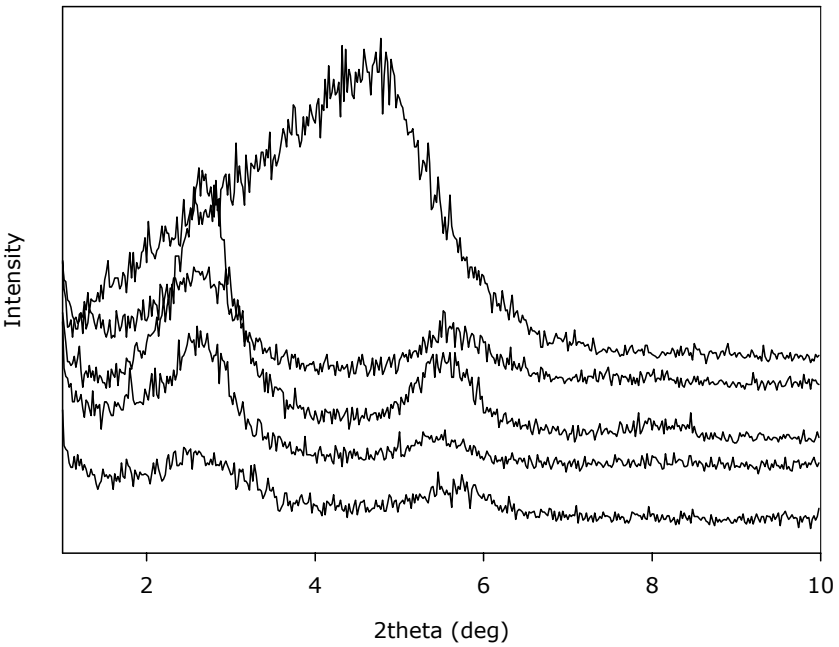


**Figure 4.3** X-ray diffraction patterns of nanocomposites containing 5 wt. % clay. (From top to bottom: C25A, PC-I, PC, All-S, and PI-C).

Figures 4.1 through 4.3 show that, after melt blending, the intensity of the diffraction peak corresponding to C25A is reduced while a set of new peaks appear. In Figure 4.2, PC-I, PC, and All-S patterns contain diffraction peaks characteristic of the intercalated structure. Whereas, CI-P and PI-C represent an exfoliated structure since the peaks decrease in height and get broader as delamination increases (Dennis et al., 2001). In other words, the polymer that enters the galleries pushes the platelets far enough apart so that the platelets may not be parallel to each other indicating an exfoliated structure and the irregular platelet separation exceeds the sensitivity of X-ray diffraction. Thus, no peak is detected by XRD.

It is apparent in Figure 4.3 that, the X-ray diffraction pattern of PI-C is almost featureless compared with the others, only exhibiting a very broad, extremely weak reflection at approximately 2θ of 2.47°.

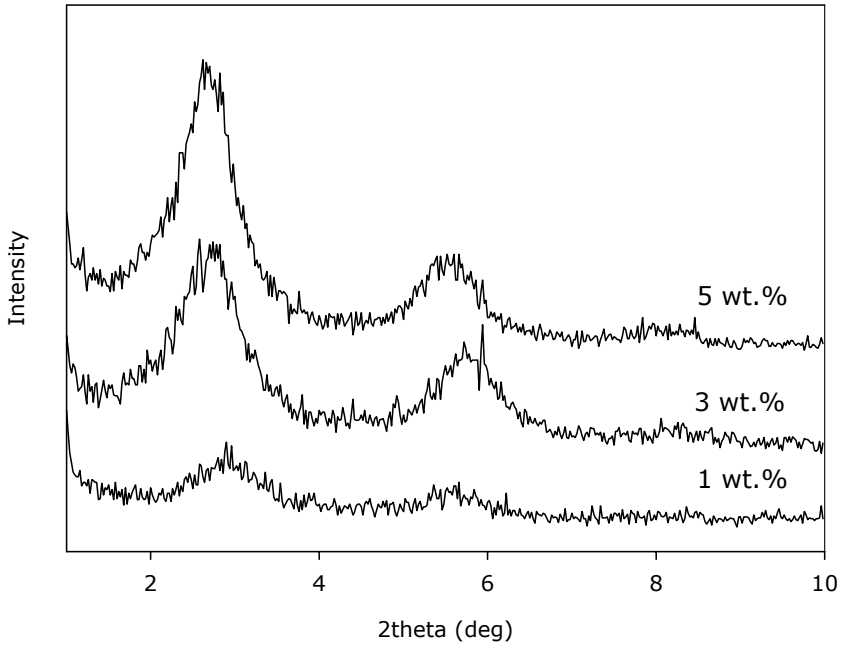


**Figure 4.4** X-ray diffraction patterns of PET/clay nanocomposites with different clay concentrations.

Figure 4.4 shows X-ray diffraction patterns for PET/clay nanocomposites at varying clay concentrations.

The intensity of diffraction peaks increases as a function of the clay concentration. This indicates more ordered structures in the nanocomposites at higher clay concentrations. At low clay concentration, part of the stacking structure is disrupted by the imposed shear stress during the melt blending (Xianbo and Lesser, 2003). More stacking structure was observed when the clay concentration was higher. To conclude, exfoliated structures are observed for addition orders designated as PI-C, CI-P and All-S. In all these cases, clay layers are subjected to high shear stresses since the shear stress is proportional to the viscosity at constant shear rate. Additionally, melt flow index values of the formulations will be given in Section 4.2, supporting this explanation.

### 4.1.2 Scanning Electron Microscopy (SEM) Analysis

There are several techniques that can be applied to evaluate the morphology of polymer blends, SEM plays an important part for a better understanding of the surface. In this study, both polymer matrix nanocomposites and polymer blends are focused on since newly developed material is composed of the three components: PET, impact modifier (E-MA-GMA) and clay (C25A). It is known that the two polymers used in this study form a polymer blend. For this reason, SEM was chosen to interpret the morphology regarding the compatibility between PET and E-MA-GMA. SEM images of fractured surfaces of all the formulations will be presented here with the same magnifications of x250 and x3500. The hair indicated at these magnifications corresponds to 100 μm and 10 μm respectively.

Figure 4.5 represents the impact fractured surfaces of twice extruded PET at magnifications of x250 and x3500, respectively. PET has a smooth structure. Almost no fragmentation is observed and few straight crack lines are apparently seen indicating low impact strength.

In Figures 4.6 and 4.7, SEM micrographs of PET/E-MA-GMA blends with varying E-MA-GMA concentrations are shown at magnifications of x250 and x3500, respectively. It is obvious that featureless structure of pure PET disappears when melt blended with E-MA-GMA. In Figures 4.6 (a) and 4.6 (b), the continuous and interpenetrated phases of PET and E-MA-GMA are clearly seen. This suggests that there is a very good adhesion between PET and E-MA-GMA and it is a result of intermolecular reactions between the two polymers.

Figures 4.6 (c), 4.6 (d), and 4.7 show that, at higher concentrations of the impact modifier, the morphology is similar. The point is that E-MA-GMA is an elastomeric material, which reduces the effective area bearing the tensile load. Elastomers may also create cavitation which is a major mechanism of stress relief. It is observed that, from 5 wt. % through 20 wt. % E-MA-GMA concentrations, cavitations become larger, which alleviate the triaxial stresses causing the cracks to grow (Sperling, 1997). Additionally, in order to observe the morphology easily, techniques like etching by acids, swelling by solvents and dissolving out one or the other component could have been used.

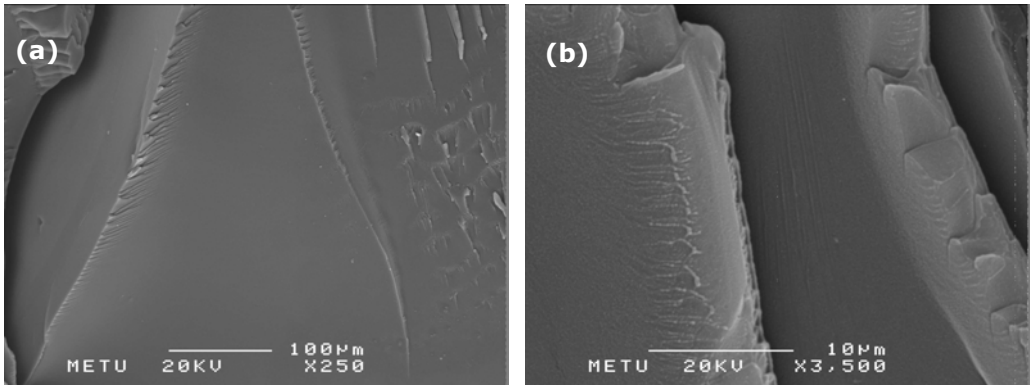


**Figure 4.5** SEM micrographs of double extruded, pure PET with magnifications: (a) x250; (b) x3500.

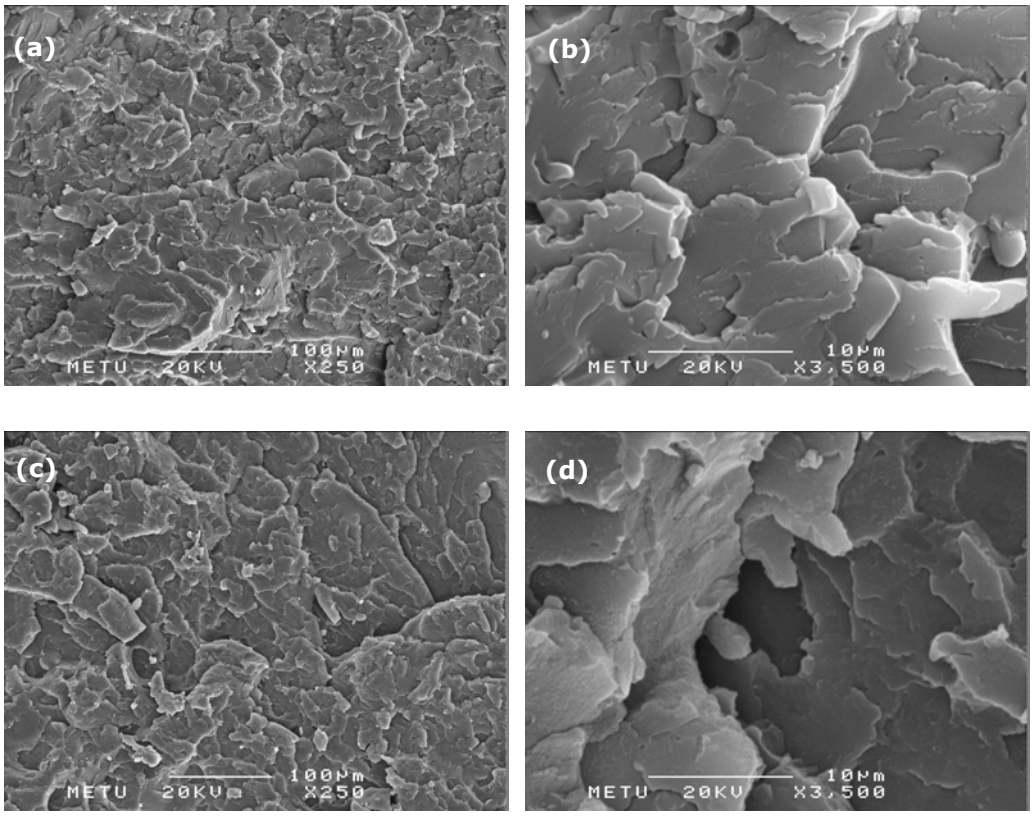


**Figure 4.6** SEM micrographs of PET/E-MA-GMA blends with different E-MA-GMA concentrations: (a) 5 wt. %, x250; (b) 5 wt. %, x3500; (c) 10 wt. %, x250; (d) 10 wt. %, x3500.

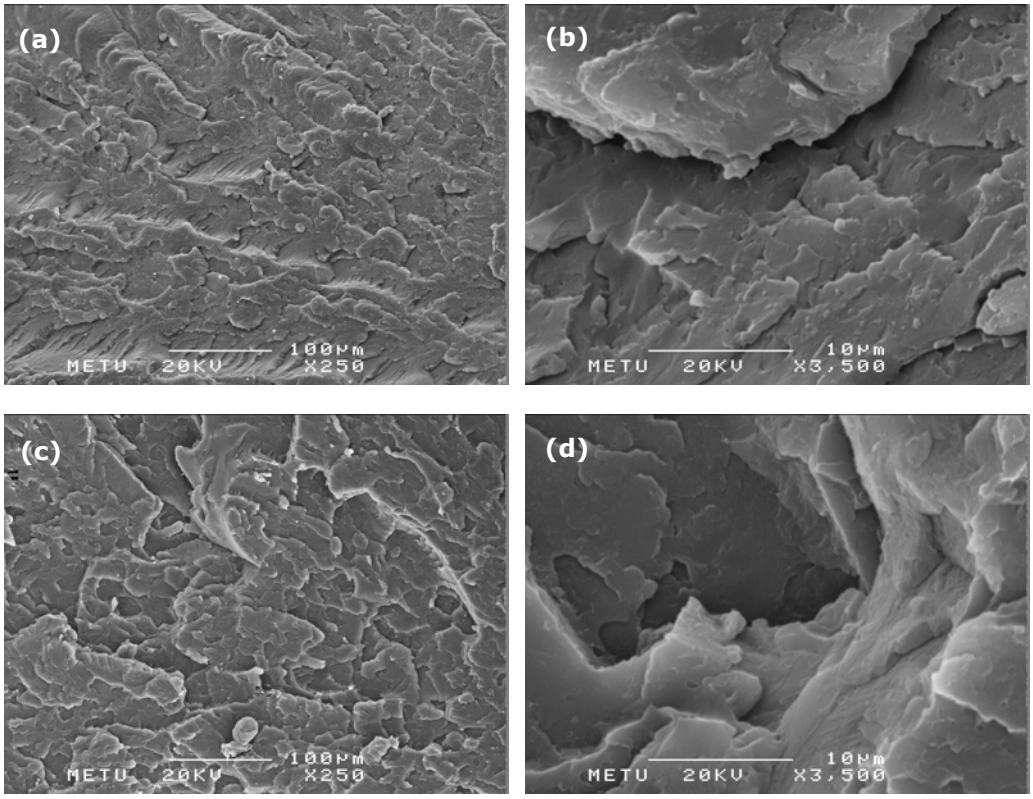


**Figure 4.7** SEM micrographs of PET/E-MA-GMA blends with different E-MA-GMA concentrations: (a) 15 wt. %, x250; (b) 15 wt. %, x3500; (c) 20 wt. %, x250; (d) 20 wt. %, x3500.

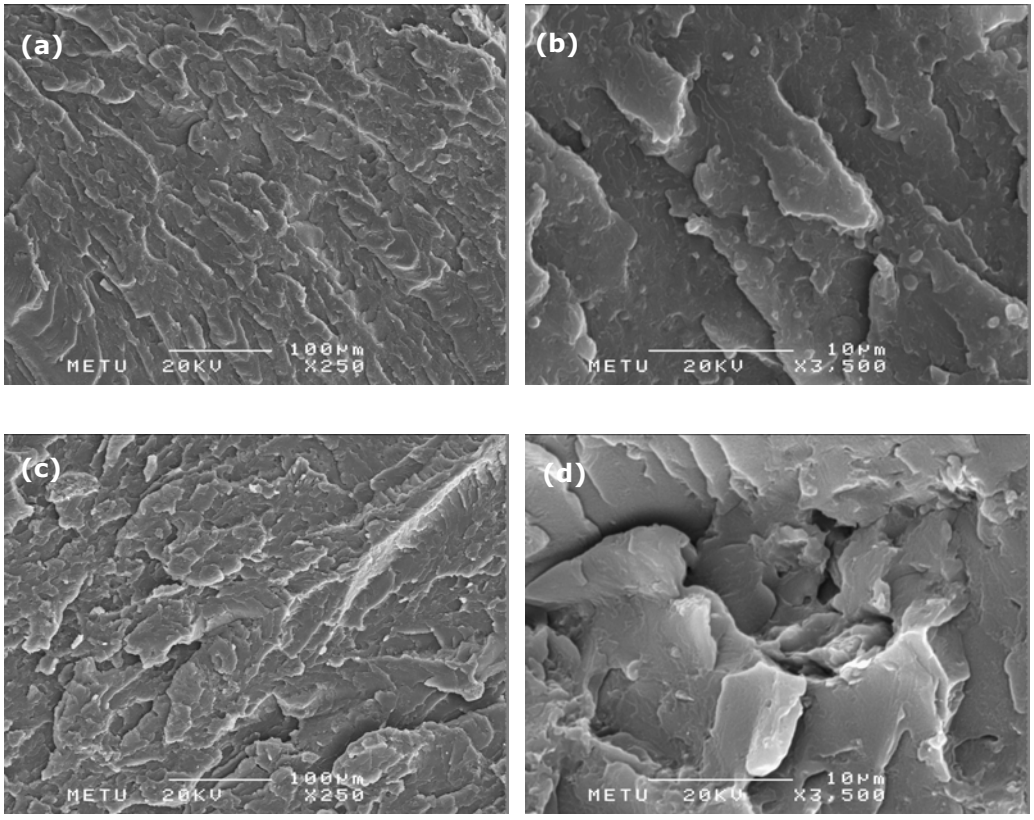


**Figure 4.8** SEM micrographs of PET/E-MA-GMA/C25A nanocomposites: (a) CI-P with 1 wt. % C25A, x250; (b) CI-P with 1 wt. % C25A, x3500; (c) CI-P with 3 wt. % C25A, x250; (d) CI-P with 3 wt. % C25A, x3500.

Figure 4.8 through 4.12 represent SEM micrographs of ternary nanocomposites prepared by different addition orders. When the blend has tough behavior, cavitation and extensive deformation of the matrix occur (Chapleau, 2003). However, it is very difficult to interpret the morphology of the nanocomposites based on the effect of clay. The influence of clay concentration looks almost the same in all of the images. For this reason, other electron microscopy techniques such as Transmission electron microscopy (TEM), which have higher resolution, should be utilized. In the previous section, whether the clay is intercalated or exfoliated was discussed in light of X-ray diffraction analysis. However, it should be supported by TEM since the features of the local microstructure from TEM give useful detail to understand the overall picture which is supported by XRD results.

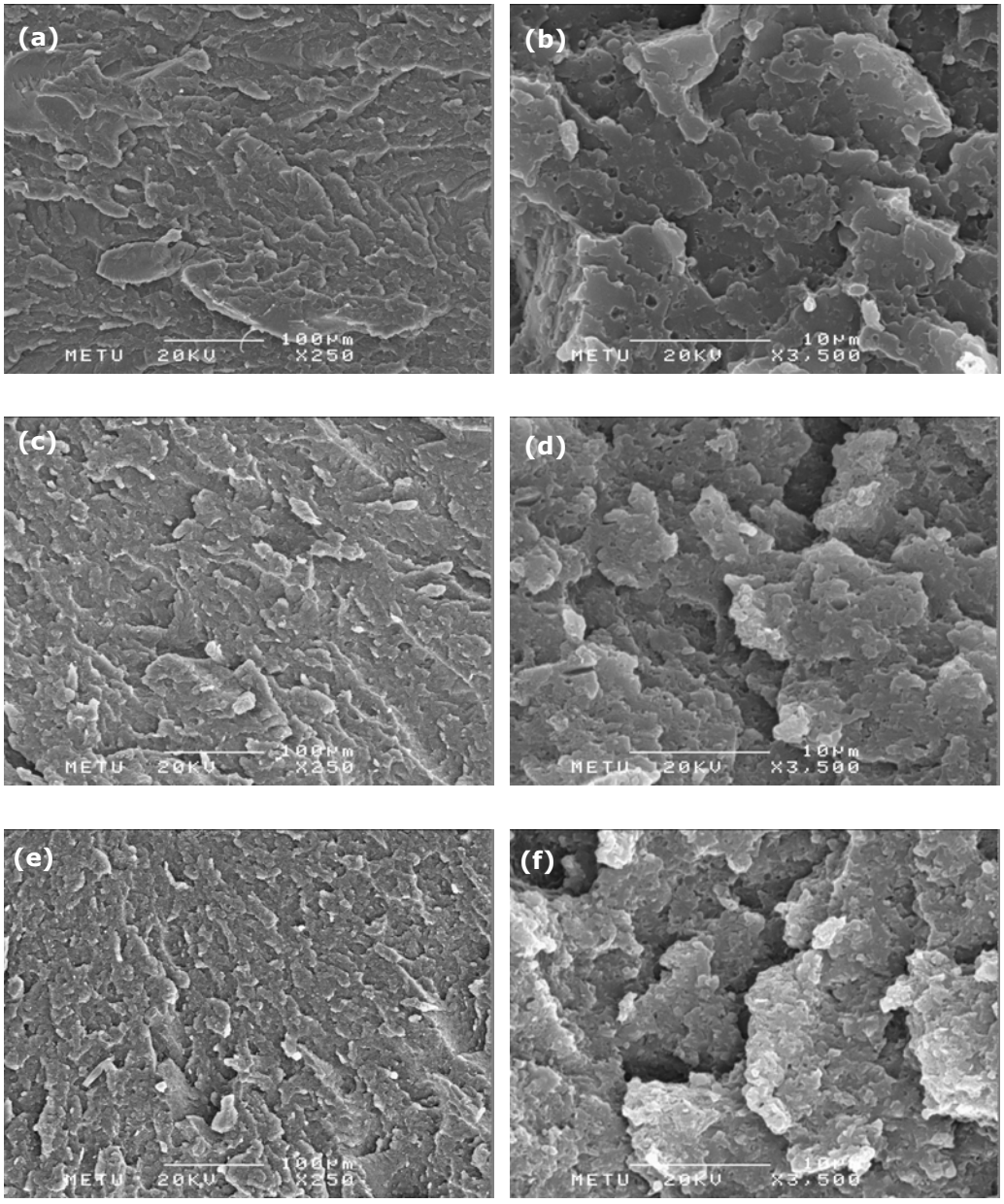


**Figure 4.9** SEM micrographs of PET/E-MA-GMA/C25A nanocomposites: (a) PC-I with 1 wt. % C25A, x250; (b) PC-I with 1 wt. % C25A, x3500; (c) PC-I with 3 wt. % C25A, x250; (d) PC-I with 3 wt. % C25A, x3500; (e) PC-I with 5 wt. % C25A, x250; (f) PC-I with 5 wt. % C25A, x3500.

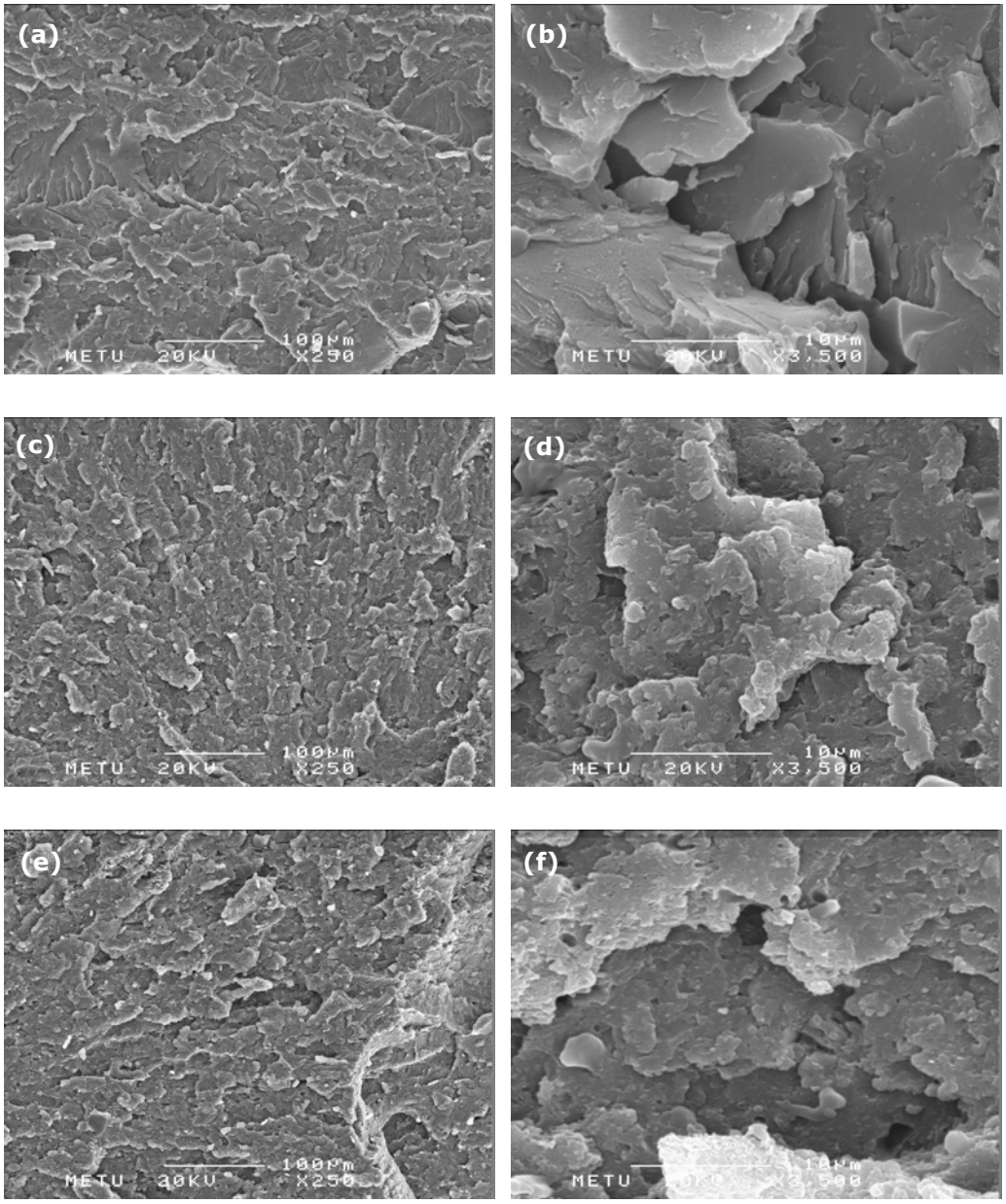


**Figure 4.10** SEM micrographs of PET/E-MA-GMA/C25A nanocomposites: (a) PI-C with 1 wt. % C25A, x250; (b) PI-C with 1 wt. % C25A, x3500; (c) PI-C with 3 wt. % C25A, x250; (d) PI-C with 3 wt. % C25A, x3500; (e) PI-C with 5 wt. % C25A, x250; (f) PI-C with 5 wt. % C25A, x3500.

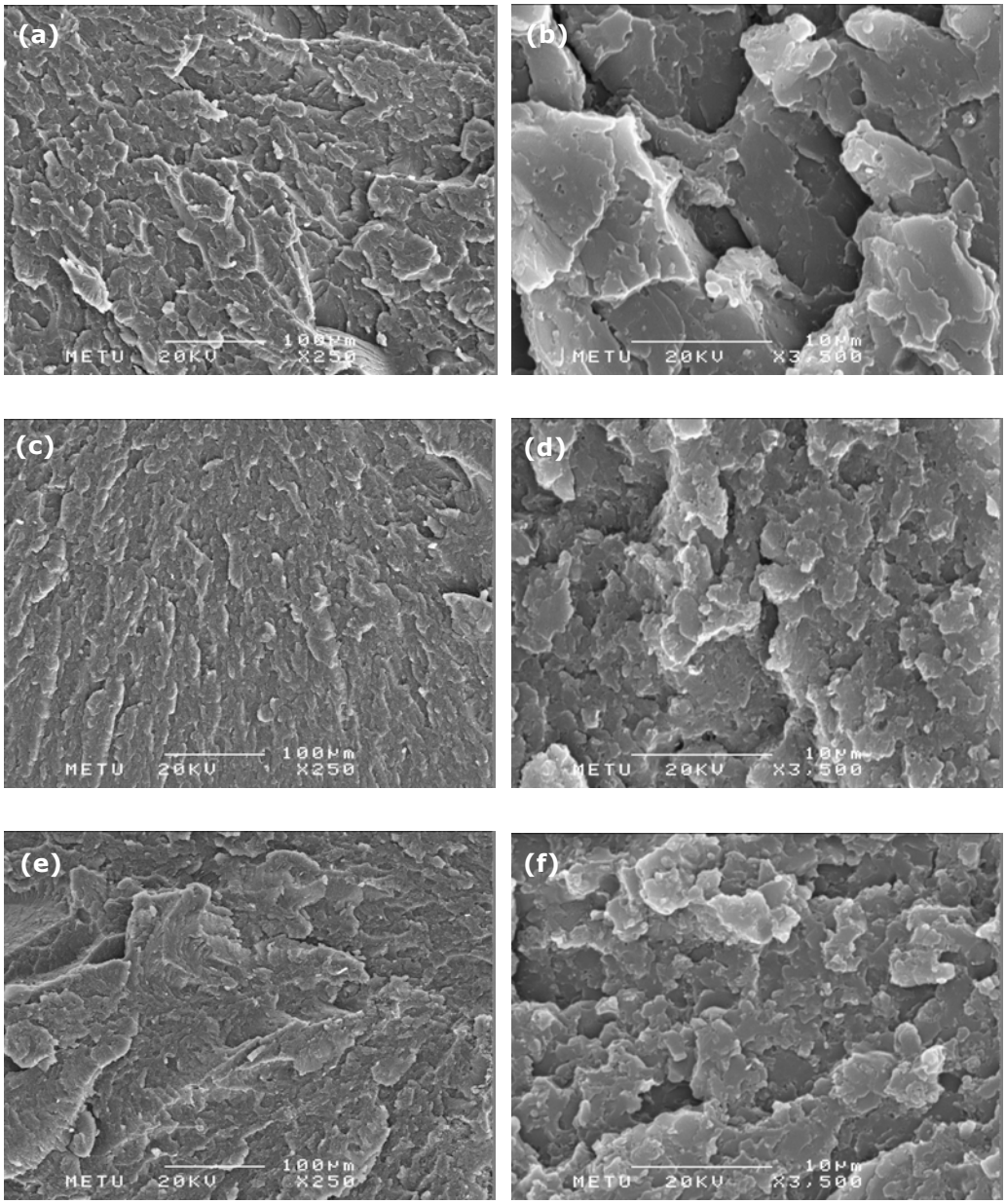


**Figure 4.11** SEM micrographs of PET/E-MA-GMA/C25A nanocomposites: (a) All-S with 1 wt. % C25A, x250; (b) All-S with 1 wt. % C25A, x3500; (c) All-S with 3 wt. % C25A, x250; (d) All-S with 3 wt. % C25A, x3500; (e) All-S with 5 wt. % C25A, x250; (f) All-S with 5 wt. % C25A, x3500.

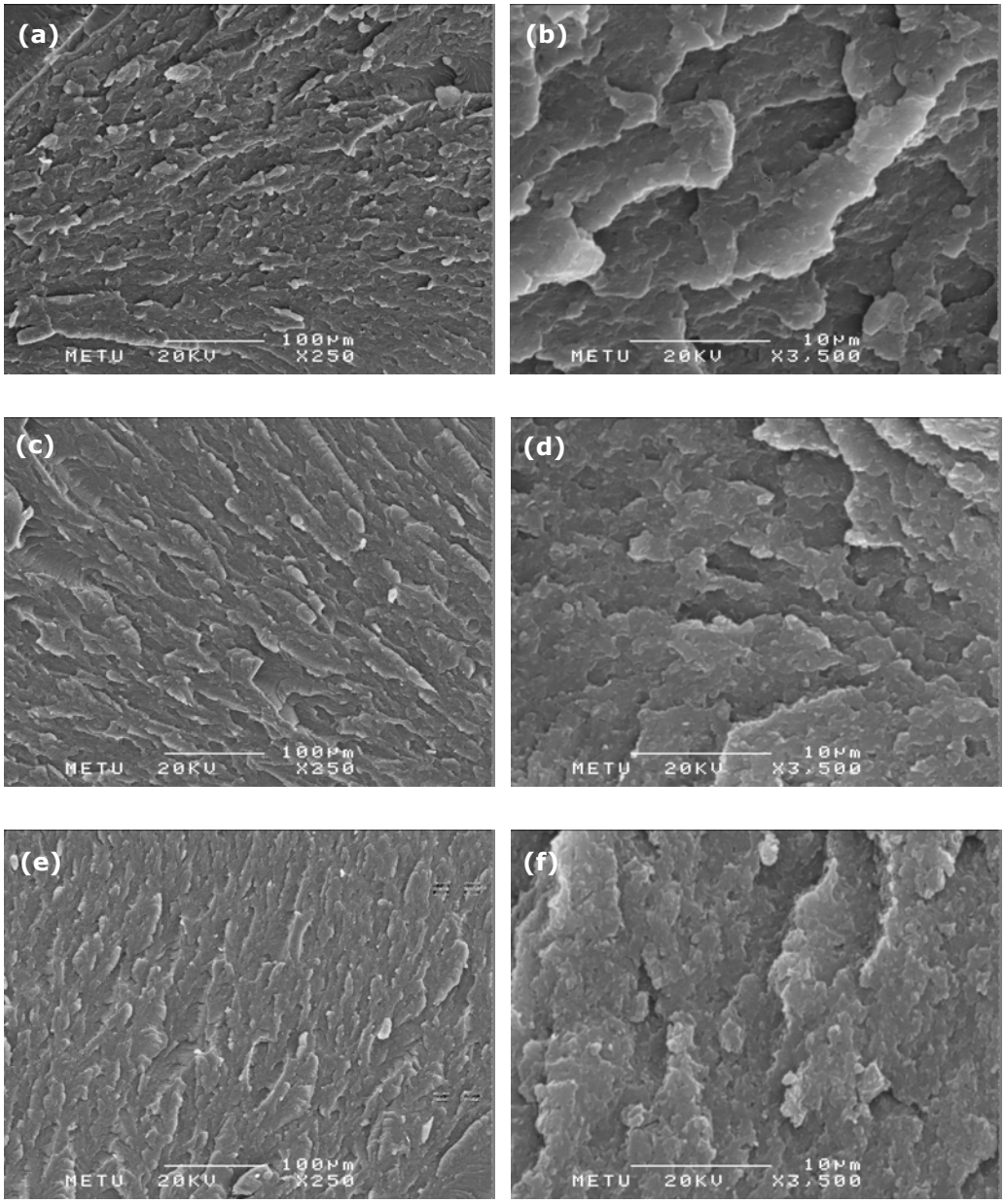


**Figure 4.12** SEM micrographs of binary PET/C25A nanocomposites with different clay concentrations: (a) 1 wt. % C25A, x250; (b) 1 wt. % C25A, x3500; (c) 3 wt. % C25A, x250; (d) 3 wt. % C25A, x3500; (e) 5 wt. % C25A, x250; (f) 5 wt. % C25A, x3500.

## 4.2 Flow Characteristics

Melt flow index measurements were carried out under a specified load of 2.16 kg and at a specified temperature of 260°C. As is known, melt flow index is inversely related to the melt viscosity. Additionally, the melt viscosity is related to the molecular weight of the material. In Table 4.2, melt flow index values of all the formulations are given.

At the end of the analysis, the followings are observed:

(a) The MFI of pure PET increases (i.e. the viscosity decreases) upon extrusion indicating chain scission.

(b) The MFI of E-MA-GMA is much lower than that of PET under the same load and at the same temperature. Thus, in PI blends; as the impact modifier content increases, the MFI decreases.

(c) Clay decreases the MFI (increases the viscosity) since it acts as a filler, as observed from PC materials.

(d) Upon addition of E-MA-GMA to PC blends, the MFI decreases (the viscosity increases) as expected. However, this decrease in MFI is not the same for all the mixing sequences. CI-P and PI-C give the lowest MFI (highest viscosity). It should be noted that these sequences gave rise to exfoliated structures.

In the case of PI-C, the epoxy functionality of GMA reacts with PET and forms a viscous mixture. Thus, high shear stresses are applied on the clay layers and exfoliation takes place. Likewise, in the case of CI-P, E-MA-GMA with high viscosity also exfoliates the clay layers in the same manner. However, in PC-I, this mechanism does not take place. The pure PET can not exfoliate the clay layers.

**Table 4.2** MFI values of all formulations.

| **Pure PET (not extruded)** | **MFI (g/10 min)** |
|---|---|
| | 610 |
| **Impact Modifier (E-MA-GMA)** | **MFI (g/10 min)** |
| | 26 |
| **PI** | |
| **Impact Modifier (wt. %)** | **MFI (g/10 min)** |
| 5 | 166 |
| 10 | 147 |
| 15 | 143 |
| 20 | 61 |
| **PC** | |
| **Clay (wt. %)** | **MFI (g/10 min)** |
| 0 | 809 |
| 1 | 496 |
| 3 | 358 |
| 5 | 262 |
| **CI-P** | |
| **Clay (wt. %)** | **MFI (g/10 min)** |
| 1 | 140 |
| 3 | 124 |
| **PC-I** | |
| **Clay (wt. %)** | **MFI (g/10 min)** |
| 1 | 236 |
| 3 | 207 |
| 5 | 184 |
| **PI-C** | |
| **Clay (wt. %)** | **MFI (g/10 min)** |
| 1 | 115 |
| 3 | 112 |
| 5 | 110 |
| **All-S** | |
| **Clay (wt. %)** | **MFI (g/10 min)** |
| 1 | 214 |
| 3 | 183 |
| 5 | 167 |

## 4.3 Mechanical Behavior

### 4.3.1 Effect of Impact Modifier

In order to optimize impact modifier (E-MA-GMA) content for ternary nanocomposites composed of PET, impact modifier, and clay; mechanical behavior of binary PET/E-MA-GMA blends was studied. At the end, the impact modifier content providing balanced mechanical properties was determined.

Figure 4.13 presents typical stress-strain curves for pure PET and for impact modified PET blends at various impact modifier contents. Pure PET shows brittle behavior and fractures at about 5% strain. In contrast, all PET/impact modifier blends are ductile with the formation of a stable neck propagating along the gauge section before fracturing. It should be noted that pure E-MA-GMA has a reported strain at break of 1100%.

As is seen in Figure 4.13, the stress-strain curves for impact modified PET blends show well-defined yield points. Since the area under the curve is a measure of the energy required to break the material, it is obvious that the energy to fracture in stress-strain increases with increasing the modifier content. Besides, the addition of the modifier decreases the tensile stress at yield. The elongation at break increases significantly, jumping from 5% for pure PET to between 100 and 300% for the modified PET, depending on the modifier concentration.

Young's modulus values of PET/impact modifier blends are shown as a function of impact modifier content in Figure 4.14. Pure E-MA-GMA has a reported Young's Modulus of 8 MPa. Young's Modulus decreases from 1155 MPa for not extruded, pure PET to nearly 600 MPa for PET containing 20 wt. % impact modifier. Use of 5 wt. % modifier leads to a Young's modulus of 910 MPa. On the other hand, PET at 5 wt. % loading level of impact modifier leads to lower elongation at break compared with the ones containing 10, 15, and 20 wt. % modifier. Percent tensile strain at break values of these blends are shown in Figure 4.15. As a conclusion, the lower impact modifier content of PET blends possibly explains the higher modulus and the lower elongation at break for these blends.

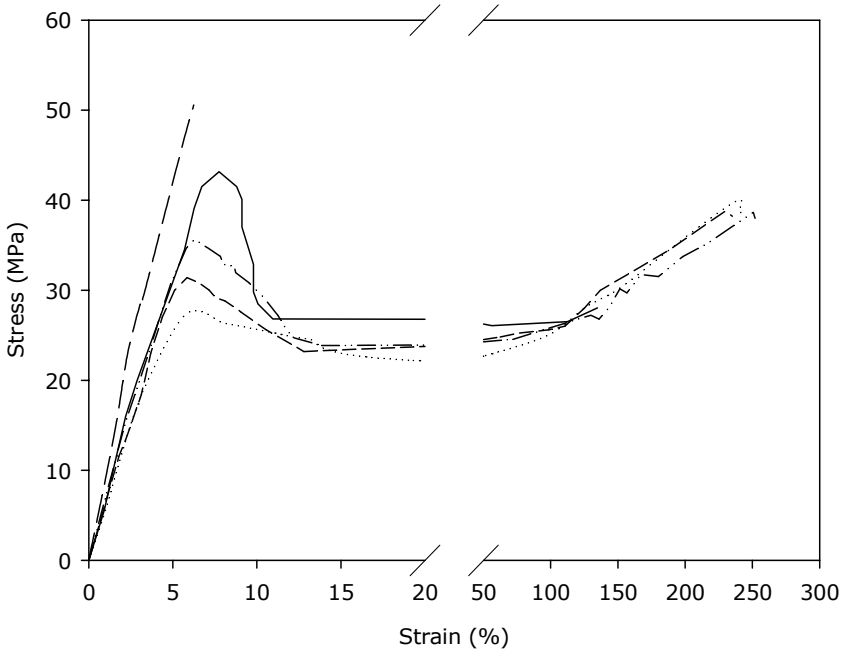


**Figure 4.13** The stress-strain curves for PET (P) containing different amounts of impact modifier (I). (From top to bottom: (– – -) pure P, (——) PI with 5 wt. %, (– · · –) PI with 10 wt. %, (- - - -) PI with 15 wt. %, (·····) PI with 20 wt. % impact modifier content.

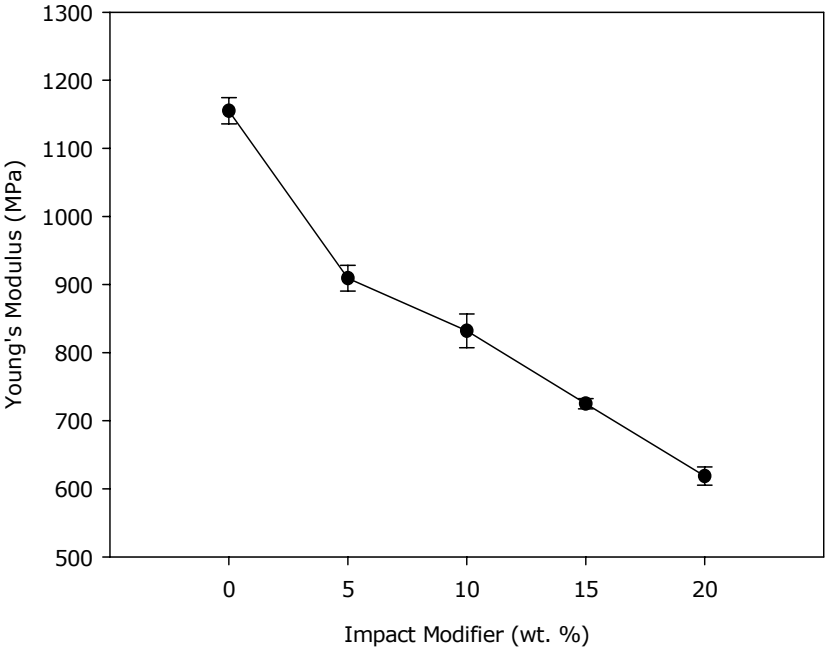


**Figure 4.14** Young's modulus values of PET/impact modifier blends as a function of the impact modifier content.

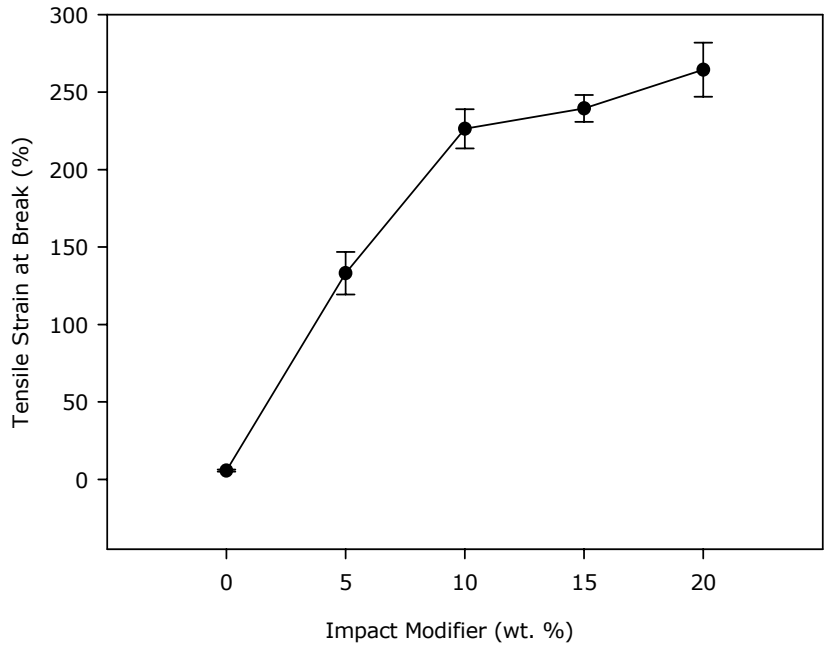


**Figure 4.15** Tensile strain at break values of PET/impact modifier blends as a function of the impact modifier content.

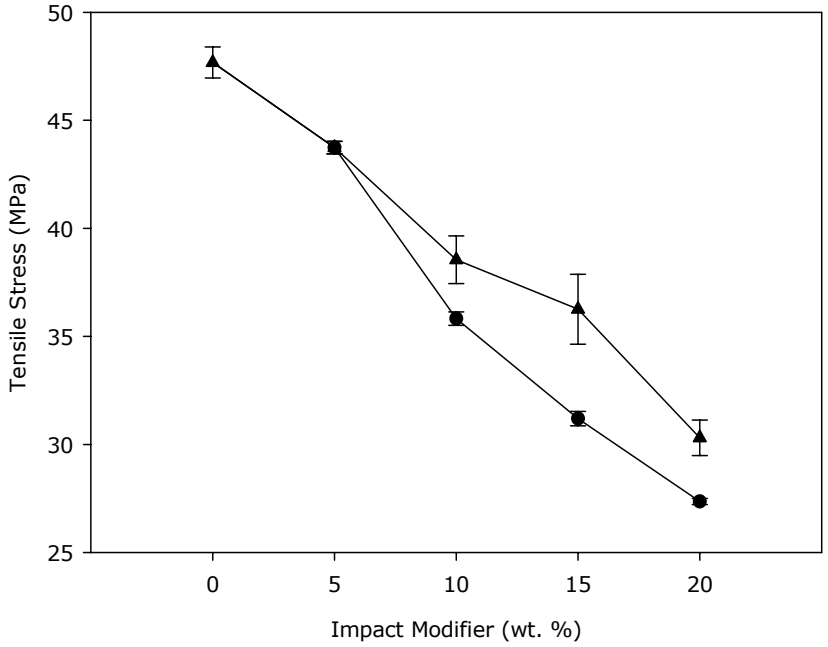


**Figure 4.16** Tensile stress values of PET/impact modifier blends as a function of the impact modifier content. (●); tensile stress at yield, (▲); tensile strength.

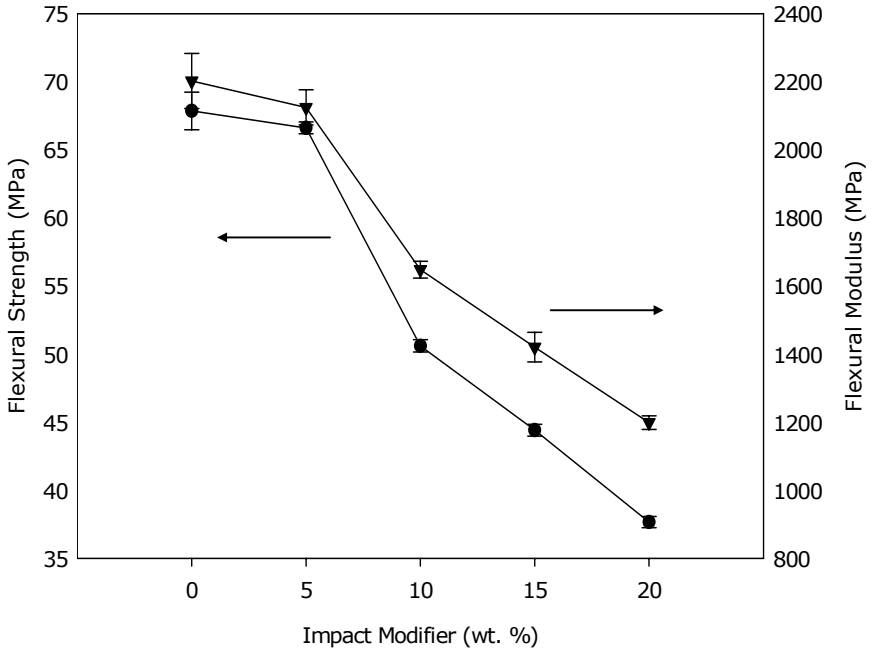


**Figure 4.17** Flexural strength and flexural modulus values of PET/impact modifier blends as a function of the impact modifier content.

Tensile stress at yield and tensile strength of all investigated PET/impact modifier blends are reported in Figure 4.16. Since there is no yield point in the stress-strain curve for pure PET, PET has only tensile strength value at fracture, which is the highest stress value in Figure 4.16. At 5 wt. % E-MA-GMA content, the tensile stress at yield also gives the tensile strength of the material. The tensile strength and tensile stress at yield decrease relatively linearly with the impact modifier content. The property reduction is the expected result owing to the lower strength of the modifier, reported as 4 MPa.

Figure 4.17 shows flexural strength and flexural modulus values for PET/impact modifier blends with varying impact modifier concentration. As the modifier concentration increases, flexural strength values and flexural moduli for blends decrease in a similar fashion. It is apparently seen that both flexural strength and flexural modulus values are greater than those of tensile testing. The reason is that in flexural testing, the lower half of the specimen is in tension and the upper half is in compression.

Besides, cracks do not play such an important role in compression than in tension because the stresses tend to close the cracks rather than open them (Nielsen and Landel, 1994).

### 4.3.2 Effects of Addition Order and Clay Concentration

After the impact modifier concentration was chosen as 5 wt. % owing to its balanced mechanical properties, the effects of different addition orders and clay concentrations on mechanical properties were investigated.

Figure 4.18 shows the typical stress-strain curves of PC nanocomposites in the absence of impact modifier. Figures 4.19 through 4.22 illustrate the stress-strain curves for PET/impact modifier/clay nanocomposites prepared by different addition sequences.

For the sake of reminding, the addition orders investigated can be summarized as follows: P, I and C stand for PET, Impact Modifier (E-MA-GMA), and Clay respectively. The first two letters indicate the materials mixed in the first run. This mixture was compounded with the third ingredient in the subsequent run. The following sequences were prepared:

Sequence 1 (PI-C),

Sequence 2 (PC-I),

Sequence 3 (CI-P),

Sequence 4 (All-S) All simultaneous feeding.

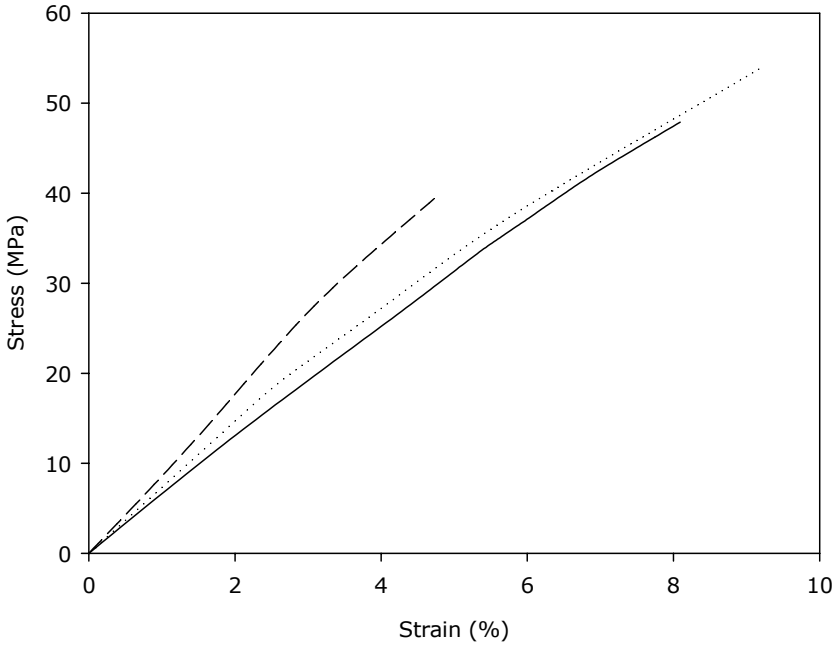


**Figure 4.18** The stress-strain curves of PET/clay (PC) nanocomposites containing different amounts of clay. (——) PC with 1 wt. %; (·····) PC with 3 wt. %; (----) PC with 5 wt. % clay.

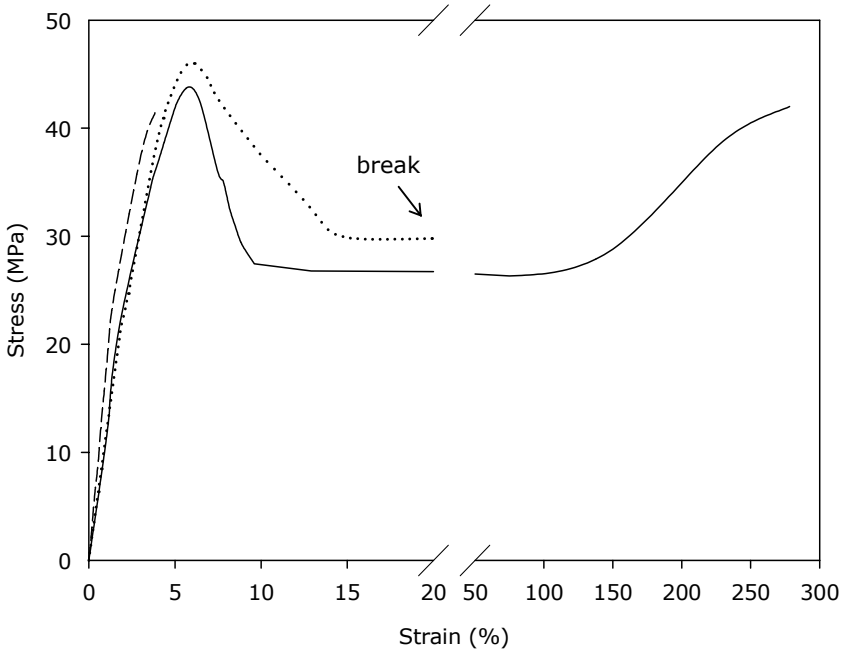


**Figure 4.19** The stress-strain curves of PET/impact modifier/clay (PI-C) nanocomposites containing different amounts of clay. (——) PI-C with 1 wt. %; (·····) PI-C with 3 wt. %; (----) PI-C with 5 wt. % clay.

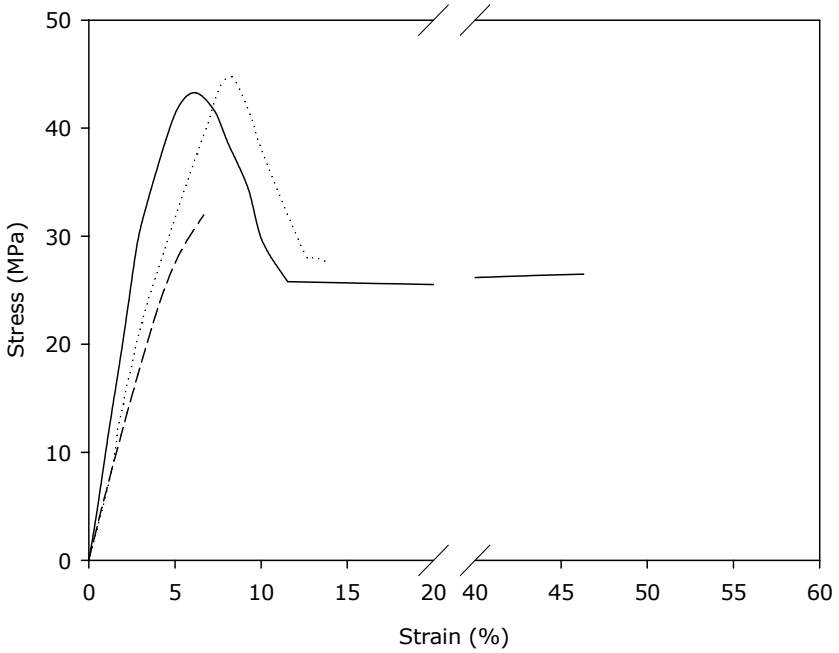


**Figure 4.20** The stress-strain curves of PET/impact modifier/clay (PC-I) nanocomposites containing different amounts of clay. (——) PC-I with 1 wt. %; (·····) PC-I with 3 wt. %; (----) PC-I with 5 wt. % clay.

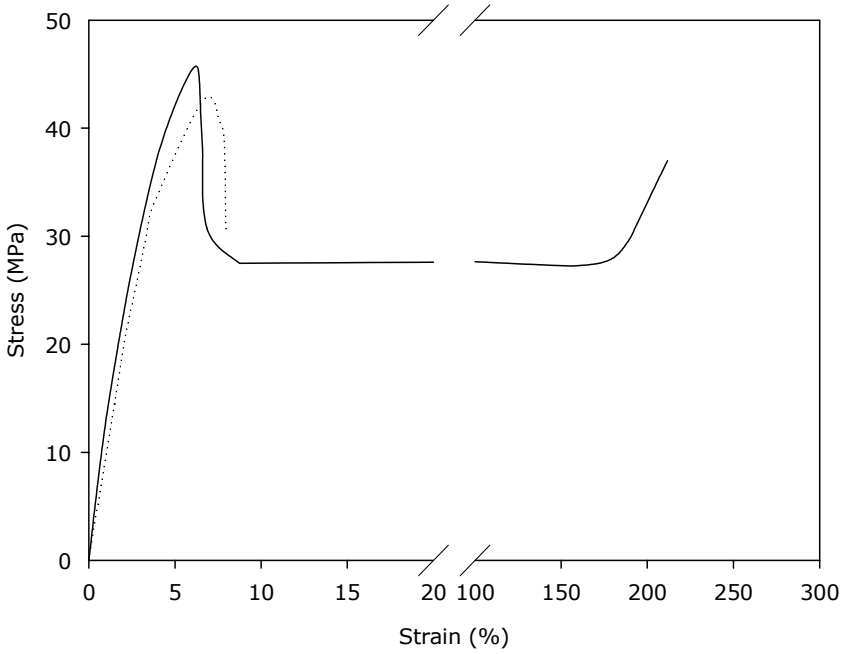


**Figure 4.21** The stress-strain curves of PET/impact modifier/clay (CI-P) nanocomposites containing different amounts of clay. (——) CI-P with 1 wt. %; (·····) CI-P with 3 wt. % clay.

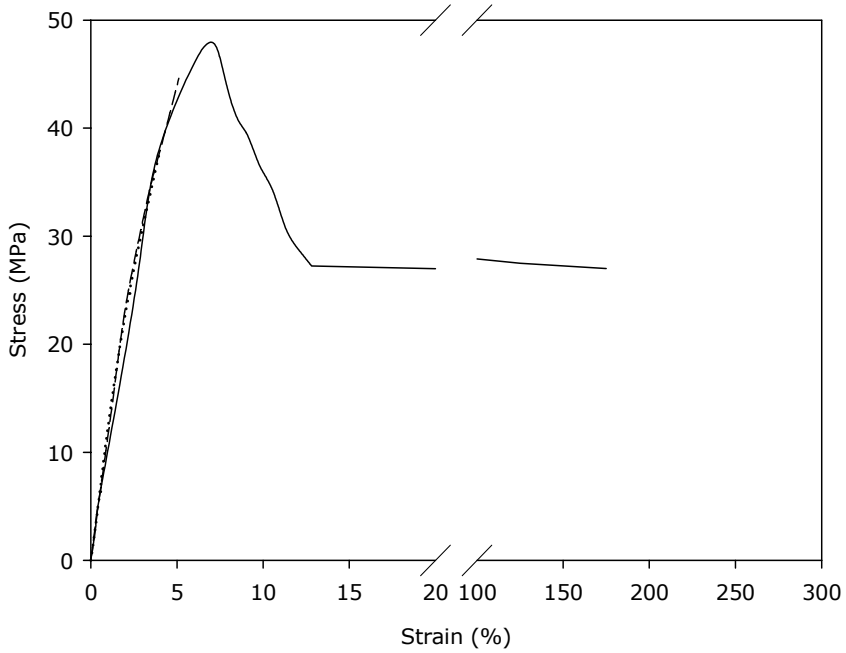


**Figure 4.22** The stress-strain curves of PET/impact modifier/clay (All-S) nanocomposites containing different amounts of clay. (——) All-S with 1 wt. %; (·····) All-S with 3 wt. %; (----) All-S with 5 wt. % clay.

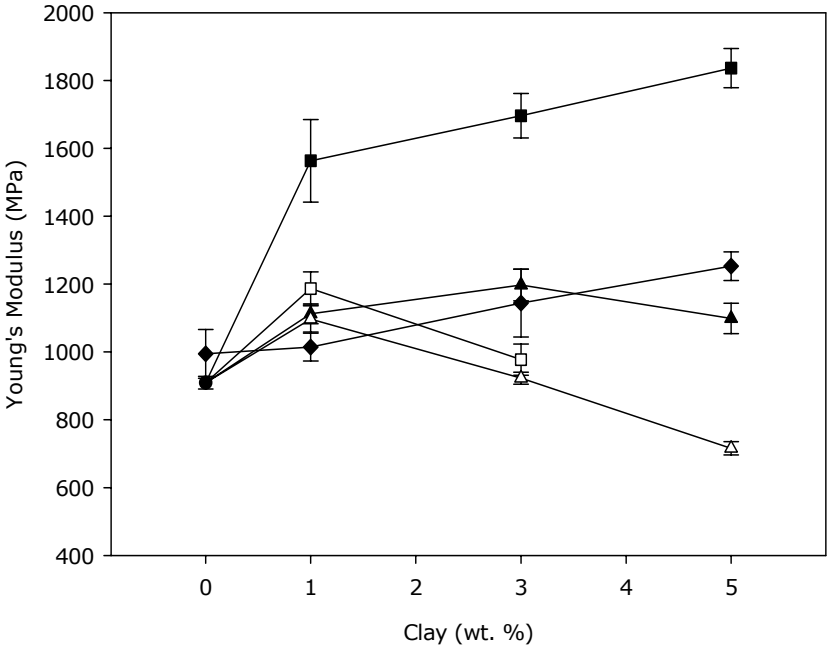


**Figure 4.23** Young's modulus values of all formulations as a function of clay concentration: (■) PI-C; (□) CI-P; (▲) All-S; (Δ) PC-I; (♦) PC; (●)PI.

Figure 4.23 displays Young's Modulus values of both binary and ternary nanocomposites with respect to the amount of clay. It is seen from Figures 4.18 through 4.23 that, Young's modulus is greatly influenced by the content of clay and by the addition sequence of the three components.

In these figures, the characteristic behavior of polymer/layered silicate nanocomposite materials is observed (Alexandre and Dubois, 2000). Obviously, Young's Modulus of PET/organoclay nanocomposites (PC) increases with increasing clay content since any filler whose modulus is greater than that of the polymer increases the modulus of a mixture with that polymer.

For PI-C; there is a sharp increase of Young's modulus for very small clay loadings (1 wt. %) followed by a much slower increase beyond 5 wt. % loading. On the other hand, with increasing clay content, Young's modulus values of All-S, CI-P, and PC-I do not change markedly up to loading levels of 3 wt. % clay when compared with Young's modulus of PI (0 wt. % clay). These observations support the fact that better dispersion of the clay in PET and strong interaction between PET and the clay are essential for achieving higher Young's modulus.

In other words, as the polymer/clay adhesion is improved -as for example when the functional groups of the impact modifier (terpolymer), which can react with groups on the filler surface, are incorporated in the matrix- the stresses are much more effectively transferred from the polymer matrix to the inorganic filler, and thus a higher increase in Young's modulus is expected (Manias et al., 2001). For this reason, compared to binary PET/clay nanocomposites (PC), ternary PET/clay/impact modifier nanocomposites are characterized by larger modulus increases for the same clay loading. In addition, E-MA-GMA acts as a chain extender for PET.

Based on Young's modulus, PI-C is the best addition sequence at which PET was first compounded with the modifier. Later, this mixture was compounded with the clay in the subsequent run. The modification of the PET prior to compounding with the clay may have resulted in promoting the exfoliation of clay layers owing to the high molecular weight obtained in comparison to pure PET.

While the highest Young's modulus is revealed at 5 wt.% clay for PI-C, the lowest value obtained is at 5 wt. % clay loading for PC-I.

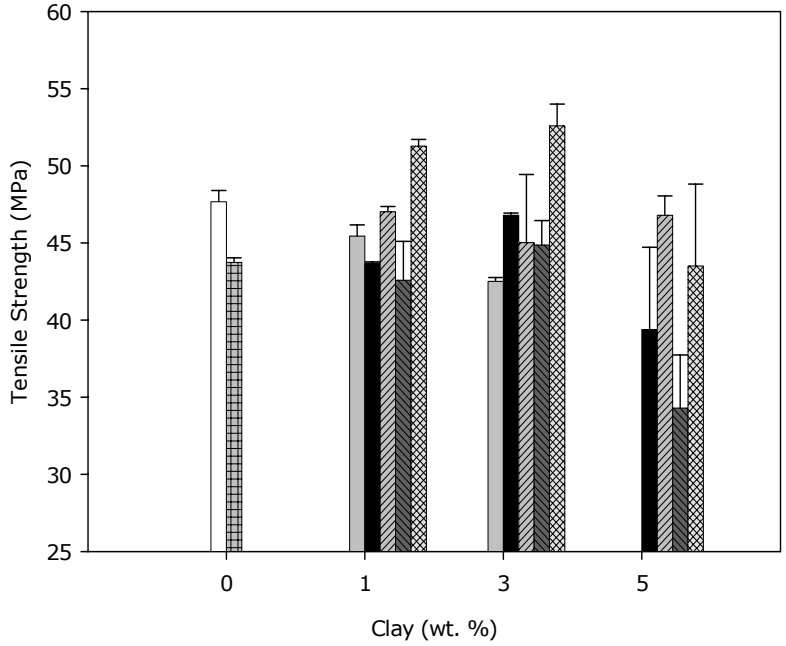


**Figure 4.24** Tensile strength as a fuction of clay content.
P, PI, CI-P, PI-C, All-S, PC-I, PC.

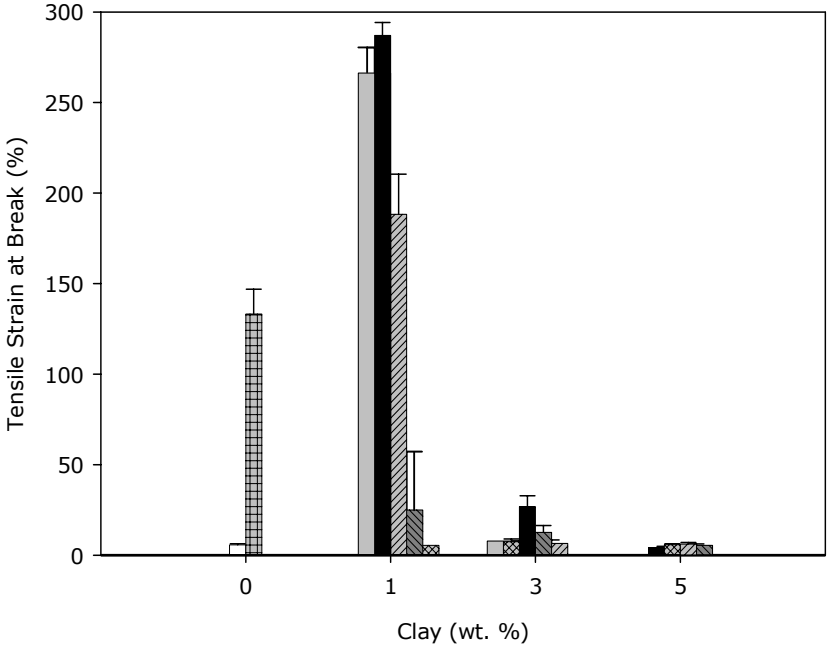


**Figure 4.25** Tensile strain at break (%) as a function of clay content.
P, PI, CI-P, PI-C, All-S, PC-I, PC.

Figures 4.24 and 4.25 exhibit the tensile strength and the tensile strain at break of the materials studied. It is observed that addition of E-MA-GMA decreases the tensile strength of the pure PET and PET-clay binary nanocomposite materials, since E-MA-GMA has a lower tensile strength than that of PET. The order of the addition does not significantly affect the tensile strength of the nanocomposites. In general, the tensile strength values of the materials with 1 wt. % and 3 wt. % clay contents are higher than those of the materials with 5 wt. % clay content. This is probably due to higher levels of exfoliation as observed by XRD.

The tensile strain at break values, on the other hand, are significantly higher at 1 wt. % clay content owing to high levels of exfoliation. While pure PET does not show yielding and breaks at very low strains, addition of E-MA-GMA results in a ductile material that elongates to very high extension after the yield point. At 1 wt. % clay content, the mixing sequences of CI-P, PI-C, and to a degree All-S exhibit yielding followed by elongation to very high strains. As observed earlier, these mixing orders have exfoliated structure. At higher clay content (3 wt. %), materials mixed with these sequences still exhibit yield, but do not elongate to high strains owing to the stress concentration effect of unexfoliated clay particles. The strain at break further decreases at 5 wt. % clay concentration.

Figure 4.26 confirms the previous discussion. At 0 wt. % clay content, pure PET does not exhibit yielding whereas PET/E-MA-GMA does. At 1 wt. % clay content, PI-C, CI-P, All-S, and PC-I mixing sequences show yielding. At 3 wt. % clay content, PI-C, CI-P and All-S mixing sequences also exhibit yielding. The level of yield stress, when yielding exists, is insensitive to the mixing order and the clay content. However, at the amount of 5 wt. % clay content, the nanocomposites break without yielding.

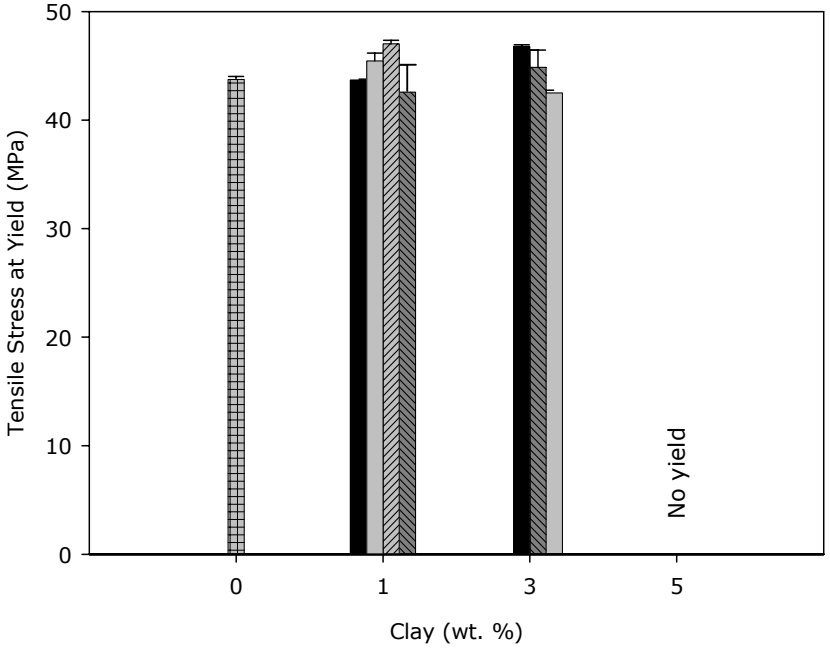


**Figure 4.26** Tensile stress at yield as a function of clay content.
PI, PI-C, CI-P, All-S, PC-I.

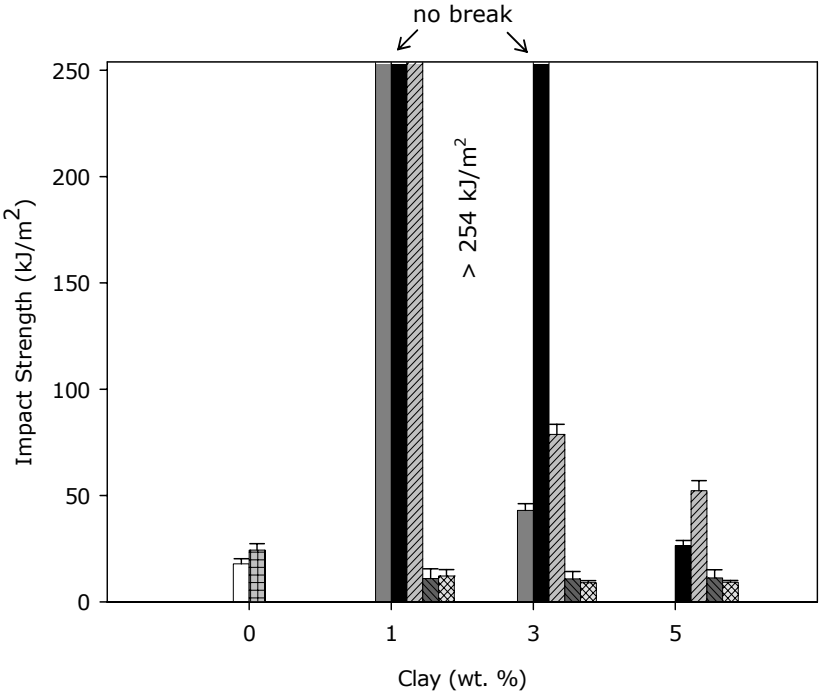


**Figure 4.27** Impact strength as a function of clay content.
P, PI, CI-P, PI-C, All-S, PC-I, PC.

The unnotched charpy impact strengths of all the materials at room temperature are summarized in Figure 4.27. The pristine PET has a poor impact resistance with a value of nearly 20 kJ/m$^2$. Adding 5 wt. % impact modifier did not significantly change the impact strength of pure PET, whereas the impact strength results drastically changed when the modifier was added as a third component in the PET/clay nanocomposites.

It should be noted that while pure PET specimens always broke completely upon impact, the tough nanocomposites indicated in Figure 4.27 did not break, and their impact strength is recorded in excess of 254 kJ/m$^2$. The impact values are consistent with the presence or absence of yielding. At 0 wt. % clay content, the impact strength of the PET increases with the addition of E-MA-GMA. At 1 wt. % clay content, the exfoliated structures of CI-P, PI-C and All-S mixing sequences did not break and thus, their impact strength is higher than 254 kJ/m$^2$. At 3 wt. % clay content, the same is true for the PI-C mixing order. The impact strength values of the materials with CI-P and All-S mixing sequences are still high. The impact strength decreases at 5 wt. % clay content owing to the stress concentration effect of unexfoliated clay.

Based on the impact and the strain at break results, the best sequence of component addition is once more selected as (PI-C). In this case, the polymer matrix mixture prepared in the first run (PI) has higher melt viscosity than does pure PET as observed by MFI. Thus this matrix can apply high shear stresses on the clay particles and delaminate the clay layers resulting in best mechanical properties. However, in other addition sequences such as PC-I, the matrix can not apply high shear stresses owing to its lower viscosity.

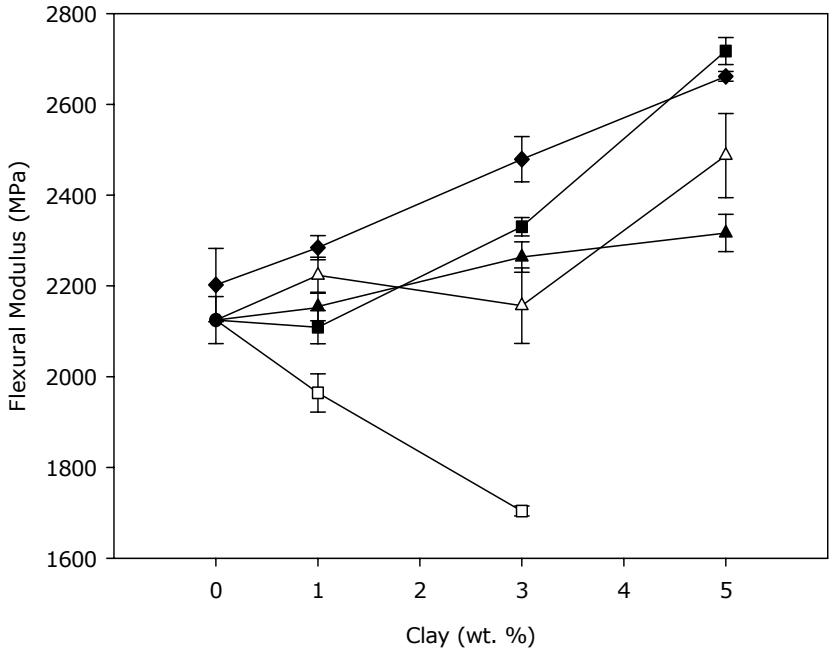


**Figure 4.28** Flexural modulus as a function of clay content:
(■) PI-C; (□)CI-P; (▲) All-S; (Δ) PC-I; (♦) PC; (●) PI.

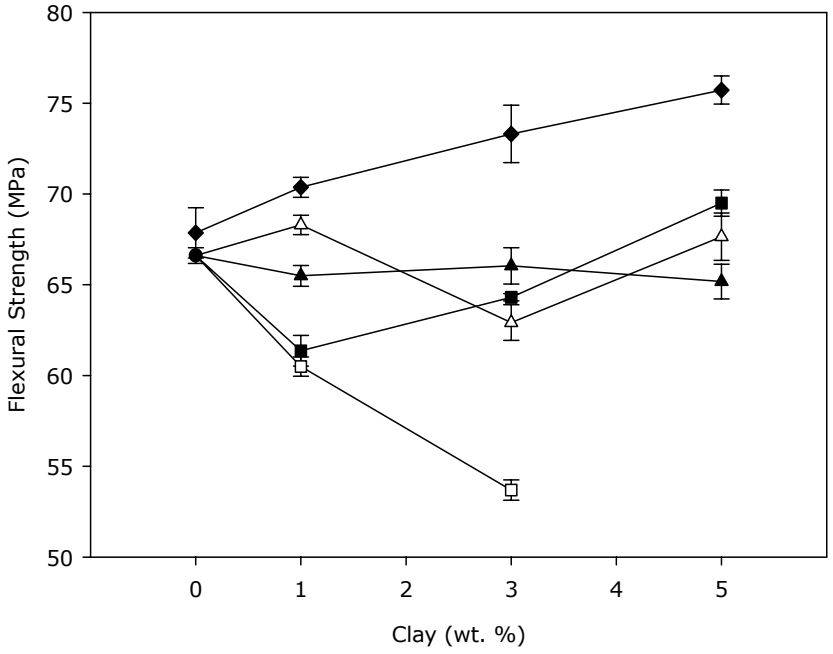


**Figure 4.29** Flexural strength as a function of clay content:
(■) PI-C; (□) CI-P; (▲) All-S; (Δ) PC-I; (♦) PC; (●) PI.

The flexural modulus and strength values are shown in Figures 4.28 and 4.29 respectively. Generally speaking, the flexural modulus increases with the addition of rigid clay particles. E-MA-GMA decreases the modulus, since it is a rubbery material. Thus, PC binary nanocomposites have the highest modulus in general. The flexural modulus is not sensitive to the mixing order. It is the components and their contents which are effective in determining the modulus, as implied by several theories on modulus (Nielsen and Landel, 1994).

The level of flexural modulus is significantly higher than the tensile modulus due to the nature of the flexural test as observed in other composites. Flexural strength is not significantly affected by the mixing sequence and the clay content studied here. The PC nanocomposites exhibit the highest level of flexural strength owing to the lack of E-MA-GMA with low strength. The flexural strength is also higher than the tensile strength, since in flexural test the cracks formed can not propagate easily towards the upper part of the specimen which is in compression.

Lastly, in flexural testing break point was observed only on the PC nanocomposites with 5 wt. % clay content, and the PC-I ternary nanocomposites with 5 wt. % clay content owing to the extensibility imparted by E-MA-GMA. Flexural strain at break (%) values of these materials are nearly 5% and 6% respectively.

## 4.4 Thermal Analysis

Poly(ethylene terephthalate) used in this study, has a glass transition temperature ($T_g$) at 76.7°C, a melting temperature ($T_m$) at 253.9°C with an onset temperature of 235.6°C, and a crystallization temperature at 138.7°C with an onset temperature of 132.5°C. Generally speaking, the $T_g$ and the $T_m$ of polymers containing aromatic moieties such as phenylene are high when compared with those of polymers derived from aliphatic containing reactants (Seymour and Carraher, 1984). The high $T_g$ and $T_m$ values of PET are the result of the rigidity of the aromatic portion of the polymer. Another stiffening group known as carboxyl group is also present in the structure of PET.

On the other hand, the glass transition temperature of the impact modifier is below the room temperature. For this reason, it was not detected by DSC analysis. The impact modifier (E-MA-GMA) is a semi-crystalline terpolymer with a melting temperature of 68.8°C. Because of the irregularity in its structure, the $T_m$ of E-MA-GMA is lower than the $T_m$ of either of the homopolymers.

As is seen in Table 4.3, the melting temperature ($T_m$) and the glass transition temperature ($T_g$) of all the formulations remain almost the same, the variations are about 2-4°C. This suggests that the incorporation of both clay and impact modifier do not influence much the melting and glass transition behavior of the compositions. However, the highest $T_g$ values are observed for PI-C with 1 wt. % and 3 wt. % clay and All-S with 1 wt. % clay concentration, which are 79.4°C, 79.7°C, and 79.5°C respectively. It is obvious that relative to the pure PET, the composites containing exfoliated clay show higher $T_g$. This finding suggests that PET segments confined within the silicate galleries of the clay tend to retard the segmental motion of the PET matrix (Tseng et al., 2002).

As for the crystallization temperature ($T_c$); all compositions show crystallization peak during heating and the crystallization temperature during heating process decreases by the addition of the clay and impact modifier. For example, the $T_c$ values of PI-C with 1 wt. %, 3 wt. %, and 5 wt. % clay contents are 128.5°C, 122.4°C, and 118.7°C respectively. It is apparent that $T_c$ of PI-C with 1 wt. % clay concentration is about 10°C lower than that of pure PET. The effect of clay content on the crystallization temperature ($T_c$) for all the formulations can clearly be seen in Table 4.3. The influence of addition order on crystallization temperature is not significant as compared with the effect of clay

content. The results on PC and other compositions with clay indicate that the clay has a strong nucleation effect and increases the crystallization rate (Liu et al., 1999). Likewise, results on PI and other compositions with the impact modifier indicate that the impact modifier acts as a nucleating agent and decreases the crystallization temperature of pure PET.

**Table 4.3** Thermal properties of all formulations.

| **Pure PET (not extruded)** | **$T_g$(°C)** | **$T_c$(°C)** | **$T_m$(°C)** |
|---|---|---|---|
| | 76.7 | 138.7 | 253.9 |
| **Impact Modifier (E-MA-GMA)** | | | |
| | <20 | - | 68.8 |
| **PI** | | | |
| **Impact Modifier (wt. %)** | **$T_g$(°C)** | **$T_c$(°C)** | **$T_m$(°C)** |
| 5 | 76.5 | 126.3 | 255.5 |
| 10 | 76.3 | 130.6 | 255.1 |
| 15 | 77.7 | 129.0 | 254.3 |
| 20 | 78.8 | 126.2 | 254.3 |
| **PC** | | | |
| **Clay (wt. %)** | **$T_g$(°C)** | **$T_c$(°C)** | **$T_m$(°C)** |
| 0 | 77.5 | 133.8 | 255.6 |
| 1 | 78.8 | 120.6 | 256.3 |
| 3 | 78.5 | 121.9 | 256.1 |
| 5 | 76.9 | 116.1 | 253.8 |
| **CI-P** | | | |
| **Clay (wt. %)** | **$T_g$(°C)** | **$T_c$(°C)** | **$T_m$(°C)** |
| 1 | 74.6 | 130.4 | 254.9 |
| 3 | 78.1 | 121.0 | 253.9 |
| **PC-I** | | | |
| **Clay (wt. %)** | **$T_g$(°C)** | **$T_c$(°C)** | **$T_m$(°C)** |
| 1 | 77.8 | 126.0 | 257.3 |
| 3 | 74.6 | 119.4 | 253.9 |
| 5 | 76.9 | 116.4 | 255.5 |
| **PI-C** | | | |
| **Clay (wt. %)** | **$T_g$(°C)** | **$T_c$(°C)** | **$T_m$(°C)** |
| 1 | 79.4 | 128.5 | 253.8 |
| 3 | 79.7 | 122.4 | 255.1 |
| 5 | 73.6 | 118.7 | 253.9 |
| **All-S** | | | |
| **Clay (wt. %)** | **$T_g$(°C)** | **$T_c$(°C)** | **$T_m$(°C)** |
| 1 | 79.5 | 126.6 | 257.4 |
| 3 | 74.8 | 123.6 | 254.8 |
| 5 | 78.3 | 122.1 | 256.0 |

# CHAPTER 5

# CONCLUSIONS

In X-ray analysis, for PI-C, CI-P, and All-S sequences with 1 wt. % clay content, no peak was detected by XRD, which suggests that they have an exfoliated structure. PI-C and CI-P with 3 wt. % clay content also displayed an exfoliated structure. X-ray patterns showed that, as the exfoliation increased, the peaks decreased in height and got broader.

Mechanical behavior of PET/E-MA-GMA (PI) blends showed that, energy to fracture in tensile testing increased with increasing E-MA-GMA concentration. Young's modulus and the tensile stress at yield decreased with the addition of the impact modifier. Whereas, the tensile strain at break increased significantly, jumping from 5% for pure PET to 300% for PET with 20 wt. % E-MA-GMA. Additionally, the tensile strength and the tensile stress at yield decreased relatively linearly with E-MA-GMA content. Not only flexural strength values but also flexural moduli of PET/E-MA-GMA blends decreased with E-MA-GMA content.

As for the effect of clay concentration on the mechanical properties of the materials; Young's modulus of PET/clay nanocomposites increased with increasing clay content. However, Young's modulus was greatly influenced by the addition order of PI-C; sharp increase of Young's modulus was observed for very small clay loadings (1 wt. %).

The impact strength of tough nanocomposites was recorded in excess of 254 $kJ/m^2$. The impact values were consistent with the presence or absence of yielding. At 0 wt. % clay content, the impact strength of the PET increased with the addition of E-MA-GMA. At 1 wt. % clay content, the exfoliated structures of CI-P, PI-C and All-S mixing sequences did not break and thus, their impact strength was in excess of 254 $kJ/m^2$. At 3 wt. % clay content, the same was true for the PI-C mixing order. The impact strength of the materials with CI-P and All-

S mixing sequences was still high. However, the impact strength decreased at 5 wt. % clay content.

The tensile strain at break values, on the other hand, were significantly higher at 1 wt. % clay content. While pure PET did not show yielding and fractured at very low strain values, addition of E-MA-GMA resulted in a ductile material that extended to a very high strain after the yield point. At 1 wt. % clay content, the mixing sequences of CI-P, PI-C, and to a degree All-S exhibited yielding followed by elongation to very high strains.

In SEM micrographs, smooth structure of pure PET disappeared when melt blended with E-MA-GMA. The influence of clay concentration looked almost the same in all of the images.

MFI measurements showed that, the MFI of pure PET increased upon extrusion. The MFI of E-MA-GMA was much lower than that of PET under the same load and at the same temperature. Thus, in PI blends; as the impact modifier content increased, the MFI decreased. In addition, clay decreased the MFI of the compositions. Upon addition of E-MA-GMA to PC blends, the MFI decreased. However, this decrease in MFI was not the same for all the mixing sequences. CI-P and PI-C gave the lowest MFI (highest viscosity).

DSC analysis showed that, the melting temperature ($T_m$) and the glass transition temperature ($T_g$) of all formulations remained almost the same. This implied that the incorporation of both clay and impact modifier did not significantly affect the melting and glass transition behavior of the compositions. However, the highest $T_g$ values were observed for PI-C with 1 wt. % and 3 wt. % clay and All-S with 1 wt. % clay concentration, which suggested that relative to pure PET, the composites containing exfoliated clay showed higher $T_g$. The crystallization temperature during heating process decreased by the addition of the clay and impact modifier. Results on PI and other compositions with the impact modifier indicated that, the impact modifier and clay acted as a nucleating agent and decreased the crystallization temperature of pure PET.

# REFERENCES


Alexandre, M., and Dubois, P., 2000. Polymer-Layered Silicate Nanocomposites: Preparation, Properties, and Uses of a New Class of Materials, Materials Science and Engineering, 28, 1-63.

ASTM D256-92, 1993. Standart Test Method for Impact Resistance of Plastics and Electrical Insulating Materials, Annual Book of ASTM Standards, 08.01, 58-74, Philadelphia, PA.

ASTM D638M-91a, 1993. Standart Test Method for Tensile Properties of Plastics, Annual Book of ASTM standards, 08.01, 174-182, Philadelphia, PA.

ASTM D790M-92, 1993. Standart Test Methods for Flexural Properties of Unreinforced and Reinforced Plastics and Electrical Insulating Materials, Annual Book of ASTM standards, 08.01, 284-292, Philadelphia, PA.

ASTM D1238-79, 1993. Standart Test Method for Flow Rates of Thermoplastics by Extrusion Plastometer, Annual Book of ASTM Standards, 08.01, 467-479, Philadelphia, PA.

Beyer, G., 2002. Nanocomposites: a New Class of Flame Retardants for Polymers, Plastics Additives and Compounding, October, 22-28.

Billmeyer, F.W., 1984. Textbook of Polymer Science, 3rd ed., John Wiley and Sons, Inc., NY.

Broutman, L.J., and Krock R.H., 1967. Modern Composite Materials, Addison-Wesley Publishing Company, MA.

Callister, W.D., 1997. Materials Science and Engineering: an Introduction, 4th ed., John Wiley and Sons, Inc., NY.

Chapleau, N., and Huneault, M.A., 2003. Impact Modification of Poly(ethylene terephthalate), Journal of Applied Polymer Science, 90, 2919-2932.

Chazeau, L., Cavaille, J.Y., Canova, G., Dendievel, R., Boutherin, B., 1999. Viscoelastic Properties of Plasticized PVC Reinforced with Cellulose Whiskers, Journal of Applied Polymer Science, 71, 1797-1808.

Chou, N.J., Kowalczyk, S.P., Saraf, R., Tong, H.M., 1994. Characterization of Polymers, Manning Publication, Co., CT.

Concise Encyclopedia of Polymer Science and Engineering, 1990. John Wiley and Sons, Inc., NY.

Davis, C.H., Mathias, L.J., Gilman, J.W., Schiraldi, A., Shields, J.R., Trulove, P., Sutto, T.E., Delong, H.C., 2002. Effects of Melt-Processing Conditions on the Quality of Poly(ethylene terephthalate) Montmorillonite Clay Nanocomposites, Journal of Polymer Science: Part B: Polymer Physics, 40, 2661-2666.

Dennis, H.R., Hunter, D.L., Chang, D., Kim, S., White, J.L., Cho, J.W., Paul, D.R., 2001. Effect of Melt Processing Conditions on the Extent of Exfoliation in Organoclay-Based Nanocomposites, Polymer, 42, 9513-9522.

Encyclopedia of Polymer Science and Technology, 1970. Plastics, Resins, Rubbers, and Fibers, 13, John Wiley and Sons, Inc., NY.

Favier, V., Canova, G.R., Shrivastava, S.C., Cavaille, J.Y., 1997. Mechanical Percolation in Cellulose Whiskers Nanocomposites, Polymer Engineering and Science, 37, 1732-1739.

Fisher, E.G., 1976. Extrusion of Plastics, 3rd ed., Newness-Butterworths, London.

Fukushima, Y., Okada, A., Kawasumi, M., Kurauchi, T., Kamigaito, O., 1988. Swelling Behavior of Montmorillonite by Poly-6-amide, Clay Minerals, 23, 27-34.

Giannelis, E.P., 1996. Polymer Layered Silicate Nanocomposites, Advanced Materials, 8, 29-35.

Giannelis, E.P., 1998. Polymer-Layered Silicate Nanocomposites: Synthesis, Properties and Applications, Applied Organometallic Chemistry, 12, 675-680.

Giannelis, E.P., 1999. Polymer-Layered Silicate Nanocomposites: Emerging Scientific and Commercial Opportunities, Proceedings of 57th SPE Annual Technical Conference (ANTEC), 155, 3966-3968.

Giannelis, E.P., Krishnamoorti, R., Manias, E., 1999. Polymer-Silicate Nanocomposites: Model Systems for Confined Polymers and Polymer Brushes, Advances in Polymer Science, 138, 108-147.

Gibson, R.F., 1994. Principles of Composite Material Mechanics. Mc-Graw Hill, Inc., NY.

Giese, R.F., and Van Oss, C.J., 2002. Colloid and Surface Properties of Clays and Related Minerals, Surfactant Science Series, 105, Marcel Dekker, Inc., NY.

Grubb, D.T., 1974. Review: Radiation Damage and Electron Microscopy of Organic Polymers, Journal of Materials Science, 9, 1715-1736.

Hasegawa, N., Okamoto, H., Kato, M., Usuki, A., 2000. Preparation and Mechanical Properties of Polypropylene-Clay Hybrids Based on Modified Polypropylene and Organophilic Clay, Journal of Applied Polymer Science, 78, 1918-1922.

Herron, N., and Thorn, D.L., 1998. Nanoparticles: Uses and Relationships to Molecular Clusters, Advanced Materials, 10, 1173-1184.

Hert, M., 1992. Tough Thermoplastic Polyesters by Reactive Extrusion with Epoxy-containing Copolymers, Die Angewandte Makromolekulare Chemie, 196, 89-99.

Imai, Y., Nishimura, S., Abe, E., Tateyama, H., Abiko, A., Yamaguchi, A., Aoyama, T., Taguchi, H., 2002. High-Modulus Poly(ethylene terephthalate)/Expandable Fluorine Mica Nanocomposites with a Novel Reactive Compatibilizer, Chemistry of Materials, 14, 477-479.

Kalfoglou, N.K., Skafidas, D.S., Kallitsis, J.K., 1995. Comparison of Compatibilizer Effectiveness for PET/HDPE Blends, Polymer, 36, 4453-4462.

Ke, Y.C., Long, C.F., Qi, Z.N., 1999. Crystallization, Properties, and Crystal and Nanoscale Morphology of PET-Clay Nanocomposites, Journal of Applied Polymer Science, 71, 1139-1146.

Kirk, R.E., and Othmer, D.F., 1995. Encyclopedia of Chemical Technology, 4th ed., John Wiley and Sons, Inc., NY.

Le Baron, P.C., Wang, Z., Pinnavaia, T.J., 1999. Polymer-Layered Silicate Nanocomposites: an Overview, Applied Clay Science, 15, 11-29.

Liu, L., Qi, Z., Zhu, X., 1999. Studies on Nylon 6/Clay Nanocomposites by Melt-Intercalation Process, Journal of Applied Polymer Science, 71, 1133-1138.

Lobo, H., and Bonilla, J.V., 2003. Handbook of Plastics Analysis, Marcel Dekker, Inc., NY.

Loyens, W., and Groeninckx, G., 2002a. Ultimate Mechanical Properties of Rubber Toughened Semicrystalline PET at Room Temperature, Polymer, 43, 5679-5691.

Loyens, W., and Groeninckx, G., 2002b. Phase Morphology Development in Reactively Compatibilised Polyethylene Terephthalate/Elastomer Blends, Macromolecular Chemistry and Physics, 203, 1702-1714.

Manias, E., Touny, A., Wu, L., Strawhecker, K., Lu, B., Chung, T.C., 2001. Polypropylene/Montmorillonite Nanocomposites. Review of the Synthetic Routes and Materials Properties, Chemistry of Materials, 13, 3516-3523.

Mark, J.E., 1996. Ceramic Reinforced Polymers and Polymer-Modified Ceramics, Polymer Engineering and Science, 36, 2905-2920.

Morton-Jones, D.H., 1989. Polymer Processing, Chapman and Hall, Inc., NY.

Nielsen, L.E., Landel, R.F., 1994. Mechanical Properties of Polymers and Composites, 2nd ed., Marcel Dekker, Inc., NY.

Pinnavaia, T.J., and Beall, G.W., 2000. Polymer-Clay Nanocomposites, John Wiley and Sons, Inc., Chichester, England.

Polymeric Materials Encyclopedia, 1996. Vol. 8, CRC Press, Inc., NY.

Rosen, S.L., 1993. Fundamental Principles of Polymeric Materials, 2nd ed., John Wiley and Sons, Inc., NY.

Sawyer, L.C., and Grubb, D.T., 1987. Polymer Microscopy, Chapman and Hall, Inc., NY.

Schmidt, D., Shah, D., Giannelis, E.P., 2002. New Advances in Polymer/Layered Silicate Nanocomposites, Current Opinion in Solid State and Materials Science, 6, 205-212.

Schwartz, M.M., 1997. Composite Materials: Processing, Fabrication, and Applications, Prentice-Hall, Inc., NJ.

Seymour, R.B., and Carraher, C.E., 1984. Structure-Property Relationships in Polymers, Plenum Press, NY.

Seymour, R.B., and Deanin, R.D., 1987. History of Polymeric Composites, Proceedings of 192nd ACS National Meeting, VNU Science Press, Utrecht, The Netherlands.

Sherman, L.M., 1999. Nanocomposites- a Little Goes a Long Way, Plastics Technology, 45, 52-57.

Sinha Ray, S., and Okamoto, M., 2003. Polymer/Layered Silicate Nanocomposites: a Review from Preparation to Processing, Progress in Polymer Science, 28, 1539-1641.

Solomons, T.W.G., 1996. Organic Chemistry, 6th ed., John Wiley and Sons, Inc., NY.

Sperling, L.H., 1997. Polymeric Multicomponent Materials, an Introduction, John Wiley and Sons, Inc., NY.

Strong, A.B., 1996. Plastics: Materials and Processing, Prentice-Hall, Inc., NJ.

Tsai, T.Y., Hwang, C.L., Lee, S.Y., 2000. A Fresh Approach of Modified Clays for Polymer/Clay Nanocomposites, Proceedings of 58th SPE Annual Technical Conference (ANTEC), 248, 2412-2415.

Tseng, C.R., Wu, J.Y., Lee, H.Y., Chang, F.C., 2002. Preparation and Characterization of Polystyrene-Clay Nanocomposites by Free-Radical Polymerization, Journal of Applied Polymer Science, 85, 1370-1377.

Ullmann's Encyclopedia of Industrial Chemistry, 1992. 5th Ed. Vol A20, VCH Publishers, NY.

Vaia, R.A., Ishii, H., Giannelis, E.P., 1993. Synthesis and Properties of Two-Dimensional Nanostructures by Direct Intercalation of Polymer Melts in Layered Silicates, Chemistry of Materials, 5, 1694-1696.

Vaia, R.A., Klaus, D.J., Kramer, E.J., 1995. Kinetics of Polymer Melt Intercalation, Macromolecules, 28, 8080-8085.

Vaia, R.A., Jandt, K.D., Kramer, E.J., Giannelis E.P., 1996. Microstructural Evolution of Melt Intercalated Polymer-Organically Modified Layered Silicates Nanocomposites, Chemistry of Materials, 8, 2628-2635.

Watson, E.S., O'Neill, M.J., Justin, J., Brenner, N., 1964. A Differential Scanning Calorimeter for Quantitative Differential Thermal Analysis, Analytical Chemistry, 36, 1233-1238.

Xanthos, M., and Dagli, S.S., 1991. Compatibilization of Polymer Blends by Reactive Processing, Polymer Engineering and Science, 31, 929-935.

Xianbo, H., and Lesser, A.J., 2003. Effect of a Silicate Filler on the Crystal Morphology of Poly(trimethylene terephthalate)/Clay Nanocomposites, Journal of Polymer Science: Part B: Polymer Physics, 41, 2275–2289.

Yoon, J.T., Jo, W.H., Lee, M.S., Ko, M.B., 2001. Effects of Comonomers and Shear on the Melt Intercalation of Styrenics/Clay Nanocomposites. Polymer, 42, 329-336.

# APPENDIX A

## Mechanical Testing Results

**Table A.1** Arithmetic means and standard deviations of Young's modulus values for all formulations.

| **Pure PET (not extruded)** | **Young's Modulus (MPa)** | **Stdev** |
|---|---|---|
| | 1155 | 19.3 |
| **PI** | | |
| **Impact Modifier (wt. %)** | **Young's Modulus (MPa)** | **Stdev** |
| 5 | 909 | 18.9 |
| 10 | 832 | 24.9 |
| 15 | 725 | 7.5 |
| 20 | 619 | 13.4 |
| **PC** | | |
| **Clay (wt. %)** | **Young's Modulus (MPa)** | **Stdev** |
| 0 | 994 | 72.0 |
| 1 | 1014 | 41.1 |
| 3 | 1144 | 100.0 |
| 5 | 1253 | 42.2 |
| **CI-P** | | |
| **Clay (wt. %)** | **Young's Modulus (MPa)** | **Stdev** |
| 1 | 1187 | 49.0 |
| 3 | 977 | 46.0 |
| **PC-I** | | |
| **Clay (wt. %)** | **Young's Modulus (MPa)** | **Stdev** |
| 1 | 1097 | 38.7 |
| 3 | 923 | 17.7 |
| 5 | 716 | 19.5 |

**Table A.1 (Cont'd).**

| PI-C | | |
|---|---|---|
| **Clay (wt. %)** | **Young's Modulus (MPa)** | **Stdev** |
| 1 | 1563 | 121.7 |
| 3 | 1696 | 65.7 |
| 5 | 1923 | 41.3 |
| **All-S** | | |
| **Clay (wt. %)** | **Young's Modulus (MPa)** | **Stdev** |
| 1 | 1113 | 29.3 |
| 3 | 1197 | 46.6 |
| 5 | 1098 | 44.6 |

**Table A.2** Arithmetic means and standard deviations of tensile strength values for all formulations.

| **Pure PET (not extruded)** | **Tensile Strength (MPa)** | **Stdev** |
|---|---|---|
| | 49.1 | 1.33 |
| **PI** | | |
| **Impact Modifier (wt. %)** | **Tensile Strength (MPa)** | **Stdev** |
| 5 | 43.7 | 0.29 |
| 10 | 38.6 | 1.11 |
| 15 | 36.3 | 1.62 |
| 20 | 30.3 | 0.82 |
| **PC** | | |
| **Clay (wt. %)** | **Tensile Strength (MPa)** | **Stdev** |
| 0 | 47.7 | 0.72 |
| 1 | 51.3 | 0.44 |
| 3 | 52.6 | 1.42 |
| 5 | 43.5 | 5.31 |
| **CI-P** | | |
| **Clay (wt. %)** | **Tensile Strength (MPa)** | **Stdev** |
| 1 | 45.5 | 0.73 |
| 3 | 42.5 | 0.25 |
| **PC-I** | | |
| **Clay (wt. %)** | **Tensile Strength (MPa)** | **Stdev** |
| 1 | 42.6 | 2.52 |
| 3 | 44.9 | 1.60 |
| 5 | 34.3 | 3.44 |
| **PI-C** | | |
| **Clay (wt. %)** | **Tensile Strength (MPa)** | **Stdev** |
| 1 | 43.7 | 0.08 |
| 3 | 46.8 | 0.15 |
| 5 | 39.4 | 5.34 |
| **All-S** | | |
| **Clay (wt. %)** | **Tensile Strength (MPa)** | **Stdev** |
| 1 | 47.0 | 0.33 |
| 3 | 45.0 | 4.41 |
| 5 | 46.8 | 1.25 |

**Table A.3** Arithmetic means and standard deviations of tensile stress at yield values for all formulations.

| **Pure PET (not extruded)** | **Tensile Stress at Yield (MPa)** | **Stdev** |
|---|---|---|
| | no yield | - |
| **PI** | | |
| **Impact Modifier (wt. %)** | **Tensile Stress at Yield (MPa)** | **Stdev** |
| 5 | 43.7 | 0.29 |
| 10 | 35.8 | 0.31 |
| 15 | 31.2 | 0.33 |
| 20 | 27.4 | 0.14 |
| **PC** | | |
| **Clay (wt. %)** | **Tensile Stress at Yield (MPa)** | **Stdev** |
| 0 | no yield | - |
| 1 | no yield | - |
| 3 | no yield | - |
| 5 | no yield | - |
| **CI-P** | | |
| **Clay (wt. %)** | **Tensile Stress at Yield (MPa)** | **Stdev** |
| 1 | 45.5 | 0.73 |
| 3 | 42.5 | 0.25 |
| **PC-I** | | |
| **Clay (wt. %)** | **Tensile Stress at Yield (MPa)** | **Stdev** |
| 1 | 42.6 | 2.52 |
| 3 | 44.9 | 1.60 |
| 5 | no yield | - |
| **PI-C** | | |
| **Clay (wt. %)** | **Tensile Stress at Yield (MPa)** | **Stdev** |
| 1 | 43.7 | 0.08 |
| 3 | 46.8 | 0.15 |
| 5 | no yield | - |
| **All-S** | | |
| **Clay (wt. %)** | **Tensile Stress at Yield (MPa)** | **Stdev** |
| 1 | 47.0 | 0.33 |
| 3 | no yield | - |
| 5 | no yield | - |

**Table A.4** Arithmetic means and standard deviations of tensile strain at break values for all formulations.

| **Pure PET (not extruded)** | **Tensile Strain at Break (%)** | **Stdev** |
|---|---|---|
| | 5.7 | 0.59 |
| **PI** | | |
| **Impact Modifier (wt. %)** | **Tensile Strain at Break (%)** | **Stdev** |
| 5 | 133.1 | 13.73 |
| 10 | 226.3 | 12.63 |
| 15 | 239.5 | 8.66 |
| 20 | 264.5 | 17.47 |
| **PC** | | |
| **Clay (wt. %)** | **Tensile Strain at Break (%)** | **Stdev** |
| 0 | 4.5 | 0.40 |
| 1 | 5.4 | 0.55 |
| 3 | 7.5 | 0.43 |
| 5 | 5.8 | 0.51 |
| **CI-P** | | |
| **Clay (wt. %)** | **Tensile Strain at Break (%)** | **Stdev** |
| 1 | 266.2 | 0.14 |
| 3 | 7.8 | 1.15 |
| **PC-I** | | |
| **Clay (wt. %)** | **Tensile Strain at Break (%)** | **Stdev** |
| 1 | 44.0 | 46.21 |
| 3 | 12.6 | 3.84 |
| 5 | 5.4 | 0.81 |
| **PI-C** | | |
| **Clay (wt. %)** | **Tensile Strain at Break (%)** | **Stdev** |
| 1 | 287.0 | 7.19 |
| 3 | 26.8 | 6.02 |
| 5 | 4.2 | 0.62 |
| **All-S** | | |
| **Clay (wt. %)** | **Tensile Strain at Break (%)** | **Stdev** |
| 1 | 188.3 | 0.22 |
| 3 | 6.5 | 1.90 |
| 5 | 6.2 | 0.84 |

**Table A.5** Arithmetic means and standard deviations of flexural modulus values for all formulations.

| **Pure PET (not extruded)** | **Flexural Modulus (MPa)** | **Stdev** |
|---|---|---|
| | 2523 | 29.4 |
| **PI** | | |
| **Impact Modifier (wt. %)** | **Flexural Modulus (MPa)** | **Stdev** |
| 5 | 2125 | 51.7 |
| 10 | 1648 | 24.5 |
| 15 | 1420 | 43.3 |
| 20 | 1198 | 19.9 |
| **PC** | | |
| **Clay (wt. %)** | **Flexural Modulus (MPa)** | **Stdev** |
| 0 | 2202 | 80.8 |
| 1 | 2284 | 26.6 |
| 3 | 2479 | 49.8 |
| 5 | 2662 | 11.0 |
| **CI-P** | | |
| **Clay (wt. %)** | **Flexural Modulus (MPa)** | **Stdev** |
| 1 | 1964 | 42.2 |
| 3 | 1704 | 11.2 |
| **PC-I** | | |
| **Clay (wt. %)** | **Flexural Modulus (MPa)** | **Stdev** |
| 1 | 2223 | 39.6 |
| 3 | 2156 | 83.3 |
| 5 | 2487 | 92.7 |
| **PI-C** | | |
| **Clay (wt. %)** | **Flexural Modulus (MPa)** | **Stdev** |
| 1 | 2109 | 36.6 |
| 3 | 2331 | 20.4 |
| 5 | 2718 | 29.8 |
| **All-S** | | |
| **Clay (wt. %)** | **Flexural Modulus (MPa)** | **Stdev** |
| 1 | 2152 | 31.8 |
| 3 | 2264 | 29.0 |
| 5 | 2317 | 40.9 |

**Table A.6** Arithmetic means and standard deviations of flexural strength values for all formulations.

| **Pure PET (not extruded)** | **Flexural Strength (MPa)** | **Stdev** |
|---|---|---|
| | 77.9 | 1.38 |
| **PI** | | |
| **Impact Modifier (wt. %)** | **Flexural Strength (MPa)** | **Stdev** |
| 5 | 66.6 | 0.43 |
| 10 | 50.6 | 0.45 |
| 15 | 44.4 | 0.43 |
| 20 | 37.7 | 0.41 |
| **PC** | | |
| **Clay (wt. %)** | **Flexural Strength (MPa)** | **Stdev** |
| 0 | 67.9 | 1.38 |
| 1 | 70.4 | 0.55 |
| 3 | 73.3 | 1.58 |
| 5 | 75.7 | 0.77 |
| **CI-P** | | |
| **Clay (wt. %)** | **Flexural Strength (MPa)** | **Stdev** |
| 1 | 60.5 | 0.53 |
| 3 | 53.7 | 0.56 |
| **PC-I** | | |
| **Clay (wt. %)** | **Flexural Strength (MPa)** | **Stdev** |
| 1 | 68.3 | 0.53 |
| 3 | 62.9 | 0.98 |
| 5 | 67.6 | 1.30 |
| **PI-C** | | |
| **Clay (wt. %)** | **Flexural Strength (MPa)** | **Stdev** |
| 1 | 61.4 | 0.85 |
| 3 | 64.3 | 0.20 |
| 5 | 69.5 | 0.72 |
| **All-S** | | |
| **Clay (wt. %)** | **Flexural Strength (MPa)** | **Stdev** |
| 1 | 65.5 | 0.57 |
| 3 | 66.1 | 0.87 |
| 5 | 65.2 | 0.95 |

**Table A.7** Arithmetic means and standard deviations of impact strength values for all formulations.

| **Pure PET (not extruded)** | **Impact Strength (kJ/m$^2$)** | **Stdev** |
|---|---|---|
| | 24.3 | 3.12 |
| **PI** | | |
| **Impact Modifier (wt. %)** | **Impact Strength (kJ/m$^2$)** | **Stdev** |
| 5 | 30.5 | 6.15 |
| 10 | no break (>254) | - |
| 15 | no break (>254) | - |
| 20 | no break (>254) | - |
| **PC** | | |
| **Clay (wt. %)** | **Impact Strength (kJ/m$^2$)** | **Stdev** |
| 0 | 17.9 | 2.44 |
| 1 | 12.2 | 2.94 |
| 3 | 9.0 | 1.03 |
| 5 | 9.3 | 0.77 |
| **CI-P** | | |
| **Clay (wt. %)** | **Impact Strength (kJ/m$^2$)** | **Stdev** |
| 1 | no break (>254) | - |
| 3 | 43.1 | 3.17 |
| **PC-I** | | |
| **Clay (wt. %)** | **Impact Strength (kJ/m$^2$)** | **Stdev** |
| 1 | 11 | 4.61 |
| 3 | 10.8 | 3.47 |
| 5 | 11.3 | 3.80 |
| **PI-C** | | |
| **Clay (wt. %)** | **Impact Strength (kJ/m$^2$)** | **Stdev** |
| 1 | no break (>254) | - |
| 3 | no break (>254) | - |
| 5 | 26.5 | 2.38 |
| **All-S** | | |
| **Clay (wt. %)** | **Impact Strength (kJ/m$^2$)** | **Stdev** |
| 1 | no break (>254) | - |
| 3 | 78.7 | 4.78 |
| 5 | 52.3 | 4.76 |

# APPENDIX B

## DSC Thermograms

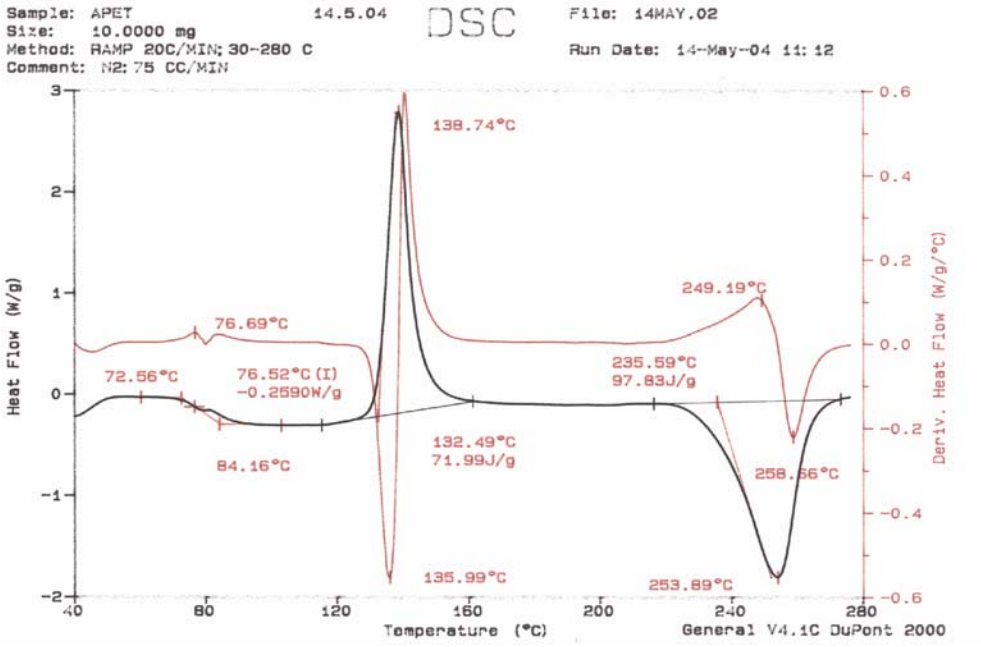


**Figure B.1** DSC thermogram of not extruded, pure PET.

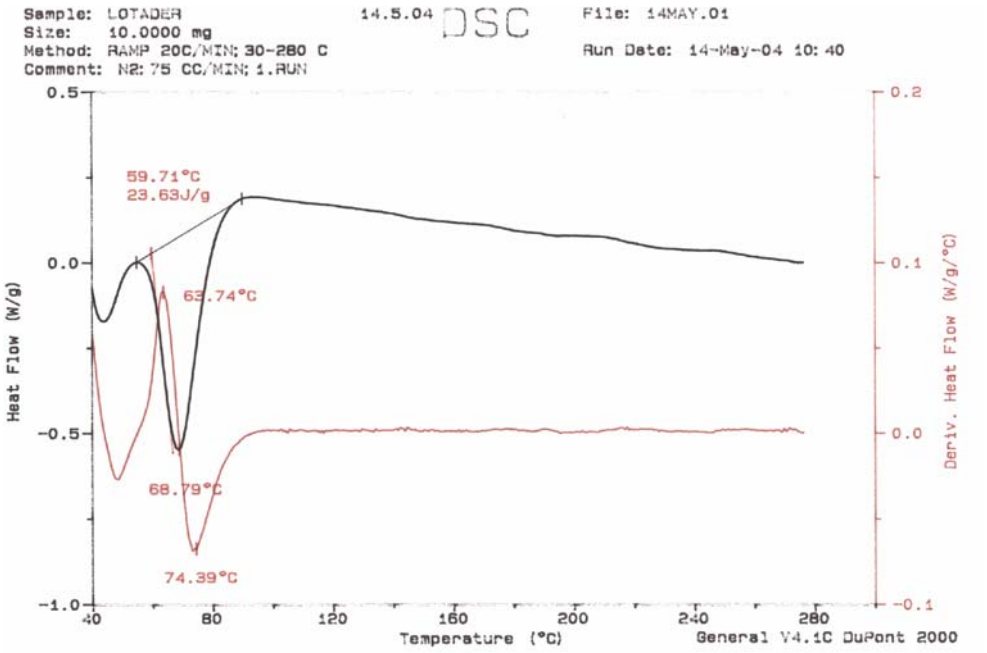


**Figure B.2** DSC thermogram of impact modifier (E-MA-GMA).

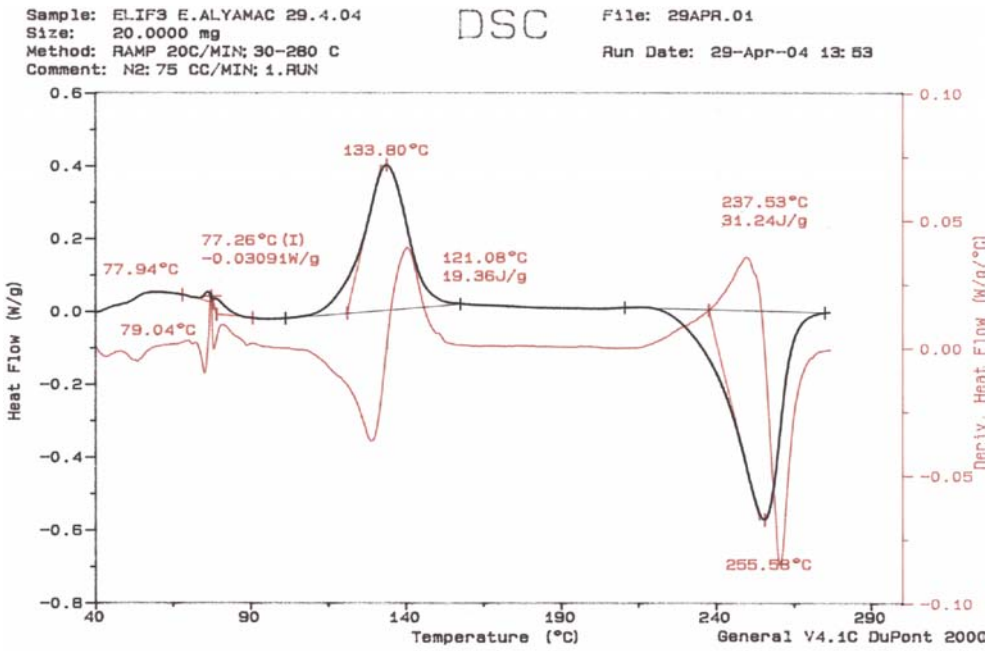


**Figure B.3** DSC thermogram of double extruded PET.

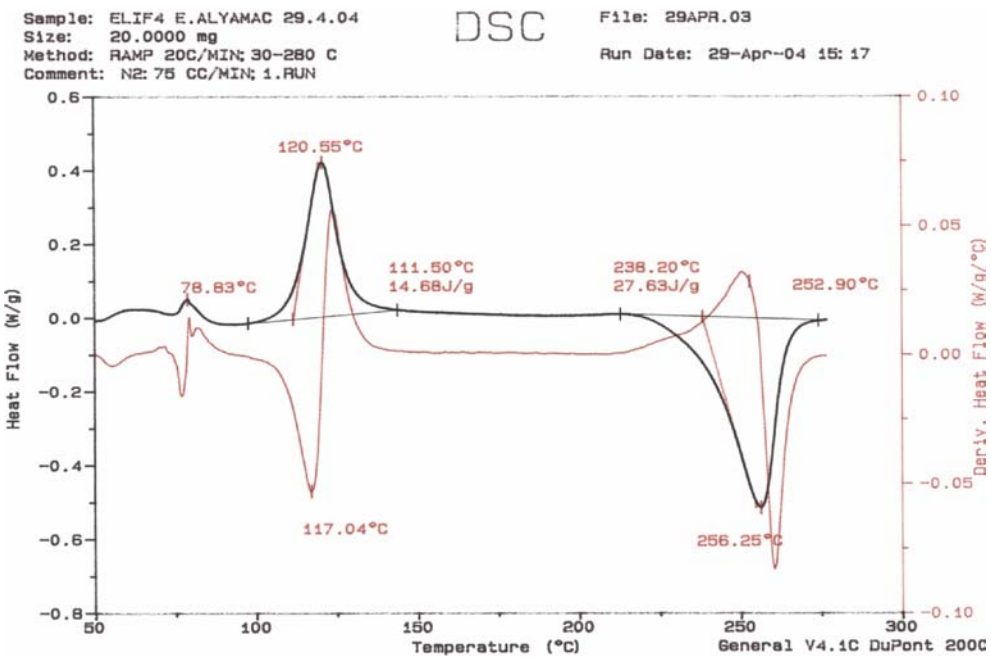


**Figure B.4** DSC thermogram of PC with 1 wt. % clay content.

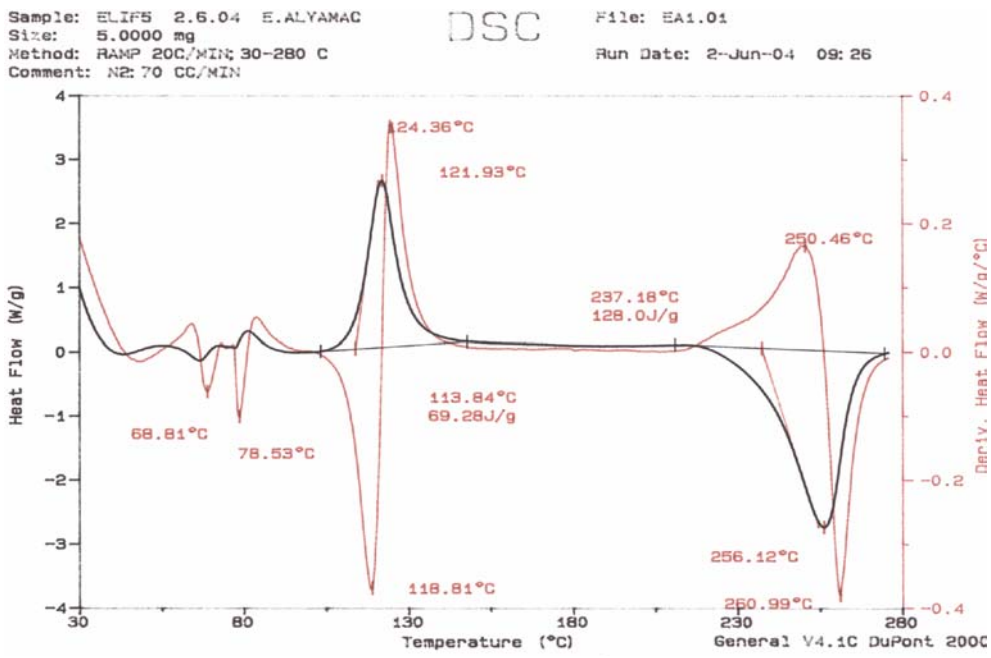


**Figure B.5** DSC thermogram of PC with 3 wt. % clay content.

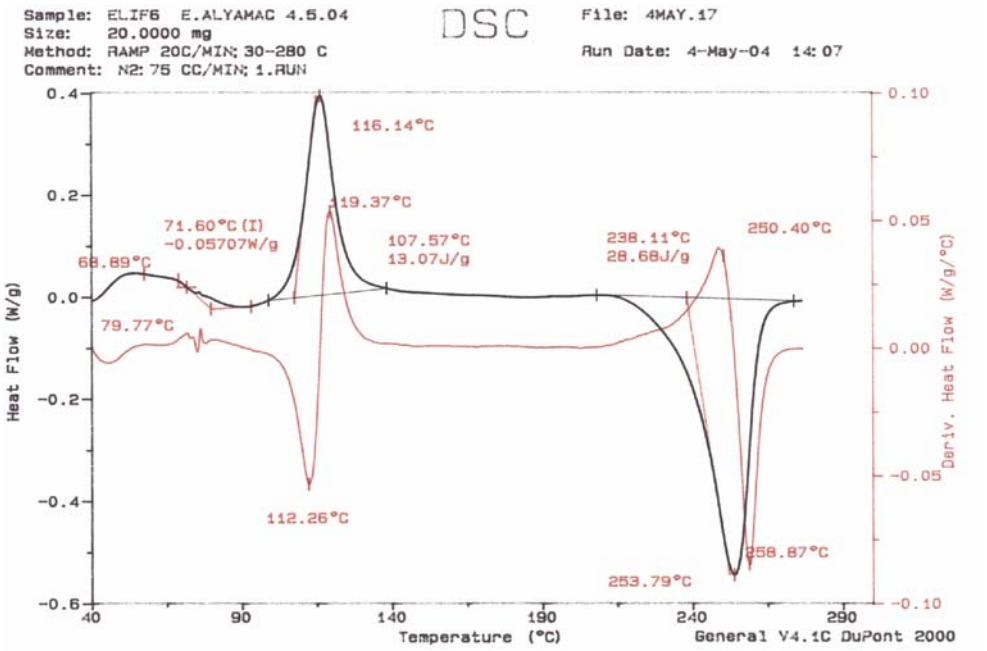


**Figure B.6** DSC thermogram of PC with 5 wt. % clay content.

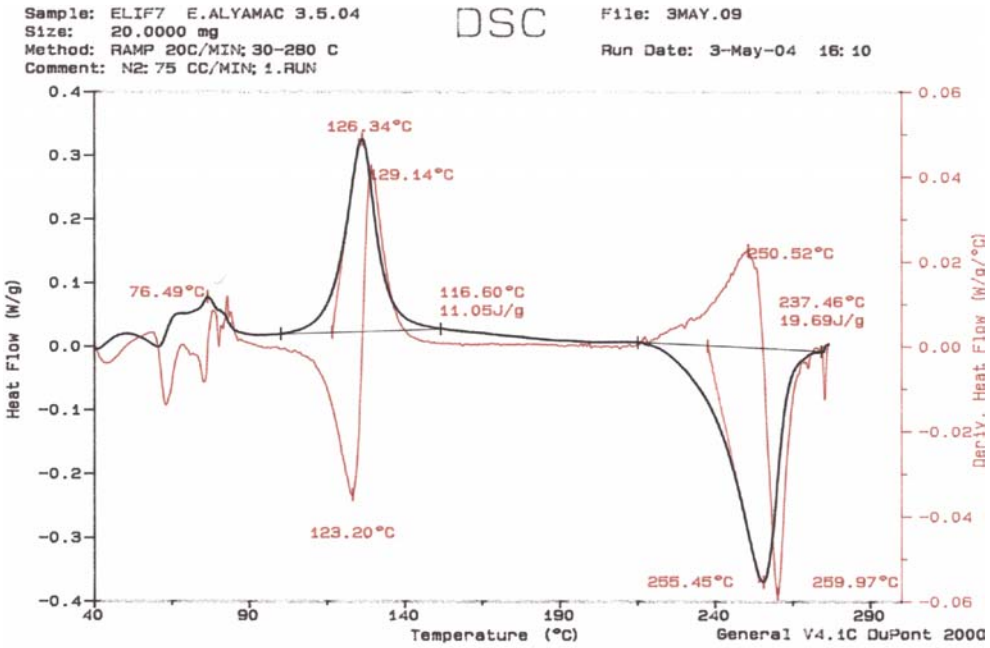


**Figure B.7** DSC thermogram of PI with 5 wt. % E-MA-GMA content.

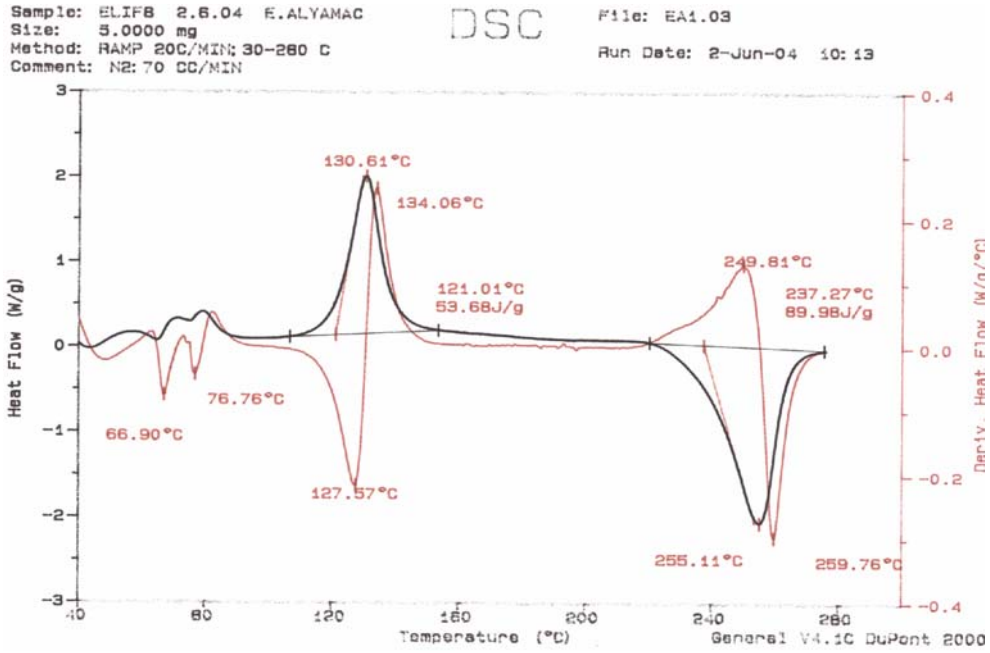


**Figure B.8** DSC thermogram of PI with 10 wt. % E-MA-GMA content.

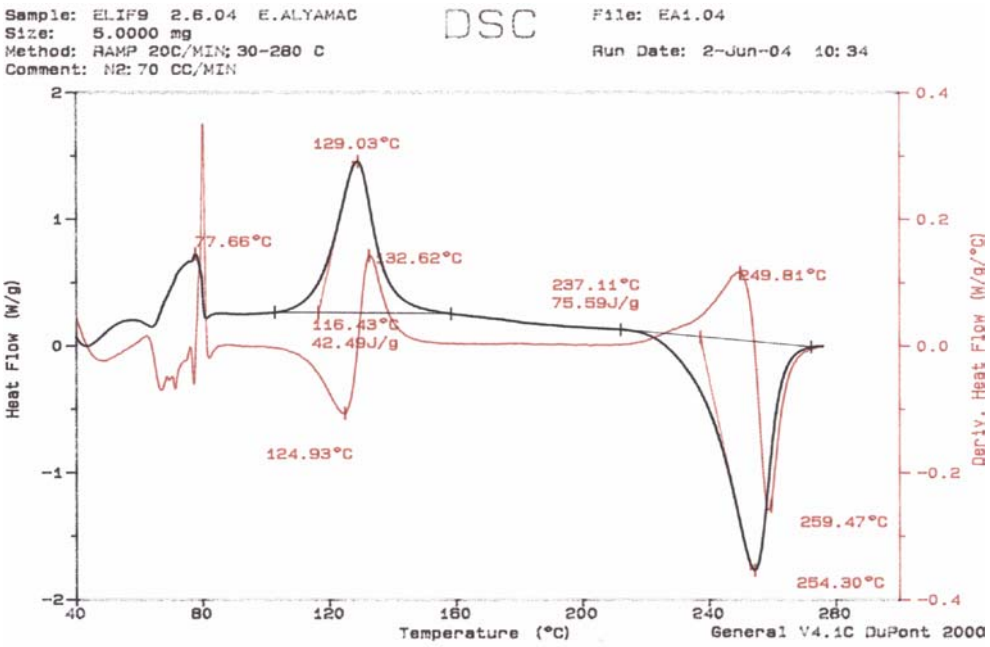


**Figure B.9** DSC thermogram of PI with 15 wt. % E-MA-GMA content.

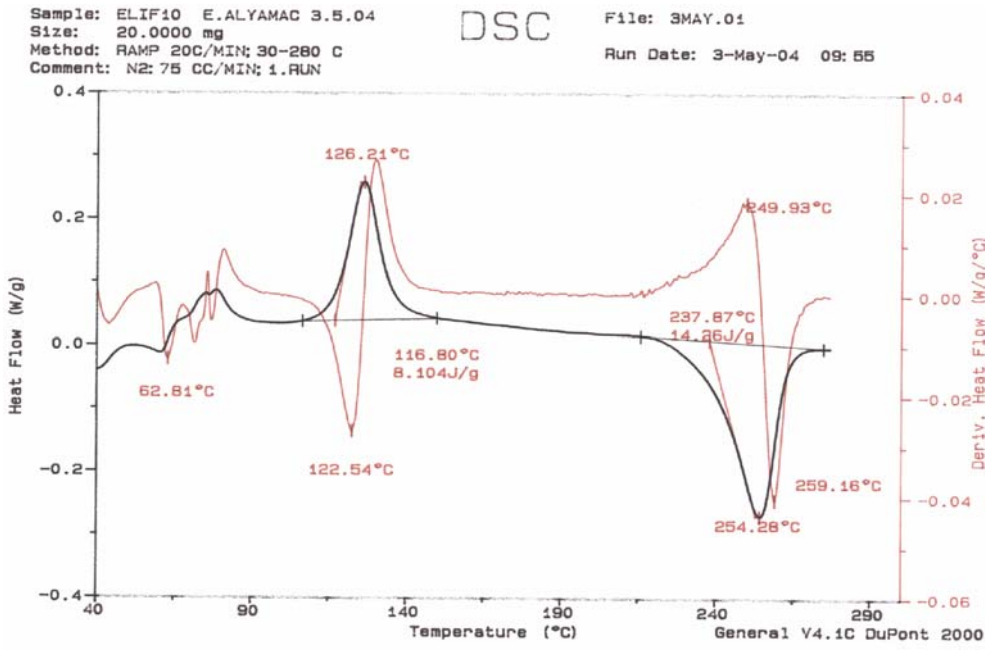


**Figure B.10** DSC thermogram of PI with 20 wt. % E-MA-GMA content.

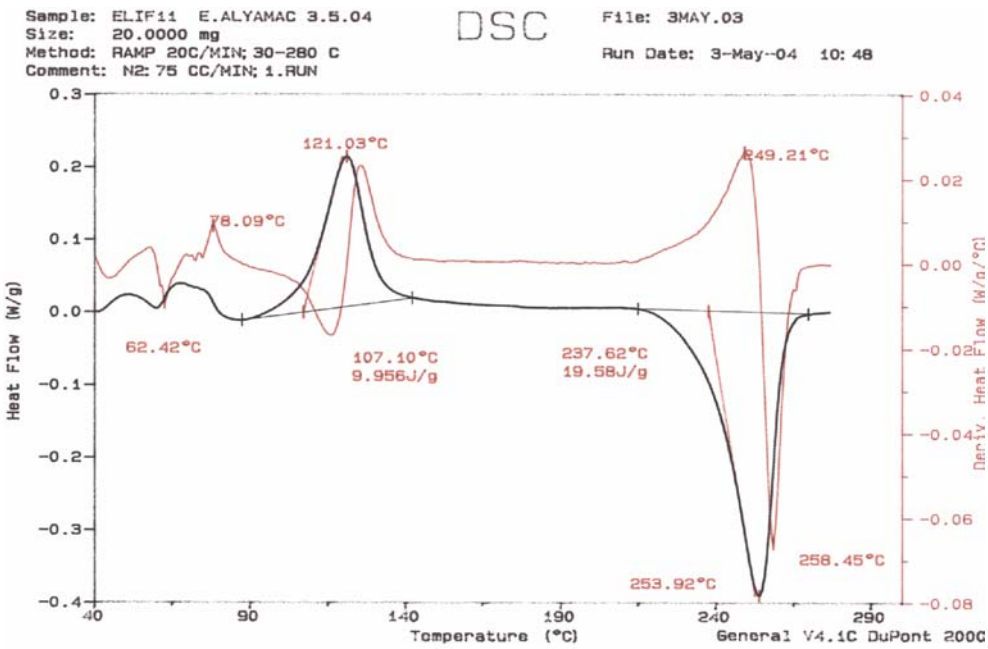


**Figure B.11** DSC thermogram of CI-P with 1 wt. % clay content.

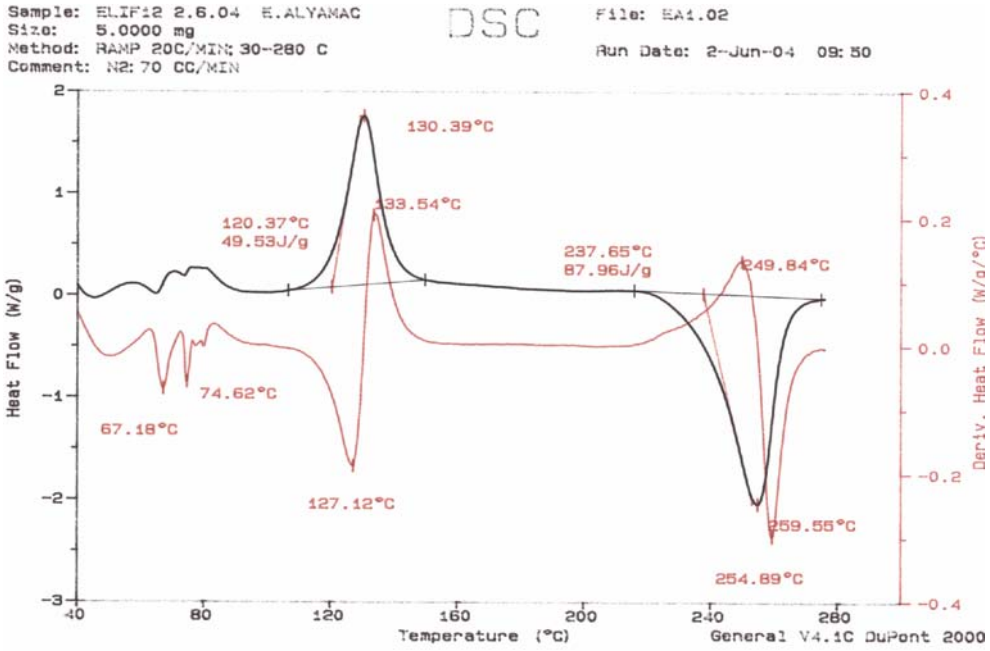


**Figure B.12** DSC thermogram of CI-P with 3 wt. % clay content.

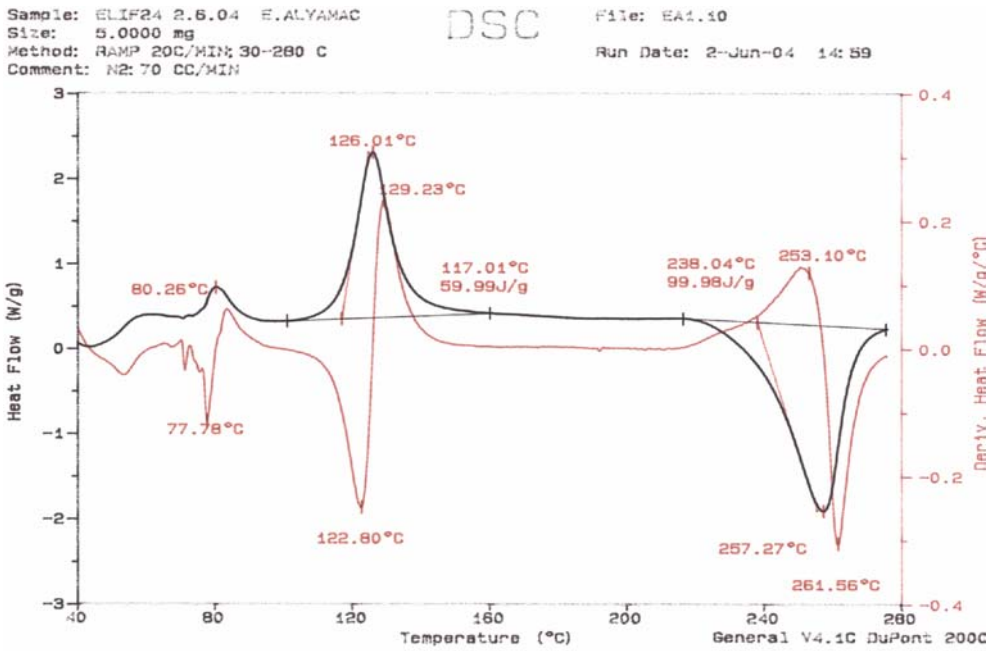


**Figure B.13** DSC thermogram of PC-I with 1 wt. % clay content.

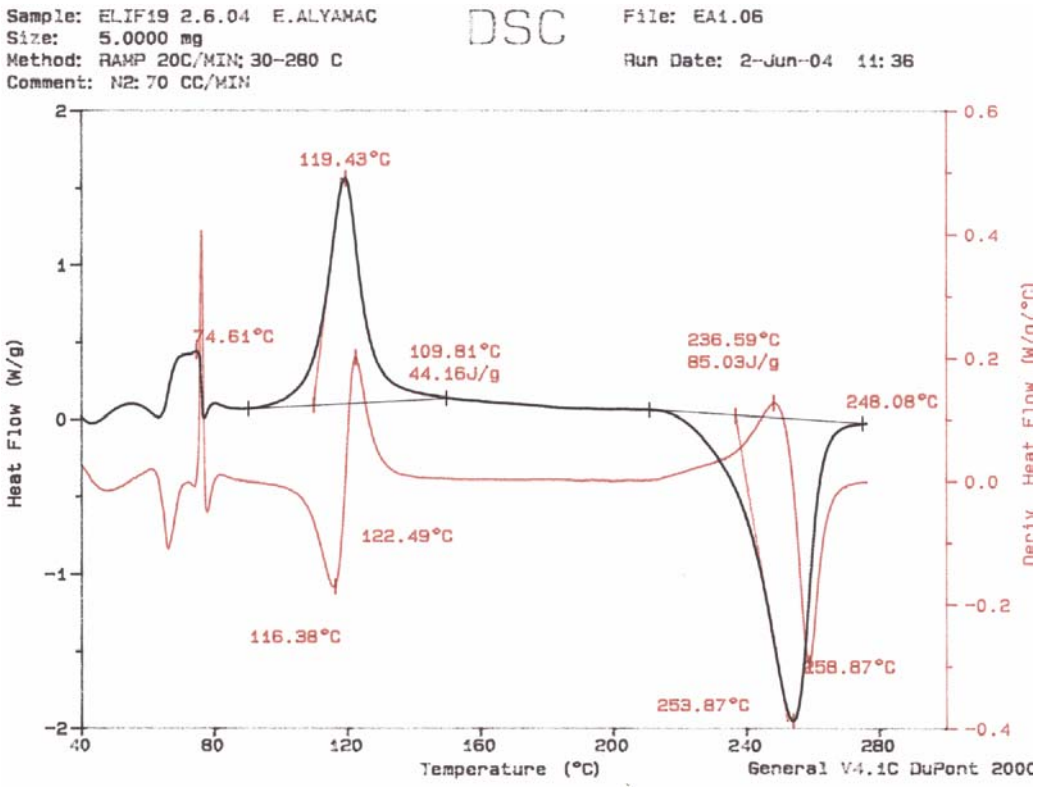


**Figure B.14** DSC thermogram of PC-I with 3 wt. % clay content.

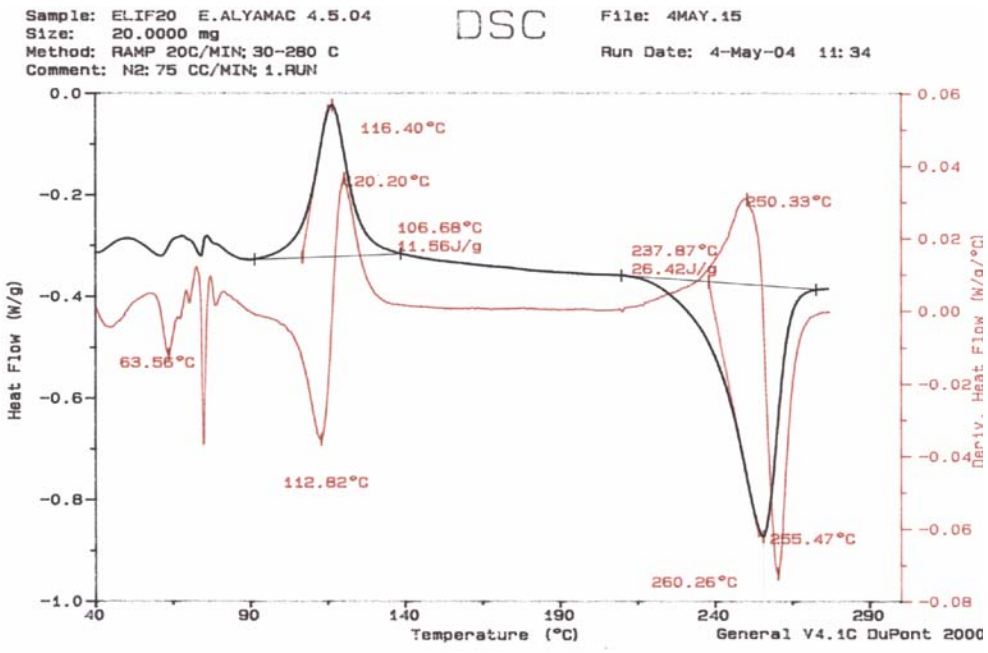


**Figure B.15** DSC thermogram of PC-I with 5 wt. % clay content.

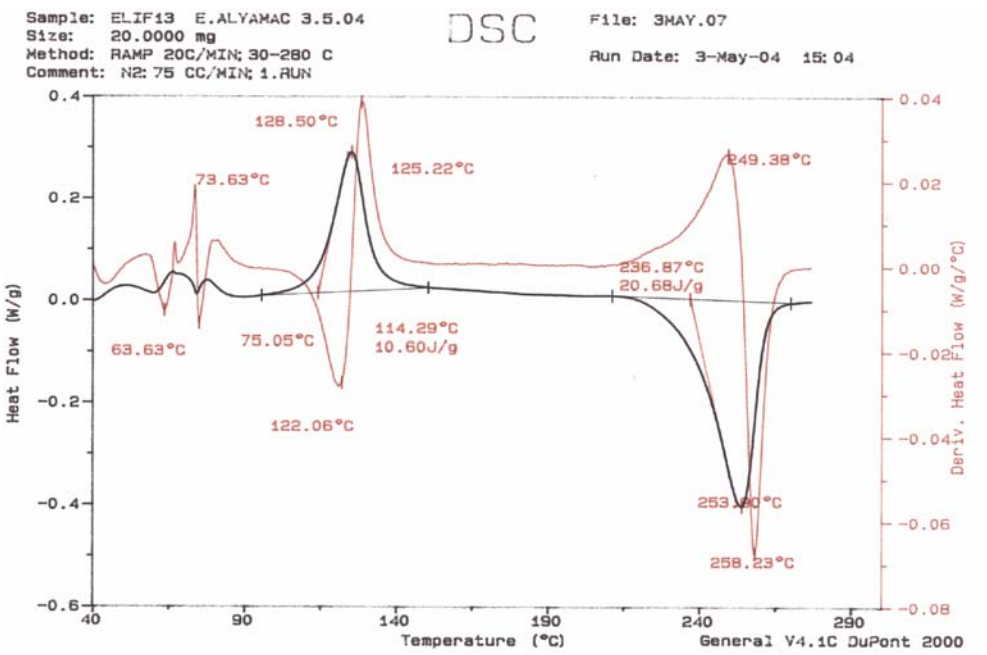


**Figure B.16** DSC thermogram of PI-C with 1 wt. % clay content.

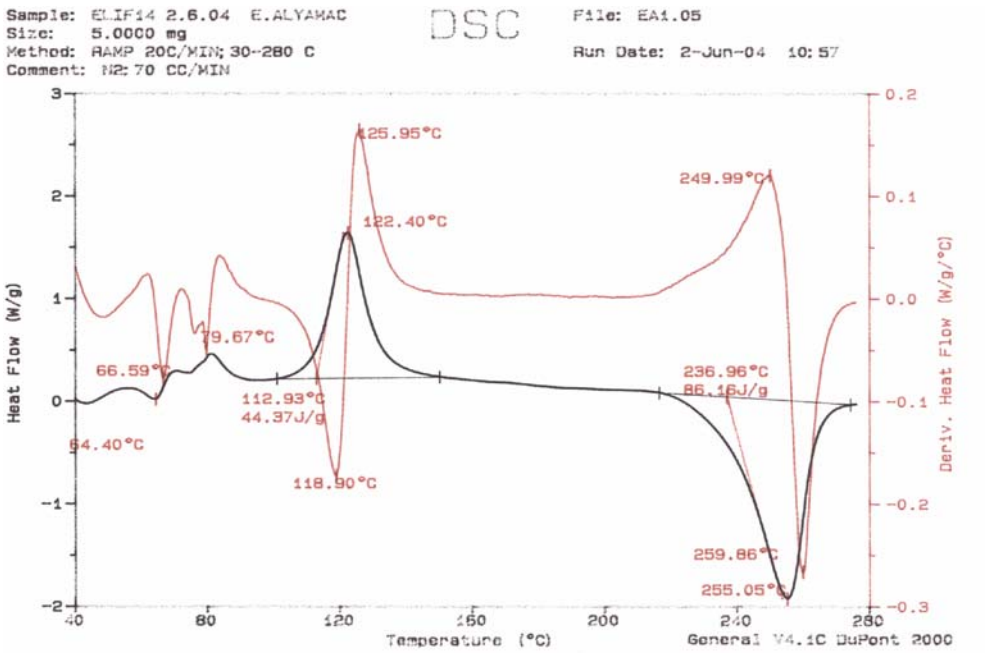


**Figure B.17** DSC thermogram of PI-C with 3 wt. % clay content.

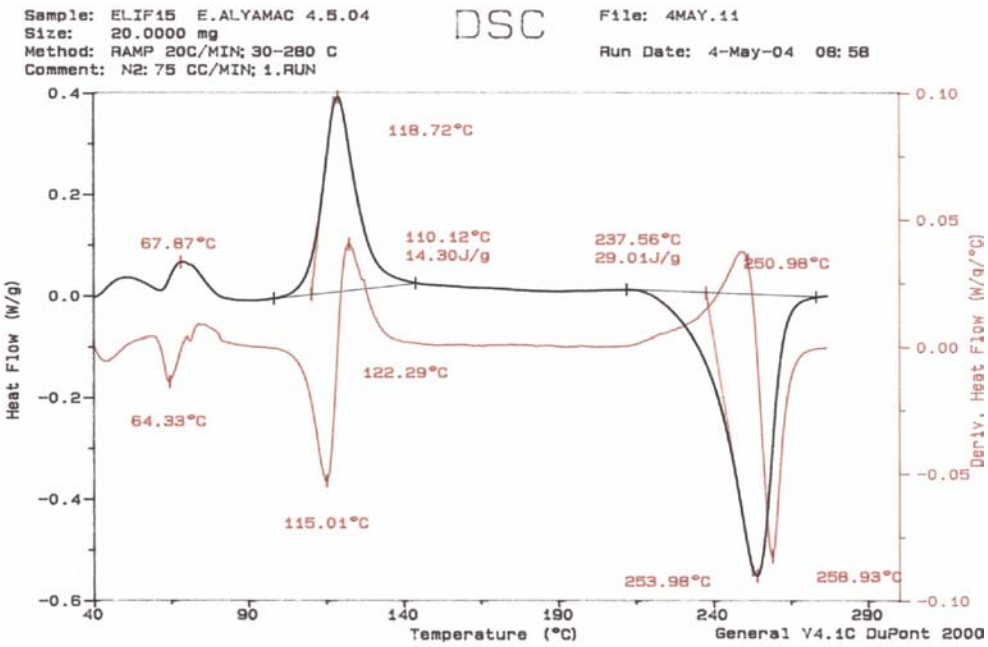


**Figure B.18** DSC thermogram of PI-C with 5 wt. % clay content.

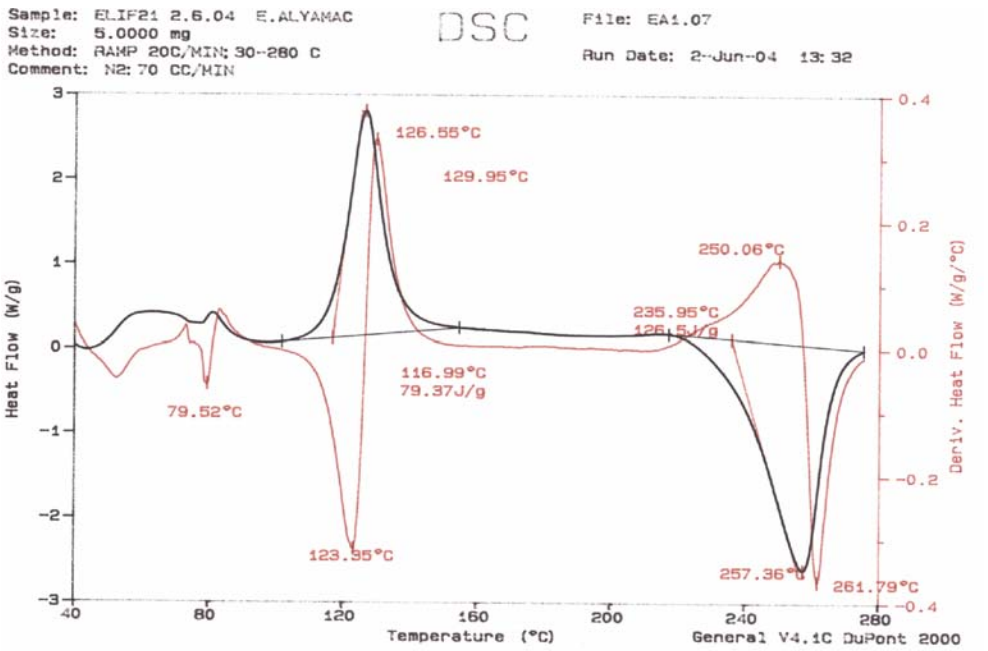


**Figure B.19** DSC thermogram of All-S with 1 wt. % clay content.

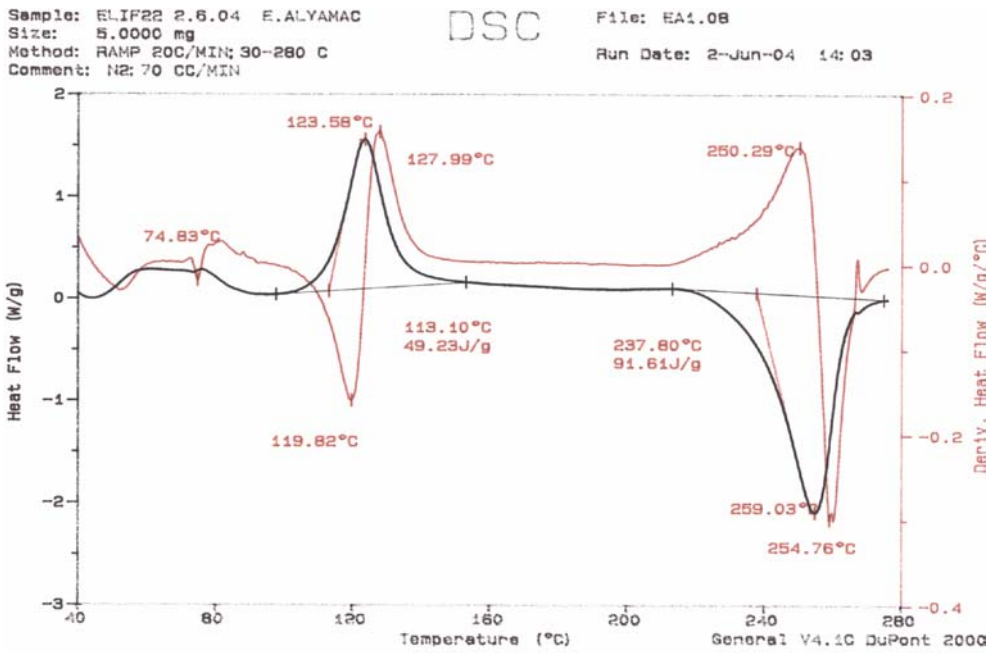


**Figure B.20** DSC thermogram of All-S with 3 wt. % clay content.

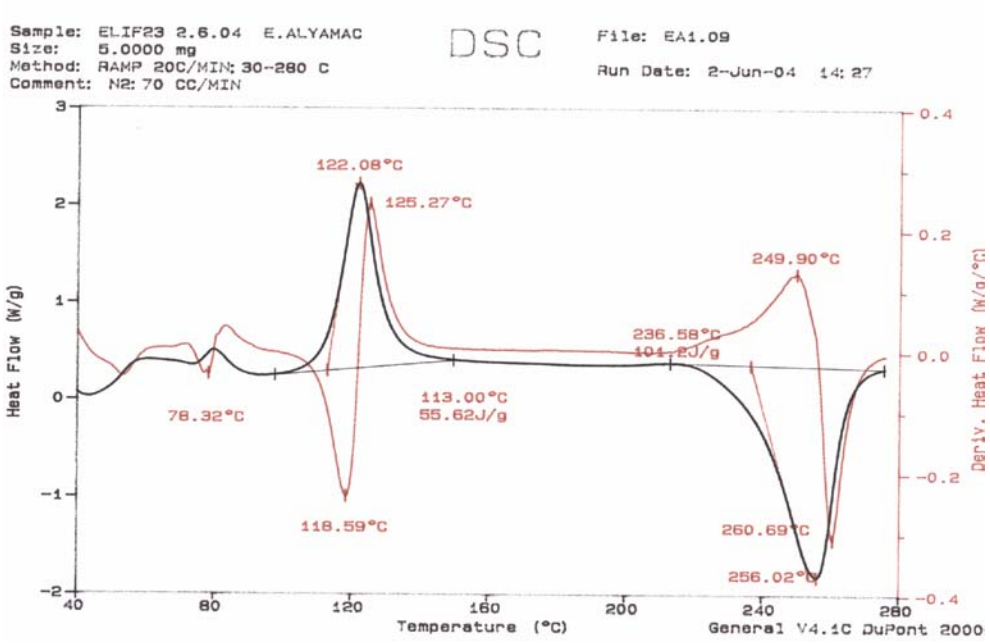


**Figure B.21** DSC thermogram of All-S with 5 wt. % clay content

# APPENDIX C

## X-Ray Diffraction Patterns

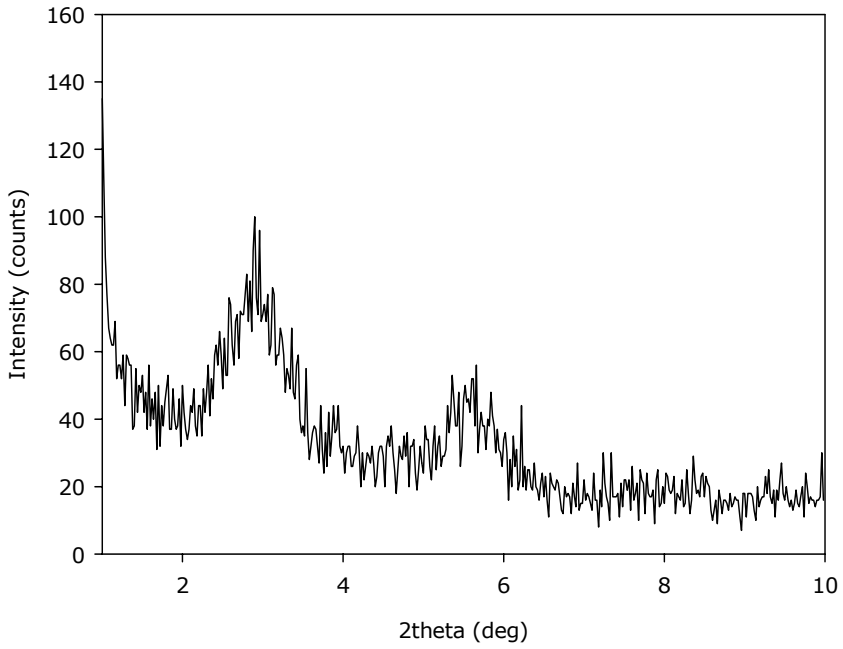


**Figure C.1** X-ray diffraction patterns of PC with 1 wt. % clay content.

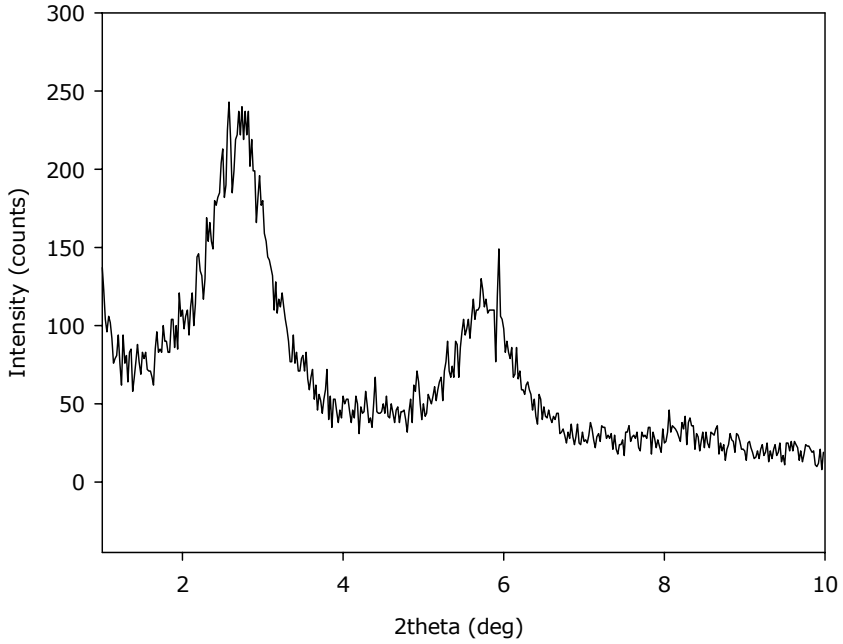


**Figure C.2** X-ray diffraction patterns of PC with 3 wt. % clay content.

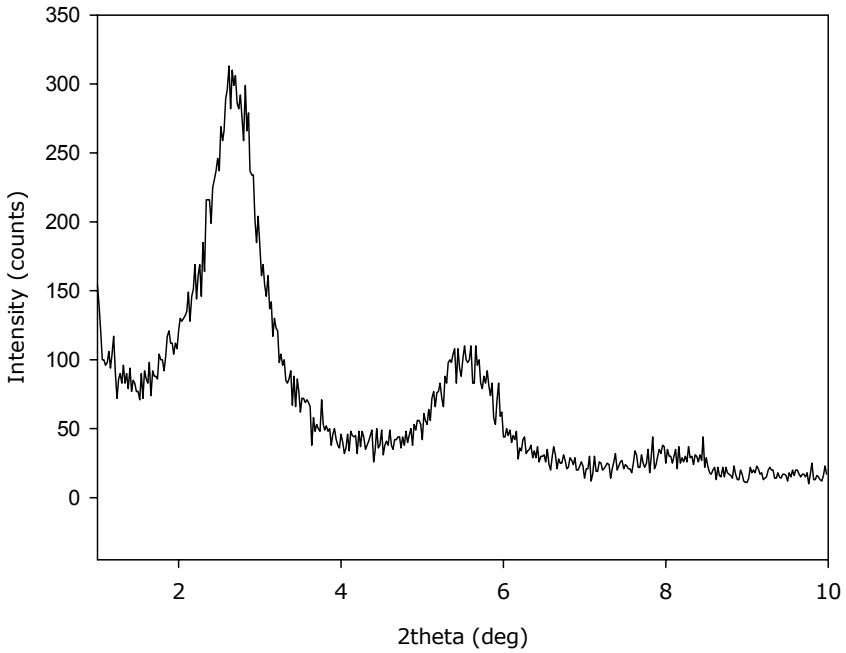


**Figure C.3** X-ray diffraction patterns of PC with 5 wt. % clay content.

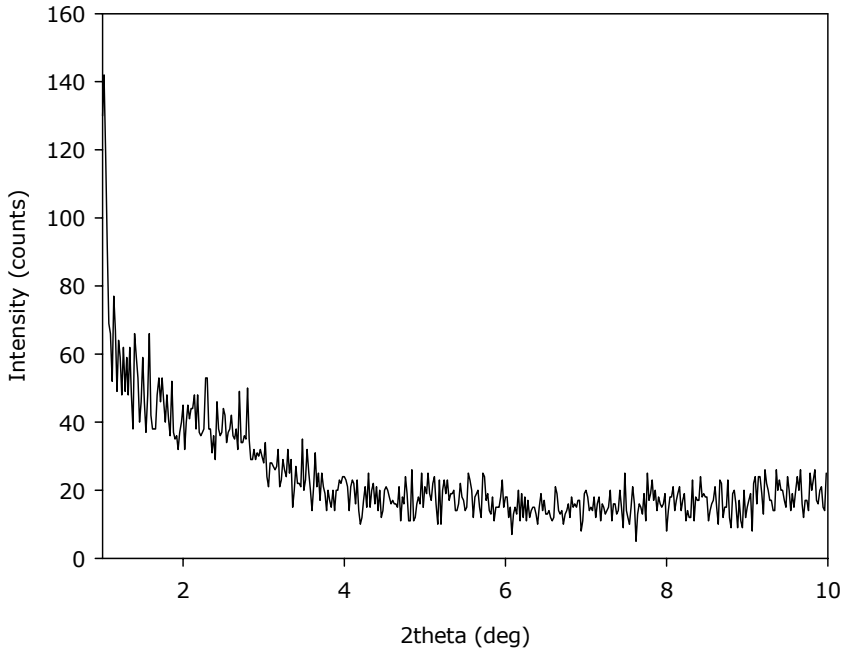


**Figure C.4** X-ray diffraction patterns of CI-P with 1 wt. % clay content.

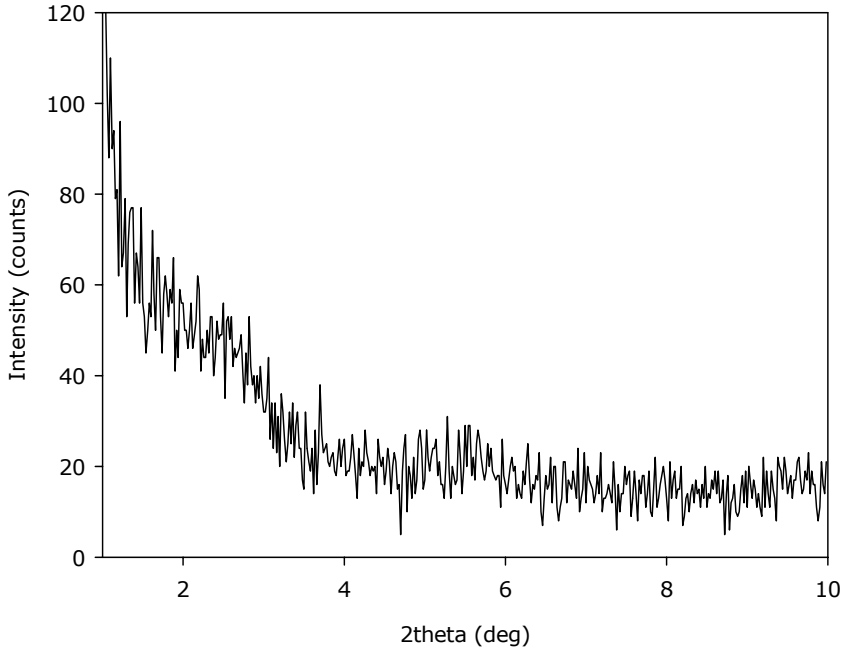


**Figure C.5** X-ray diffraction patterns of CI-P with 3 wt. % clay content.

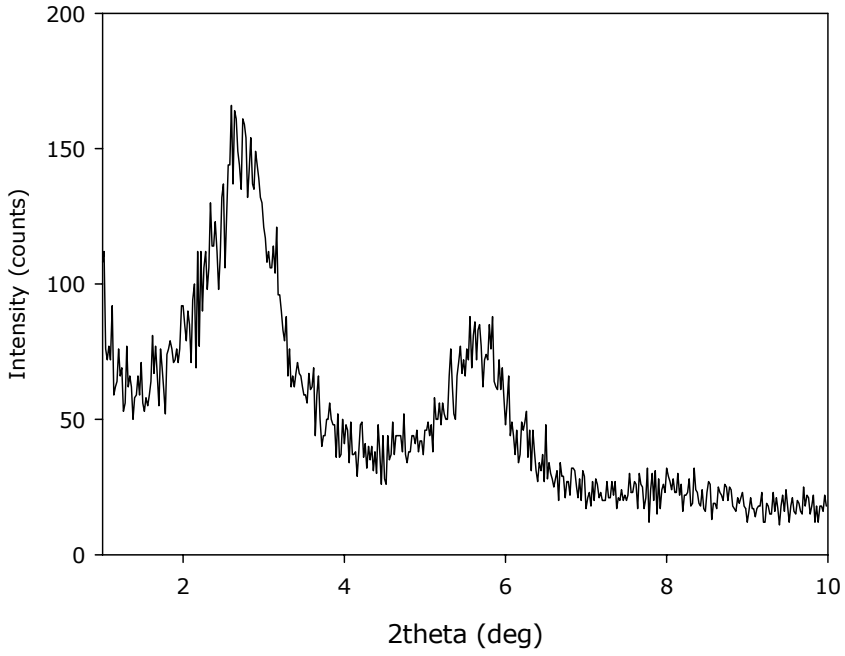


**Figure C.6** X-ray diffraction patterns of PC-I with 1 wt. % clay content.

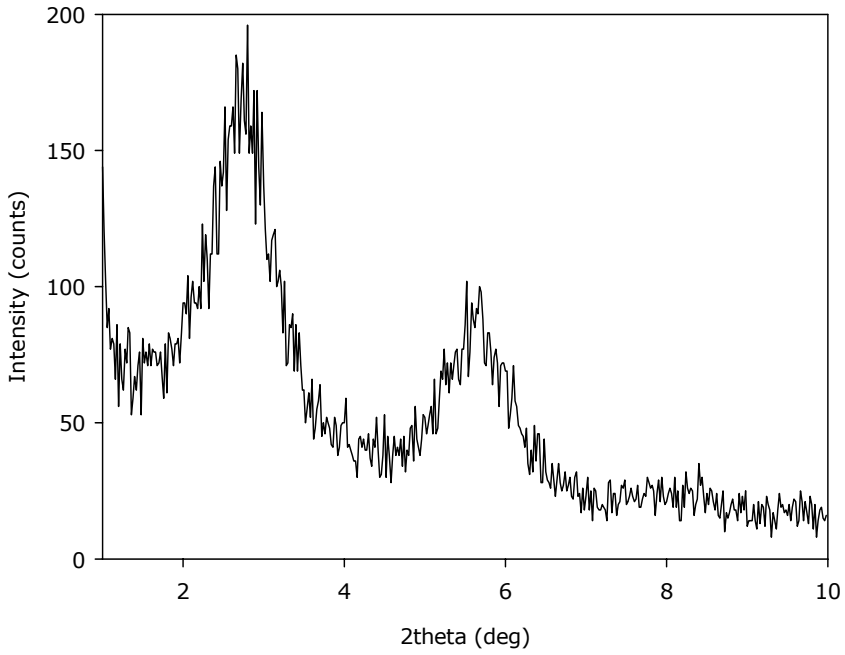


**Figure C.7** X-ray diffraction patterns of PC-I with 3 wt. % clay content.

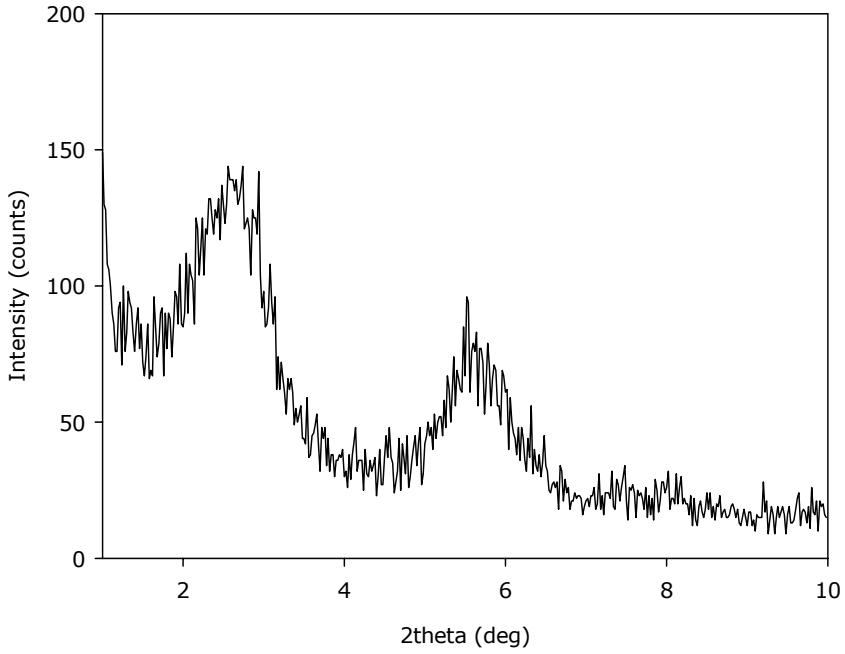


**Figure C.8** X-ray diffraction patterns of PC-I with 5 wt. % clay content.

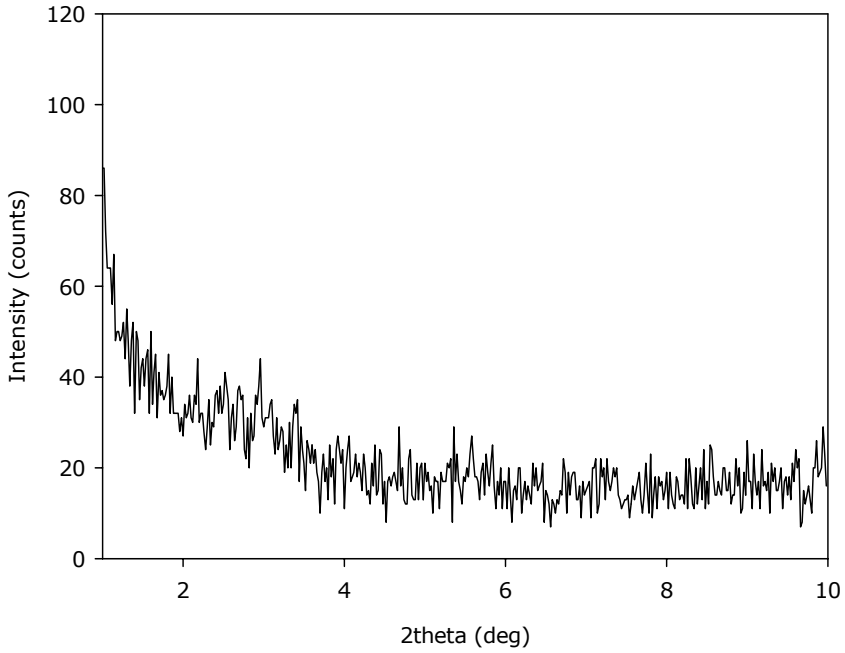


**Figure C.9** X-ray diffraction patterns of PI-C with 1 wt. % clay content.

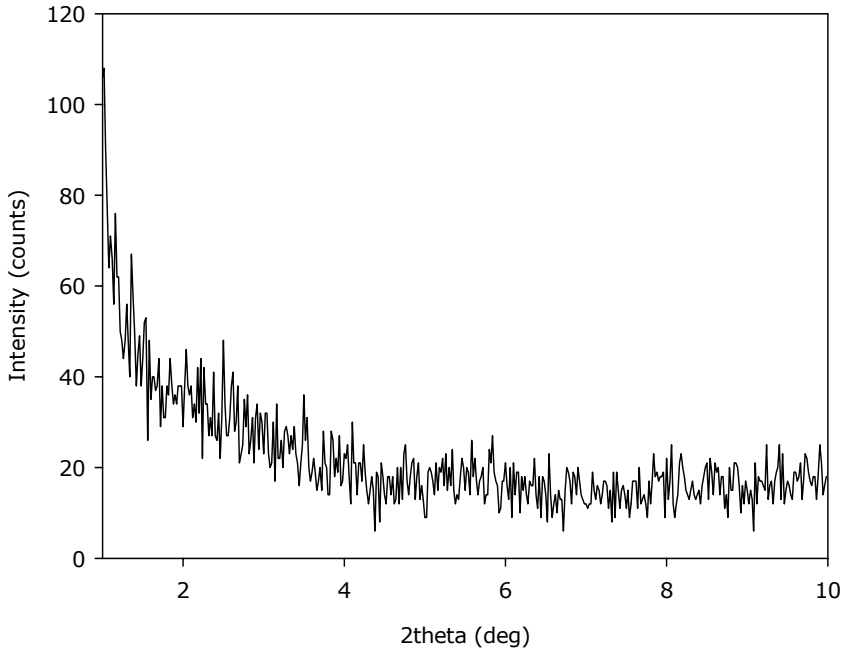


**Figure C.10** X-ray diffraction patterns of PI-C with 3 wt. % clay content.

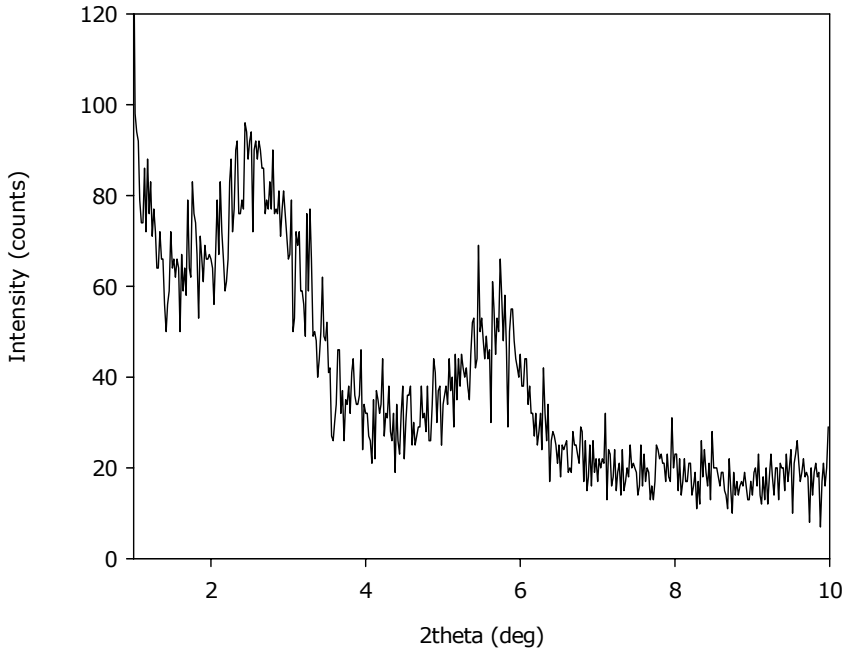


**Figure C.11** X-ray diffraction patterns of PI-C with 5 wt. % clay content.

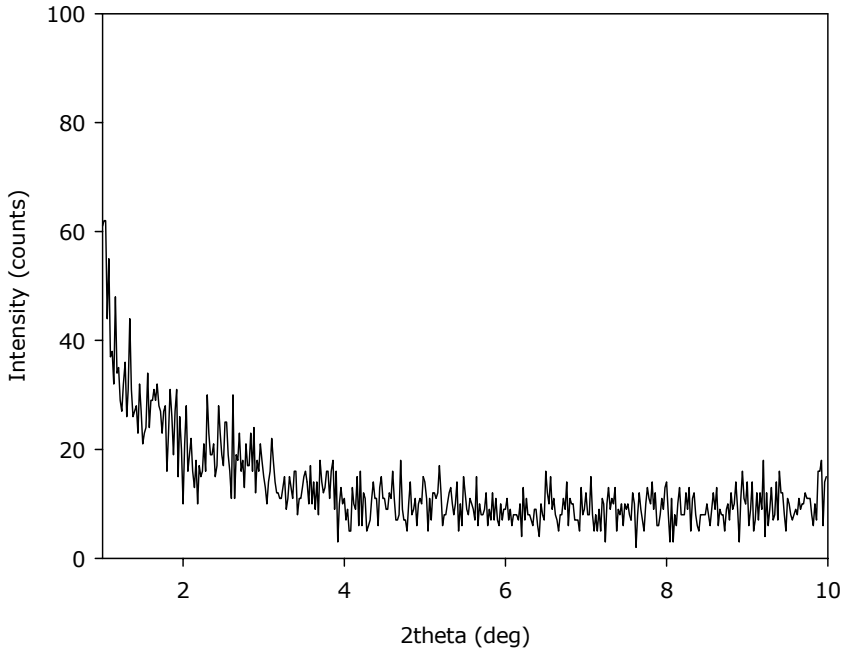


**Figure C.12** X-ray diffraction patterns of All-S with 1 wt. % clay content.

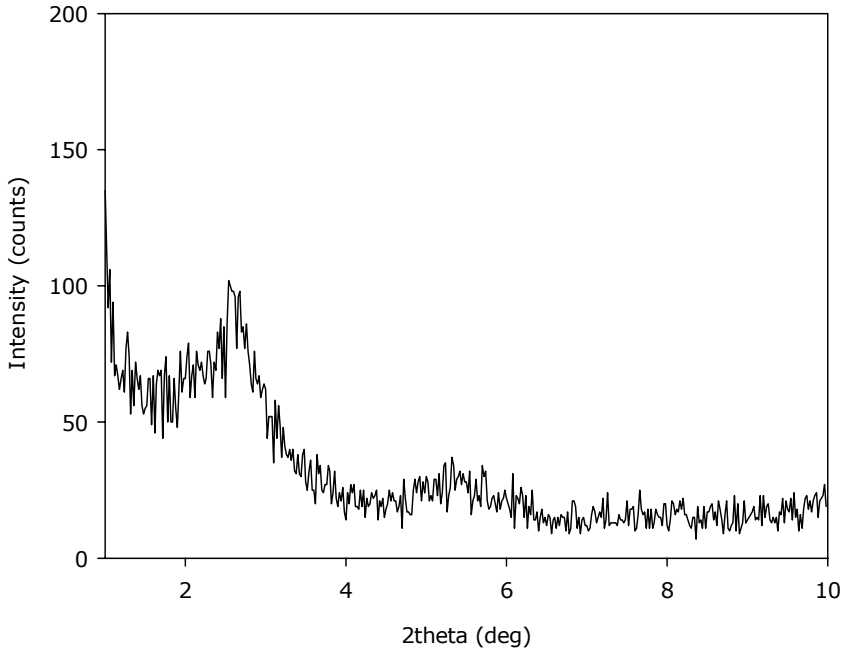


**Figure C.13** X-ray diffraction patterns of All-S with 3 wt. % clay content.

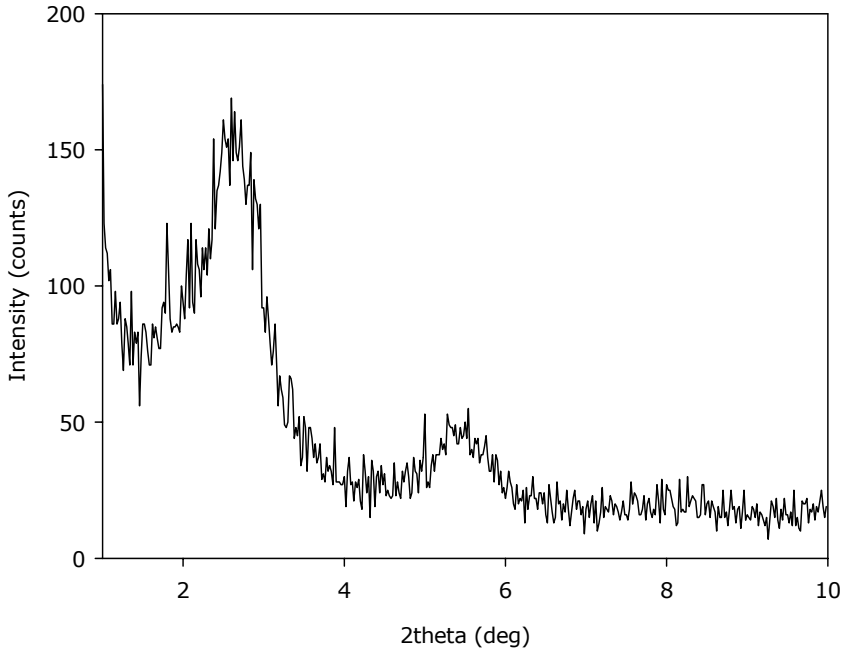


**Figure C.14** X-ray diffraction patterns of All-S with 5 wt. % clay content.